A PRECISION MEASUREMENT OF THE L_{II}-L_{III} X-RAY ENERGY LEVEL DIFFERENCE IN SOME HEAVY ELEMENTS AND A COMPARISON WITH THE PREDICTIONS OF THE SCHAWLOW-TOWNES THEORY OF THE NUCLEAR SIZE EFFECT

Thesis by

Robert Lee Shacklett

In Partial Fulfillment of the Requirements

for the Degree of

Doctor of Philosophy

California Institute of Technology

Pasadena, California

1956

ACKNOWLEDGMENTS

During the course of this work the author has received assistance and encouragement from many individuals of whom only a few can be mentioned here because of space limitations. He has profited in many ways from his association with Professor Jesse DuMond who suggested this investigation and provided the help and stimulation necessary for its successful completion. Several profitable discussions on the significance of the experimental results were enjoyed with Professor Robert Christy.

Assisting in various phases of the experiment were John J. Merrill who deserves a great deal of credit for his active interest in the work, Phillip Miller who helped in the design and construction of some of the apparatus, and Tom Layton who took care of the entire job of programming and coding the vertical divergence problem for the Jet Propulsion Laboratory's Datatron computer.

The author's wife, Jeanne, in addition to typing this thesis also assisted in the task of the reduction of data.

This work was done under a research contract with the U. S. Atomic Energy Commission which also made available on loan the plutonium used in this experiment.

ABSTRACT

The recent experimental determinations of the radius of the nuclear charge distribution all tend to give an approximate value of $R = r_o A^{1/3}$ with $r_o = 1.2 \times 10^{-13}$ cm. However, the theoretical work of Schawlow and Townes on the effect of the finite nuclear size on the L_{II}-L_{III} X-ray level splitting, through a comparison with already existing X-ray data, yielded a value of $r_o = 2.1 \times 10^{-13}$ cm. This thesis describes an experimental determination of the L_{II}-L_{III} splitting for six of the heavy elements based on two-crystal spectrometer measurements of the Bragg angles of the L_{α_2} and L_{β_1} X-ray lines of W, Pt, Bi, Th, U, and Pu. The Bragg angles of these lines, corrected for vertical divergence, temperature, and crystal diffraction pattern asymmetry, are reported with a mean standard deviation of about 0.2 second of arc. The values of the L_{II}-L_{III} splitting calculated from the wavelengths of the lines have a relative accuracy of about 50 parts per million. When the experimental splittings are compared to the theoretical values which include the nuclear size effect, a value of $r_o = 1.07 \times 10^{-13}$ cm is obtained. The suggestion is made that inaccuracies in the previous measurements of the L_{α_2} wavelengths for several high Z elements might have contributed to the large value of r_o obtained by Schawlow and Townes. When the theoretical splitting is calculated with corrections for vacuum polarization and a nuclear radius constant of $r_o = 1.2 \times 10^{-13}$ cm, a comparison with experiment shows that a discrepancy remains which is then used to evaluate an empirical correction term. The sign, magnitude, and Z-dependence of this term suggest that the remaining discrepancy might arise from the Lamb shift effect.

TABLE OF CONTENTS

PART I

INTRODUCTION

During the past few years, considerable effort has been expended toward getting as many facts as possible about (1) the size of the nucleus and (2) the nature of its charge distribution. That these two problems are intimately related is evident, for the word "size" presupposes some sort of boundary, and the type of boundary is dependent upon the nucleon distribution. Certain experiments are more sensitive to the distribution of nucleons while others reveal more information about the distribution of charge. Among the former we would place neutron and proton scattering experiments and α-decay lifetime measurements. Among the latter are measurements of isotope shifts, X-ray level splitting in heavy elements, mesonic X-rays, electron scattering by nuclei, β-decay, and nuclear Coulomb energy. It is therefore important that we distinguish between the radius of the distribution of charge and the radius of the distribution of nucleons, for these radii may be significantly different. (1) Henceforth, we usually shall have reference to the former unless otherwise stated.

Recent experiments in high energy electron scattering (2), (3) and mesonic X-rays (4) have indicated that the proton distribution probably consists of a central region of uniform density with an extended "tail" at the periphery of the latter and with a root mean square radius of $R = r_0 A^{1/3}$ where A is the atomic mass number and $r_0 \approx 1.2 \times 10^{-13}$ cm. This value of r_0 is significantly smaller than the usually accepted value, $r_0 = 1.5 \times 10^{-13}$ cm. Cooper and Henley (5)

and Ford and Hill (6) have compared these and the other methods yielding information on the charge distribution and find, with one exception, that the results of the various experiments are consistent with the smaller nuclear radius.

This exception is the value of r_0 as deduced by Schawlow and Townes.* (7) Briefly, their theory is based on the fact that in the heavy elements the finite extent of the nucleus causes a perturbation of the energy levels of those electrons whose wave functions are different from zero in the region of the nucleus. This perturbation is small for the $2p_{1/2}$ electrons and negligible for the $2p_{3/2}$ electrons. Thus the $L_{II} - L_{III}$ level splitting is subject to a small change due to nuclear size which is shown by Schawlow and Townes to increase rapidly with atomic number. By comparing their theoretical calculations with existing X-ray data on the $L_{II} - L_{III}$ level splitting in heavy elements they find that in order to get reasonable agreement a value of $r_0 = 2.1 \times 10^{-13}$ cm (assuming a fictitious uniformly charged, sharply bounded nucleus) is required.

Before this discrepancy became apparent, the present work was planned as an attempt to improve on the precision of the X-ray measurements which enter into the Schawlow-Townes theory. As other experiments began to suggest a smaller value of r_0, it became clear that highly precise X-ray measurements were necessary to eliminate a possible source of the discrepancy.

---

* This reference to the work of Schawlow and Townes was not published until after the major portion of the present work was completed. Professor Townes had kindly supplied us with the unpublished manuscript, however, which formed a basis for planning portions of this experiment.

The $L_{II} - L_{III}$ energy level difference can be measured in several different ways, each having its own peculiar set of experimental difficulties. This study is concerned with a two-crystal spectrometer determination of the wavelengths of the $L\alpha_2$ and the $L\beta_1$ lines of six of the heavy elements, ${}_{74}W$, ${}_{78}Pt$, ${}_{83}Bi$, ${}_{90}Th$, ${}_{92}U$, and ${}_{94}Pu$. The energy difference of these two lines is that of the L_{II} and L_{III} levels. The advantages of using these particular lines to obtain the level splitting will be discussed later.

Part II presents a synopsis of the theoretical work that has been done in evaluating the effect of the finite extent of the nucleus on the atomic electrons.

Part III gives a brief survey of the theory of X-ray reflection from a single crystal and then applies this theory to the operation of the two-crystal spectrometer in the absolute determination of Bragg angles.

Part IV presents an analysis of the effect of "vertical divergence" of the X-ray beam on the shape and position of the spectral line. The wavelength shift of an observed line due to absorption and due to asymmetry in the crystal diffraction patterns is also discussed.

Part V gives a description of the experimental apparatus.

Part VI describes the experimental procedure and presents the results of the measurements along with a discussion of their precision. A comparison with the Schawlow-Townes theory is made, and the possible significance of the results is discussed.

PART II

SYNOPSIS OF THE NUCLEAR SIZE EFFECT THEORY

A considerable amount of theoretical work has been done in attempting to evaluate the effect of the spatial extent of the nucleus on the energy levels of the atomic electrons. Most of this work has been carried out by investigators in the field of optical spectroscopy who have been interested in giving a quantitative interpretation of the phenomenon known as isotope shift.

Inasmuch as additional neutrons in a nucleus cause a slight change in its size and charge distribution, one might expect those atomic electrons most strongly affected by nuclear size to undergo small changes in their energy levels from isotope to isotope. This nuclear volume effect has been treated by first-order perturbation theory, and while in considerable error for the heavy elements, the theory serves as a convenient vantage point from which to survey the more exact approach discussed in Section B.

A. First-Order Perturbation Approach

The central problem of the perturbation method is the evaluation of the integral

$$\Delta E = \int_0^R P(r)(V + Ze^2/r)\, 4\pi r^2\, dr \qquad (2.1)$$

where ΔE is the shift in energy level of an atomic electron,

$P(r)$ is the probability density of the electron in the vicinity of a point nucleus,

R = radius of nucleus (more precisely, that distance beyond which the potential $V = -Ze^2/r$).

Rosenthal and Breit (8) have calculated an expression for ΔE starting with the Dirac radial wave equation for a central field. Since it is of some interest to compare and contrast the perturbation method with the more exact method, we shall consider briefly their approach. The two-component relativistic wave equations may be written*

$$\frac{dF}{dy} - \frac{jF}{y} = \frac{1}{2\gamma}\left(1 - \frac{E-V}{mc^2}\right) G$$

$$\frac{dG}{dy} + \frac{jG}{y} = \frac{1}{2\gamma}\left(1 + \frac{E-V}{mc^2}\right) F \qquad (2.2)$$

with $y = 2Zr/a_0$,

$\gamma = \alpha Z$,

a_0 is the first Bohr radius for hydrogen,

α is the fine structure constant,

j is a quantum number taking on values -1, +1, -2, ... for $s_{\frac{1}{2}}$, $p_{\frac{1}{2}}$, $p_{3/2}$, ... states respectively.

Assuming that V is constant for $y < y_0$ (which implies that the charge resides entirely on the nuclear surface) and making the approximation $E = mc^2$, the solutions of (2.2) for the region inside the nucleus are in terms of Bessel functions of the form

$$J_{|j\pm\frac{1}{2}|}(y\sqrt{\nu(\nu - 2)}/2\gamma)$$

---

* The notation has been changed slightly to conform to more prevalent usage.

where $v = V/mc^2$ is a constant. Since y is small and if $|v|$ is not too large ($-20 < v < 20$), the Bessel functions can be represented by their first term to a sufficient degree of accuracy; the solutions of (2.2) can be expressed in the form:

$$F = k_1 y^j; \quad G = \frac{k_2(2-v)y^{j+1}}{2\gamma(2j+1)} \qquad j > 0$$

$$F = \frac{k_1 y^{1+|j|}\, v}{2\gamma(1+2|j|)}\ ; \quad G = k_2 y^{|j|} \qquad j < 0 \tag{2.3}$$

k_1 and k_2 are constants.

Outside the nucleus, $V = -Ze^2/r = -2mc^2\gamma^2/y$; and with the approximation $E = mc^2$, the equations (2.2) become

$$\frac{dF}{dy} - \frac{jF}{y} = -\frac{\gamma G}{y}$$

$$\frac{dG}{dy} + \frac{jG}{y} = \left(\frac{1}{\gamma} + \frac{\gamma}{y}\right) F \tag{2.4}$$

The solutions of (2.4) are

$$F/\gamma = C1\left[J_{2\sigma}(2y^{\frac{1}{2}}) + C_2\, J_{-2\sigma}(2y^{\frac{1}{2}})\right]$$

$$G = C_1\left[A_{2\sigma}(2y^{\frac{1}{2}}) + C_2\, A_{-2\sigma}(2y^{\frac{1}{2}})\right] \tag{2.5}$$

with the abbreviations:

$$A_{2\sigma} = (j - \sigma)J_{2\sigma} + y^{\frac{1}{2}} J_{2\sigma+1}$$

$$A_{-2\sigma} = (j - \sigma)J_{-2\sigma} - y^{\frac{1}{2}} J_{-2\sigma-1} \qquad (2.6)$$

$$\sigma = \sqrt{j^2 - \gamma^2}$$

C_1 and C_2 are constants.

For a point nucleus (2.5) must be valid down to $y = 0$; and because of the behavior of negative order Bessel functions for small values of the argument, the constant C_2 must be set equal to zero. It is clear therefore that the finite nuclear size affects the wave functions through the constant C_2. Its value for a finite nucleus can be determined by matching the solutions (2.3) with the solutions (2.5) at the boundary of the nucleus $y = y_0$. The result is:

$$C_2 = \frac{F/\gamma G - J_{2\sigma}}{J_{-2\sigma} - (F/\gamma G)A_{-2\sigma}} \qquad (2.7)$$

where the argument of the Bessel functions is $2y_0^{\frac{1}{2}}$, and $F/\gamma G$ is determined from (2.3) with $y = y_0$.

The point nucleus wave functions F_0 and G_0 (with $C_2 = 0$) can be used to evaluate $P(r)$ in the integral (2.1). If we require the normalization

$$\int_0^\infty (F_0^2 + G_0^2)\, dr = 1 , \qquad (2.8)$$

(2.1) may be written

$$\Delta E = \int_0^R (V + Ze^2/r)(F_0^2 + G_0^2)\, dr \,. \qquad (2.9)$$

Since $y = 2Zr/a_0$ is small over the range of integration ($\lesssim 0.05$), F_0^2 and G_0^2 may be represented by the first term of an expansion in powers of y:

$$F_0^2 + G_0^2 = \frac{2C_1^2 j(j-\sigma)y^{2\sigma}}{\Gamma^2(2\sigma+1)} \qquad (2.10)$$

Assuming a constant value for $V = v\, mc^2$, the integration yields:

$$\Delta E = 2Ze^2 C_1^2 \frac{j(j-\sigma)}{\Gamma^2(2\sigma+1)} \left[\frac{1}{2\sigma} + \frac{vy_0}{2\gamma^2(2\sigma+1)}\right] y_0^{2\sigma} \,. \qquad (2.11)$$

Rosenthal and Breit have investigated the validity of the perturbation method and have found that (2.11) gives values which should be multiplied by a factor between 0.5 and 1.0. The correction they have worked out depends on the sizes of C_2 and v. Some typical values for Z = 81 and $v \cong -20$ (representing a spherical shell of charge) are:

State	j	C_2	Correction to ΔE
$s_{\frac{1}{2}}$	-1	0.0044	0.81
$p_{\frac{1}{2}}$	+1	0.0005	0.82
$p_{3/2}$	-2	negligible	1.0

It is significant that the finite nucleus perturbs the $p_{3/2}$ state to a negligible extent. This fact is of considerable importance because it allows the entire calculated shift of the L_{II} level to represent the change in the doublet splitting due to nuclear size.

The normalization constant C_1 appearing in (2.11) may be evaluated in terms of $h\Delta\nu$, the fine structure splitting, when the principal

quantum number is large enough so that relativistic effects can be neglected. Using Sommerfeld's doublet splitting formula and making the approximation

$$G = r\psi = C_1 \lim_{\gamma \to 0} A_2 \sigma ,$$

where ψ is the Schroedinger nonrelativistic wave function, Rosenthal and Breit obtain the following equation for C_1^2:

$$C_1^2 = \frac{h\Delta\nu/Ze^2}{\left[(\ell+1)^2 - \gamma^2\right]^{\frac{1}{2}} - 1 - (\ell^2-\gamma^2)^{\frac{1}{2}}} \qquad (2.12)$$

It is worth noting that the requirement that V be constant in the perturbation integral (2.9) is not necessary. In a note in proof in reference (8) Rosenthal and Breit show that the use of the general potential form for $r < R$

$$V = \left[-\frac{n+1}{n} + \frac{1}{n}\left(\frac{r}{R}\right)^n\right]\frac{Ze^2}{R}$$

requires that ΔE be multiplied by the factor

$$\frac{n+1}{2\sigma(2\sigma+1)(2\sigma+n+1)}$$

rather than by the factor

$$\frac{1}{2\sigma} + \frac{vy_0}{2\gamma^2(2\sigma+1)}$$

as in equation (2.11). Here n is a parameter which can range from -1 (charge concentrated at r = 0) to + ∞ (charge concentrated at r = R). With n=2 (uniform charge distribution) and with $v = -2\gamma^2/y_0$ (charge on surface of nucleus), comparison of the two factors shows that ΔE

for the shell model is about 1.5 times that for a uniform model.

Ford and Hill (6) have shown that the perturbation formula can be expressed as

$$\Delta E = \phi(Z) \left\langle r^{2\sigma} \right\rangle_{Av}$$

where $\left\langle r^{2\sigma} \right\rangle_{Av}$ is the average value of $r^{2\sigma}$ defined by

$$\left\langle r^{2\sigma} \right\rangle_{Av} = \frac{\int_0^\infty r^{2\sigma} \rho_N(r) 4\pi r^2 dr}{\int_0^\infty \rho_N(r) 4\pi r^2 dr} = (Ze)^{-1} \int_0^\infty r^{2\sigma} \rho_N(r) 4\pi r^2 dr \qquad (2.13)$$

and $\rho_N(r)$ is the nuclear charge density. Using electronic computer techniques they have evaluated $\left\langle r^{2\sigma} \right\rangle_{Av}$ for several different types of charge distributions. Their results will be useful in modifying the exact calculations of ΔE to conform to different nuclear models.

B. More Exact Calculations

A rather ingenious method of calculating ΔE without using the usual perturbation techniques has been developed by Broch. (9) Equation (2.2) for a point nucleus may be written

$$\frac{dF_o}{dy} - \frac{jF_o}{y} = \frac{1}{2\gamma}\left(1 - \frac{E_o - V_o}{mc^2}\right) G_o$$

$$\frac{dG_o}{dy} + \frac{jG_o}{y} = \frac{1}{2\gamma}\left(1 + \frac{E_o - V_o}{mc^2}\right) F_o \,. \qquad (2.14)$$

Multiplying the first of the above equations by -G, the second by F, the first of (2.2) by G_o, and the second of (2.2) by $-F_o$, we obtain by addition

$$\frac{d}{dy}(FG_o - F_oG) = \frac{\Delta V - \Delta E}{2\gamma mc^2}(F F_o + G G_o) \qquad (2.15)$$

where $\Delta V = V - V_o$ and $\Delta E = E - E_o$. Integrating this equation from y_o to ∞, noting that $\Delta V = 0$ outside the nucleus and that the wave functions vanish at ∞, we get

$$(FG_o - F_oG)_{y_o} = \frac{\Delta E}{2\gamma mc^2}\int_{y_o}^{\infty}(F F_o + G G_o)dy. \qquad (2.16)$$

A very good approximation to the integral in (2.16) can be made by assuming*

$$\int_{y_o}^{\infty}(F F_o + G G_o)dy \approx \int_{o}^{\infty}(F F_o + G G_o)dy = \frac{2Z}{a_o}\int_{o}^{\infty}(F_o^2 + G_o^2)dr = \frac{2Z}{a_o} \qquad (2.17)$$

since y_o is very small compared to atomic dimensions; hence

$$\Delta E = \tfrac{1}{2}c(FG_o - F_oG)_{y_o} \quad . \qquad (2.18)$$

F and G in this expression are given by (2.5) and F_o and G_o are the same functions with $C_2 = 0$. The value of C_2 is given by (2.7), but it must be pointed out that the quantity $F/\gamma G$ appearing therein must be calculated separately for each type of potential function used.

Broch's paper is concerned with deriving an accurate correction factor for Rosenthal and Breit's perturbation formula; however, Schawlow and Townes use Broch's expression for ΔE rather than

---

* Actually Broch assumes $\int_o^{\infty}(F_o^2 + G_o^2)dy = 1$, but Schawlow and Townes adhere to Rosenthal and Breit's normalization (2.8) since C_1 and C_2 are used in this more exact treatment.

correcting the perturbation calculations. Substituting the various quantities into (2.18) we obtain

$$\Delta E = Ze^2 C_1^2 C_2 y_0^{\frac{1}{2}} (J_{2\sigma+1} J_{-2\sigma} + J_{2\sigma} J_{-2\sigma-1}) \tag{2.19}$$

where the argument of the Bessel functions is $2y_0^{\frac{1}{2}}$. This can be simplified by using properties of the Bessel functions:

$$\Delta E = -2Ze^2 C_1^2 C_2 \frac{\sigma}{\Gamma(1+2\sigma)\Gamma(1-2\sigma)} . \tag{2.20}$$

An approximate expression for C_1^2 is given by (2.12) which is not too accurate for the $L_{II} - L_{III}$ splitting. Schawlow and Townes point out that more accurate values of C_1^2 can be obtained if Dirac wave functions with an appropriately screened nuclear charge are used rather than the Schroedinger wave functions used by Rosenthal and Breit. Actual calculation using a screening constant of 5.5 shows that C_1^2 as given by (2.12) should be multiplied by 0.76.

Substituting (2.12) into (2.20) and dividing by $h\Delta\nu$ we obtain as the fractional change in fine structure splitting due to nuclear size

$$\frac{\Delta E}{h\Delta\nu} = \frac{2C_2}{\left[(\ell+1)^2 - \gamma^2\right]^{\frac{1}{2}} - 1 - (\ell^2 - \gamma^2)^{\frac{1}{2}}} \frac{\sigma}{\Gamma(1+2\sigma)\Gamma(1-2\sigma)} \tag{2.21}$$

where C_2 is calculated from (2.7).

Schawlow and Townes have used the above formula to calculate $\Delta E/h\Delta\nu$ for a $2p_{\frac{1}{2}}$ electron for 5 values of Z between 60 and 95 assuming a nuclear radius of $1.5 \times 10^{-13} A^{1/3}$ cm and either a uniform model or a shell model for the charge distribution. The results appear in Table I.

Table I

Z	Uniform Model	Shell Model
60	1.09×10^{-4}	1.73×10^{-4}
70	2.51×10^{-4}	3.92×10^{-4}
81	6.35×10^{-4}	9.56×10^{-4}
90	1.38×10^{-3}	2.03×10^{-3}
95	2.17×10^{-3}	3.01×10^{-3}

The values of $\Delta E/h\Delta\nu$ in Table I can be conveniently represented by the expression

$$\frac{\Delta E}{h\Delta\nu} = De^{b(Z-60)} \qquad (2.22)$$

where $D_1 = 1.09 \times 10^{-4}$, $b_1 = 0.0858$ for uniform model

$D_2 = 1.72 \times 10^{-4}$, $b_2 = 0.0817$ for shell model

The values of Table I need to be corrected for the error in the normalization constant C_1^2, but whatever correction is used, it would be the same for each value listed and would not change the functional dependence on Z. In Part VI we will make the appropriate corrections to the values listed above, both for normalization and for smaller nuclear radius.

Comparing the ratios of the values of ΔE for the two different models as predicted by the methods of Section A and this Section we find that for Z = 81:

Perturbation method: $\dfrac{\Delta E(\text{shell})}{\Delta E(\text{uniform})} = \dfrac{3}{2\sigma + 3} = 1.54$

Exact method: $\dfrac{\Delta E(\text{shell})}{\Delta E(\text{uniform})} = \dfrac{9.56 \times 10^{-4}}{6.35 \times 10^{-4}} = 1.51$.

The close agreement between these two factors indicates that the perturbation method, while in error in predicting the size of ΔE, is probably valid for estimating its variation with the assumed nuclear model.

C. Theoretical Calculation of the $L_{II} - L_{III}$ Level Splitting

The energy difference between the $2p_{\frac{1}{2}}$ and $2p_{3/2}$ levels of an electron in the Coulomb field of a point nucleus is given by the well-known Sommerfeld formula

$$\Delta E_0 = \frac{mc^2}{2}\left\{\sqrt{4-\alpha^2Z^2} - \left[2 + 2\sqrt{1-\alpha^2Z^2}\right]^{\frac{1}{2}}\right\}^{\frac{1}{2}} = mc^2\, S(\alpha Z). \tag{2.23}$$

This energy difference expressed in Rydbergs is

$$\frac{\Delta\nu_0}{R} = \frac{2}{\alpha^2} S(\alpha Z) \tag{2.24}$$

where $R = \alpha^2 mc^2/2h$.

Equation (2.24) must be corrected to take into account the interaction between the various atomic electrons. Christy and Keller (10) have made a calculation of this type allowing for the interactions of the electrons of the K and L shells and the effect of the M shell on the $2p_{\frac{1}{2}}$ and $2p_{3/2}$ states. They show that the correction to be added to (2.24) is of the form

$$-2\alpha^2Z^3 f(\alpha Z) + B Z^2 \tag{2.25}$$

where $f(\alpha Z) = \frac{1}{\alpha^2Z^2}\left(\frac{W(\alpha Z)}{mc^2\alpha^2Z}\right)$

and B is an undetermined constant. $W(\alpha Z)$ has been calculated in

units of $mc^2\alpha^2Z$ for 6 values of αZ and is given in Table II of Christy and Keller's paper. This table is reproduced below along with the corresponding values of $f(\alpha Z)$ calculated using the value $1/\alpha = 137.0373$. (11) The calculation of $W(\alpha Z)$ is subject to a small error of the order of one per cent due to the neglect of outer shell electrons and higher order terms in the interaction Hamiltonian. Christy and Keller have estimated a correction term for the latter which we shall incorporate into the calculations of Part VI.

Table II

First three columns taken from Christy and Keller. (10) $W(\alpha Z)$ in units of $mc^2\alpha^2Z$.

$\sqrt{1-\alpha^2Z^2}$	Z(approx.)	$W(\alpha Z)$	$f(\alpha Z)$
1.00	0	0.00000	(indeterminate)
0.96	38	0.03995	0.509566
0.91	57	0.09508	0.553112
0.86	70	0.15666	0.601613
0.82	78	0.21110	0.644383
0.76	89	0.30256	0.716288

In actual computations, $f(\alpha Z)$ for a given value of Z must be interpolated or extrapolated from the values given in Table II. It was found that a plot of log $f(\alpha Z)$ against $1-\sqrt{1-\alpha^2Z^2}$ was nearly linear; Lagrange interpolation can therefore be used with a reasonable degree of accuracy.

The complete expression for the theoretical value of the fine

structure splitting including the Schawlow-Townes correction factor (2.22) for nuclear size is

$$\frac{\Delta\nu}{R} = \left[\frac{2}{\alpha^2} S(\alpha Z) - 2\alpha^2 Z^3 f(\alpha Z) + BZ^2\right]\left[1 + De^{b(Z-60)}\right] . \quad (2.26)$$

The values calculated using (2.26) are compared to the measured values, and B and D are adjusted to minimize the mean square error. Using existing X-ray data compiled by Cauchois and Hulubei, (12) Schawlow and Townes have calculated $(\Delta\nu_{th} - \Delta\nu_{exp})/\Delta\nu_{th}$ with and without the nuclear size correction. The value of b used in this calculation was 0.0837 which is midway between the value for a uniformly charged nucleus and that for one with a surface charge only. The sign and magnitude of D obtained in minimizing the errors ($D = -1.42 \times 10^{-4}$) corresponds to a decrease in the doublet separation and a nuclear radius of $R = 2.1 \times 10^{-13} A^{1/3}$ cm, assuming that a normalization correction factor of 0.76 is applied to the values in Table I. The results are shown in Figure 1, the (a) part of which indicates that a systematic error at large Z exists which cannot be interpreted as simply experimental error. Part (b) shows that by including the nuclear size correction factor, the large errors are reduced, and the residual scatter of the points can probably be attributed to experimental errors.

It is evident from Figure 1 that more definite conclusions could be drawn from the Schawlow-Townes theory if the precision of the X-ray measurements could be improved. In considering the experimental aspect of the problem at this point and the question of precision, it is necessary to investigate the various ways of determining the L_{II}-L_{III} level difference and the problems associated with each.

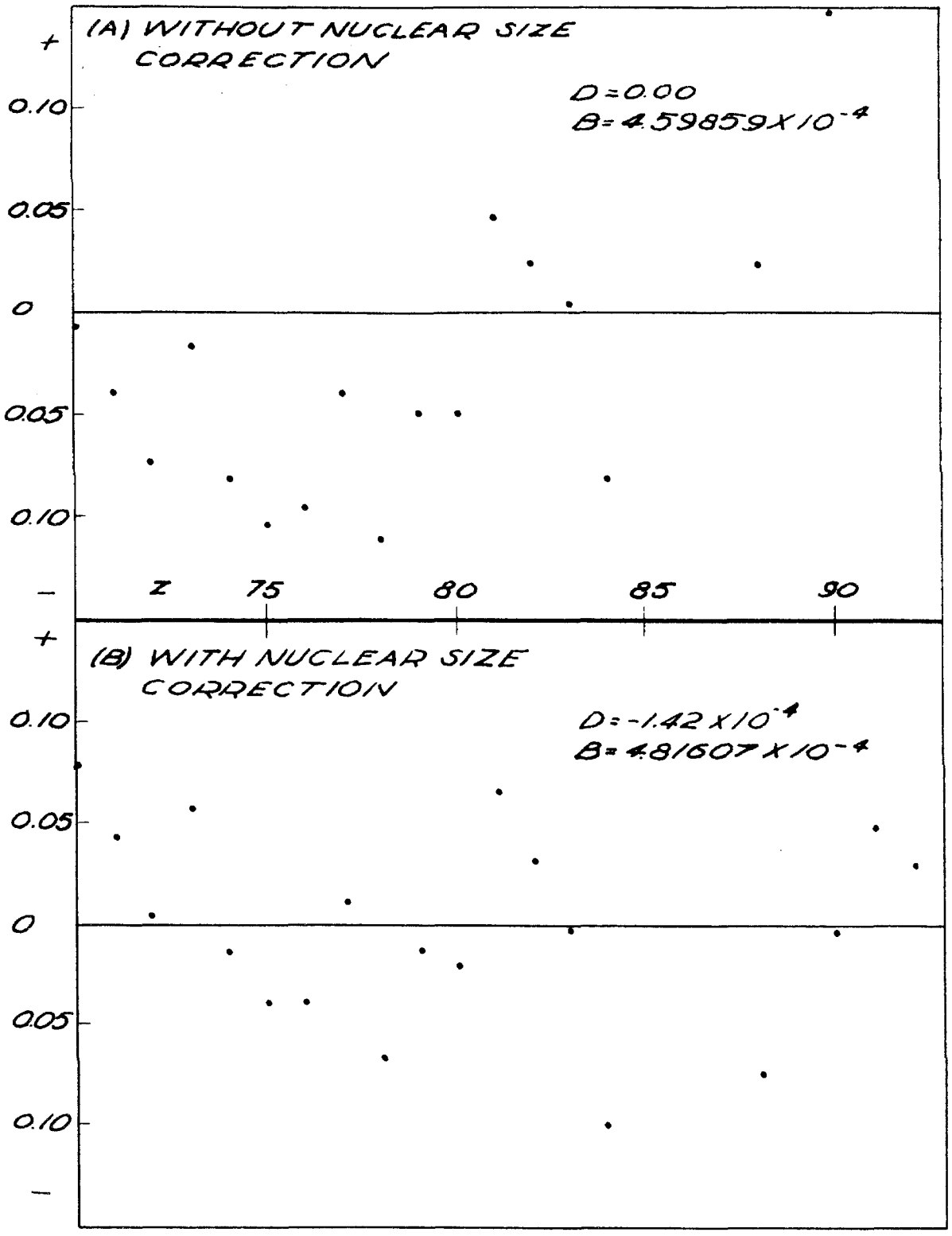

Figure 1. Schawlow and Townes' results expressed as deviations in per cent of fine structure.

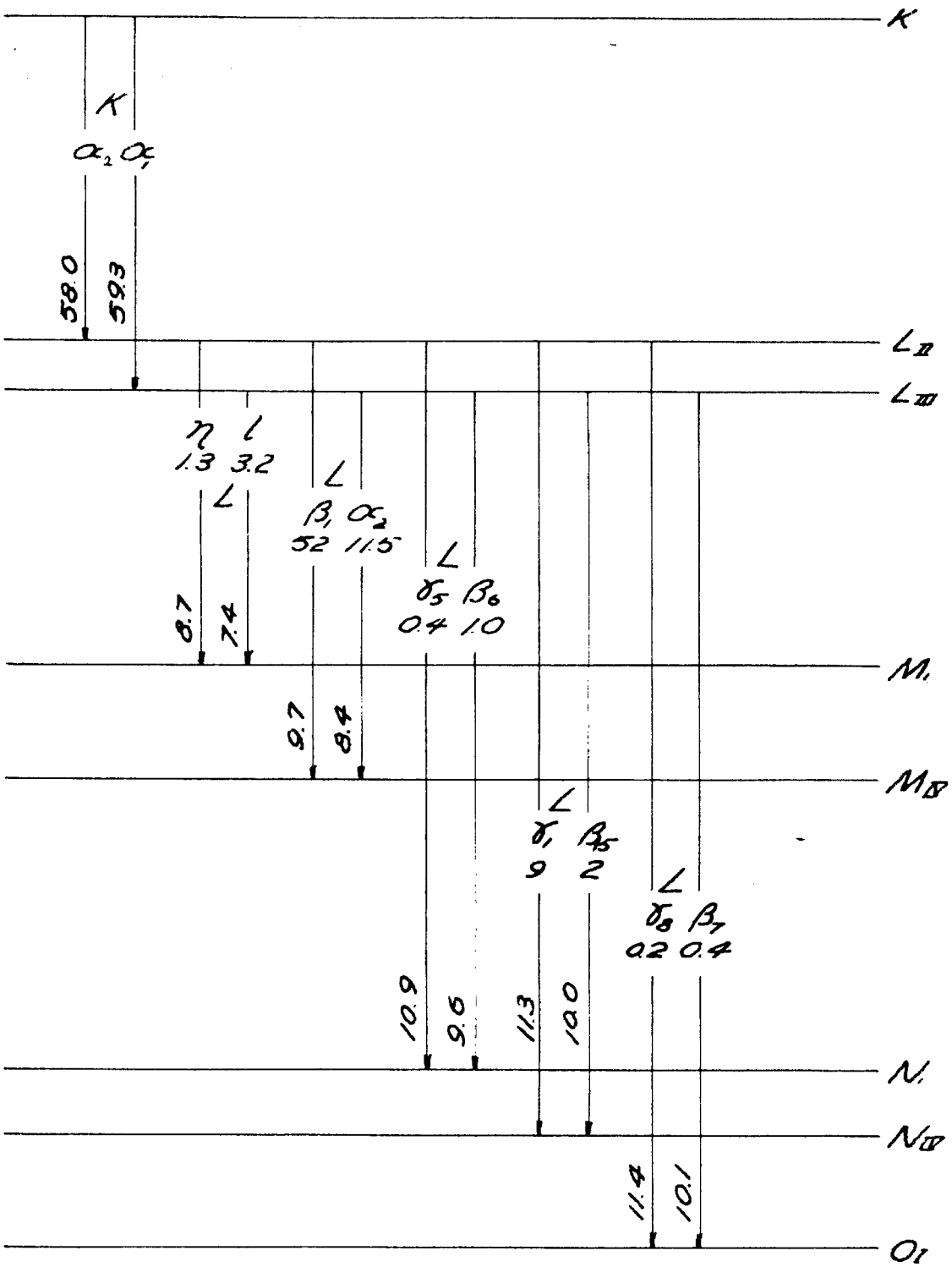

Figure 2. Energy level diagram for W(74) showing transitions giving the L_{II}-L_{III} separation. The numbers alongside the lines are the approximate energies in kilovolts, the numbers beneath the L line designations are the intensities relative to an intensity of 100 for $L\alpha_1$.

Figure 2 is an X-ray energy level diagram (not drawn to scale) showing the various pairs of transitions giving rise to the $L_{II} - L_{III}$ difference and their approximate energies for tungsten. The relative intensities for the L series lines are given, based on a relative intensity of 100 for L_{α_1}, the strongest line of the series. Another possibility not indicated in the figure is that of the direct determination of the L_{II} and L_{III} energies by absorption measurements. Of these seven possibilities, the one representing the least amount of experimental difficulty and hence the greatest possibility for precision is the measurement of the L_{α_2} and L_{β_1} lines. The rest of the L-lines are so weak that precise measurements would require an inordinate amount of time. Absorption edge measurements sometimes give misleading results because of the difficulty of interpreting the shape and structure of the observed "edge". The much larger energies of the K-lines introduce several complications into an experiment; and the fact that these lines are roughly four times broader than L series lines also places limitations on their usefulness as a precision measure of the doublet splitting.

Let us now assume that the wavelengths of the L_{α_2} and L_{β_1} lines of several heavy elements are to be measured by means of the two-crystal spectrometer using calcite crystals. Let us further assume that the degree of precision required is one-tenth of the predicted fine-structure shift due to nuclear size. We wish to find the corresponding accuracy required in the determination of the Bragg angles. Using (2.22) with $D = 1.42 \times 10^{-4}$ and $b = 0.0837$ and the experimental values of $\Delta\nu/R$ we obtain the following approximate values

for the nuclear size effect expressed in Rydbergs:

Z	$De^{b(Z-60)}$	$(\Delta\nu/R)_{exp}$	$\Delta = (\Delta\nu/R)De^{b(Z-60)}$
74	4.58×10^{-4}	98.3	0.045
94	24.32×10^{-4}	309.6	0.75

Now

$$\frac{\Delta\nu}{R} = \frac{1}{R}\left(\frac{1}{\lambda_{\beta_1}} - \frac{1}{\lambda_{\alpha_2}}\right) = \frac{1}{2Rd_1}\left(\frac{1}{\sin\theta_{\beta_1}} - \frac{1}{\sin\theta_{\alpha_2}}\right) \quad (2.27)$$

where d_1 is the grating space of calcite for first order. Differentiating the above expression, assuming that θ is the average value of θ_{β_1} and θ_{α_2} and that both angles can be measured with the same precision, we obtain:

$$\delta\theta = \left[\sqrt{2}\, Rd_1 \sin\theta \tan\theta\, (2.06\times10^{+5})\right] \delta\left(\frac{\Delta\nu}{R}\right) \quad (2.28)$$

where the factor 2.06×10^5 converts radians to seconds of arc. If we let $\delta(\Delta\nu/R) = \Delta/10$ we obtain the following values for $\delta\theta$:

$Z = 74$ $\quad \delta\theta \cong 0.2$ seconds

$Z = 94$ $\quad \delta\theta \cong 1.2$ seconds.

Inasmuch as the precision attainable on the two-crystal spectrometer is roughly independent of wavelength over this particular spectral region, it is clear that if the figure of ± 0.2 seconds can be attained in the measurements on tungsten, the nuclear size effect can be measured with an accuracy of about 2 per cent in the case of plutonium.

PART III

BRIEF THEORY OF THE TWO-CRYSTAL X-RAY SPECTROMETER

The subject of X-ray reflection from crystals has been treated extensively by many authors and some have extended the theory to cover the case of the two-crystal X-ray spectrometer. The text of Compton and Allison (13) gives a fairly comprehensive analysis of the theory of the instrument, but with somewhat greater emphasis on its use in the investigation of crystal properties rather than its use in the precise measurement of X-ray wavelengths. It is therefore necessary to investigate in somewhat greater detail the theory of the instrument as it pertains to the latter usage.

We will assume that the X-ray reflection properties of the calcite crystals used in this measurement are reasonably well represented by the theory described in the text mentioned. The validity of such an assumption can and should be subjected to experimental verification; but since such a procedure is quite involved and time consuming we will abide with the initial assumption and justify it later with several qualitative arguments.

A. X-ray Reflection From a Single Crystal

The dynamical theory of X-ray reflection in crystals, as it was developed in its more simple form by Darwin, (14) does not take into consideration the effect of the absorption of the X-rays as they penetrate the crystal. Nevertheless, the theory is sufficiently adequate so that certain salient features of the crystal "diffraction pattern" may be obtained from it. The term "diffraction pattern" is

the name commonly given to the curve of the ratio of reflected to incident intensity versus the angle of the reflected beam measured relative to the surface of the crystal. Under the assumption that the incident radiation consists of plane, polarized, monochromatic waves, where both the electric vector and the atomic reflecting planes are parallel to the crystal surface, the equation for this curve, as derived by Darwin, may be expressed in the form*

$$I^D(\ell) = \left| \frac{F/Z}{\ell \pm \sqrt{\ell^2 - F^2/Z^2}} \right|^2 \qquad (3.1)$$

The quantities appearing in this equation are defined as follows: the variable ℓ is proportional to the difference between the angle of reflection Ψ and the corrected Bragg angle θ and is given by the relation

$$\ell = (\Psi - \theta) \frac{\sin 2\theta}{2\delta} \qquad (3.2)$$

where $\delta = 1 - \mu$ is the unit difference of the refractive index. By "corrected Bragg angle" we mean the usual Bragg angle which has been corrected for index of refraction effects, namely

$$\theta = \sin^{-1} \left\{ \frac{n\lambda}{2d} \left[1 - \frac{4d^2\delta}{n^2\lambda^2} \right]^{-1} \right\} \qquad (3.3)$$

where d = actual grating space of the crystal

n = order of reflection

λ = wavelength of incident radiation.

---

* We use here the notation of Compton and Allison

Referring to (3.1) again, the quantity Z represents the number of electrons in the unit cell of the crystal and for calcite is equal to 100. F is the crystal structure factor which is the ratio of the amplitude scattered by the unit cell in the direction θ to the amplitude scattered by a single electron in that same direction. F, for a given set of crystal planes, is a function of λ and θ and takes into account the phase difference of the waves scattered from the different electrons of the unit cell. The ratio F/Z is always less than or equal to 1; for the cleavage planes of calcite at $\lambda = 0.708$ Angstrom units, $F/Z = 0.516$.

A plot of $I^D(\ell)$ for calcite at a wavelength of 0.708 A is shown in Figure 3. A scale of $\psi - \theta_0$ expressed in seconds of arc is placed immediately below the ℓ axis. The angle θ_0 is the uncorrected Bragg angle, and the separation of the two lines $\ell = 0$ and $\psi = \theta_0$ shows the effect of the index of refraction correction in (3.3).

One of the noteworthy features of the Darwin theory is that it predicts a small angular region of width $\ell = 2F/Z$ over which the crystal reflects 100 per cent of the incident intensity. Another feature is the steepness of the sides of the pattern; the width at half maximum is only 6 per cent greater than the width at the top.

While the Darwin diffraction pattern neglecting absorption gives us a first approximation to the solution of the problem of X-ray reflection from crystals, it becomes decreasingly useful for the longer wavelengths for which the absorption in the crystal becomes appreciable. Although Darwin introduced the effect of photoelectric absorption as a correction into his theory, a somewhat more general and satisfactory analysis was given later by Prins (15) who treated

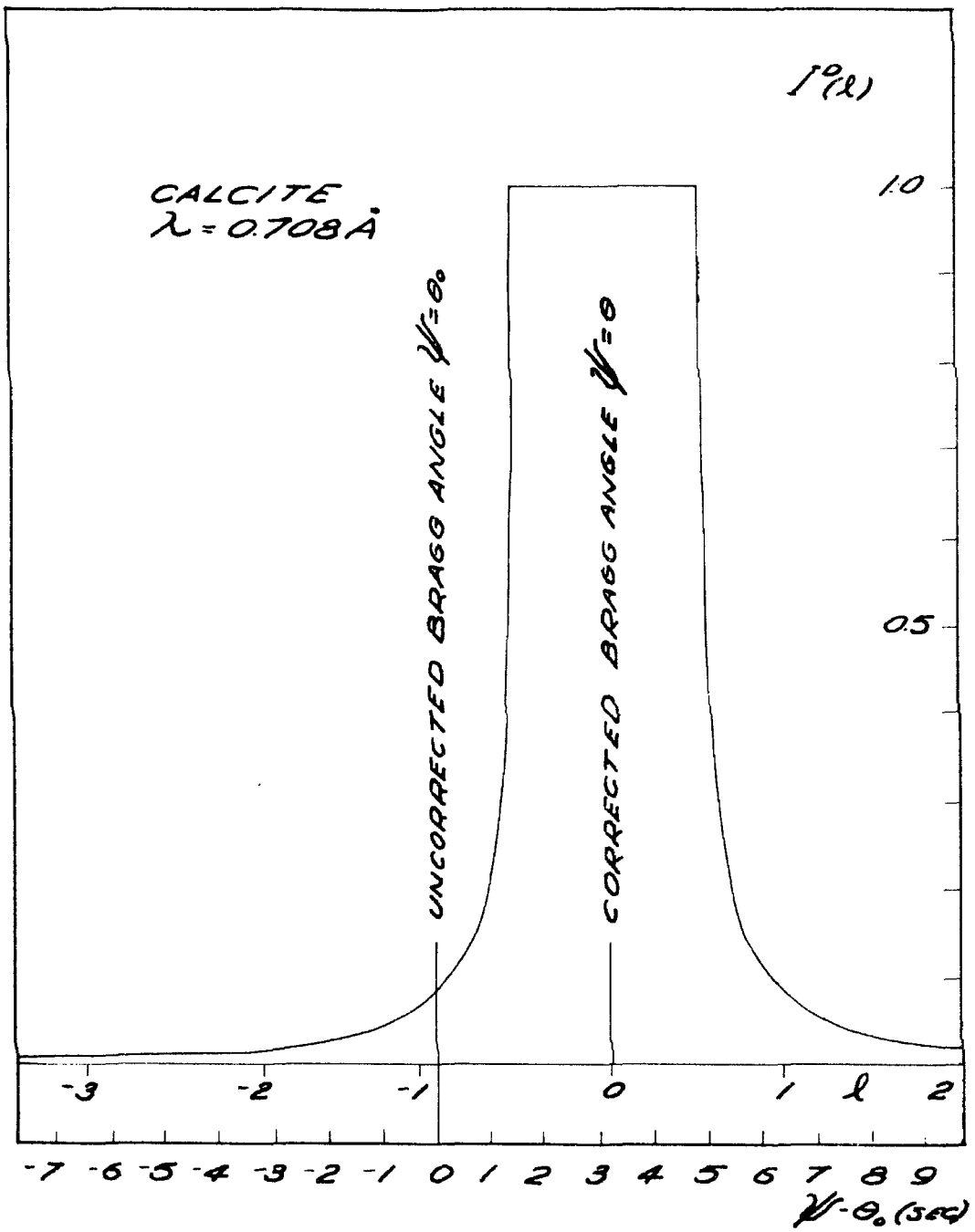

Figure 3. Darwin Diffraction Pattern as given by Equation (3.1).

the effect of absorption by considering the crystal to be a dispersive medium with a complex index of refraction. The resulting expression for the ratio of reflected to incident intensity has a form comparable to that of the Darwin formula:

$$I(\ell) = \left| \frac{(D + iB)/\delta}{\ell - i\,\beta/\delta \pm \left\{(\ell - i\,\beta/\delta)^2 - \left[(D + iB)/\delta\right]^2\right\}^{\frac{1}{2}}} \right|^2 \tag{3.4}$$

where $\beta = (\lambda/4\pi)\mu_\ell$ (includes effect of absorption)

μ_ℓ = linear absorption coefficient for the crystal

$D+iB = (\delta + i\beta)F/Z$.

It is readily seen that when $\beta = 0$ (negligible absorption) the above expression reduces to the Darwin formula.

Calculations based on (3.4) are quite laborious, but Allison (16) and Parratt (17) have published curves and tables of values of $I(\ell)$ for calcite at various wavelengths. Figure 4 shows a plot of $I(\ell)$ for 2.299 A, a wavelength considerably longer than that encountered in the present work but one for which the effect of absorption is clearly shown. The marked asymmetry is an important characteristic, and its effect on precision wavelength measurements will be discussed later.

It is necessary at this point to remark briefly about the question of polarization. It will be recalled that the Darwin formula (3.1) was based upon the assumption that the incident radiation was polarized with the electric vector parallel to the crystal planes. In discussing the other direction of polarization it is convenient to define a "plane of incidence" which is that plane normal to the surface of the crystal containing both the incident and reflected rays. The type of

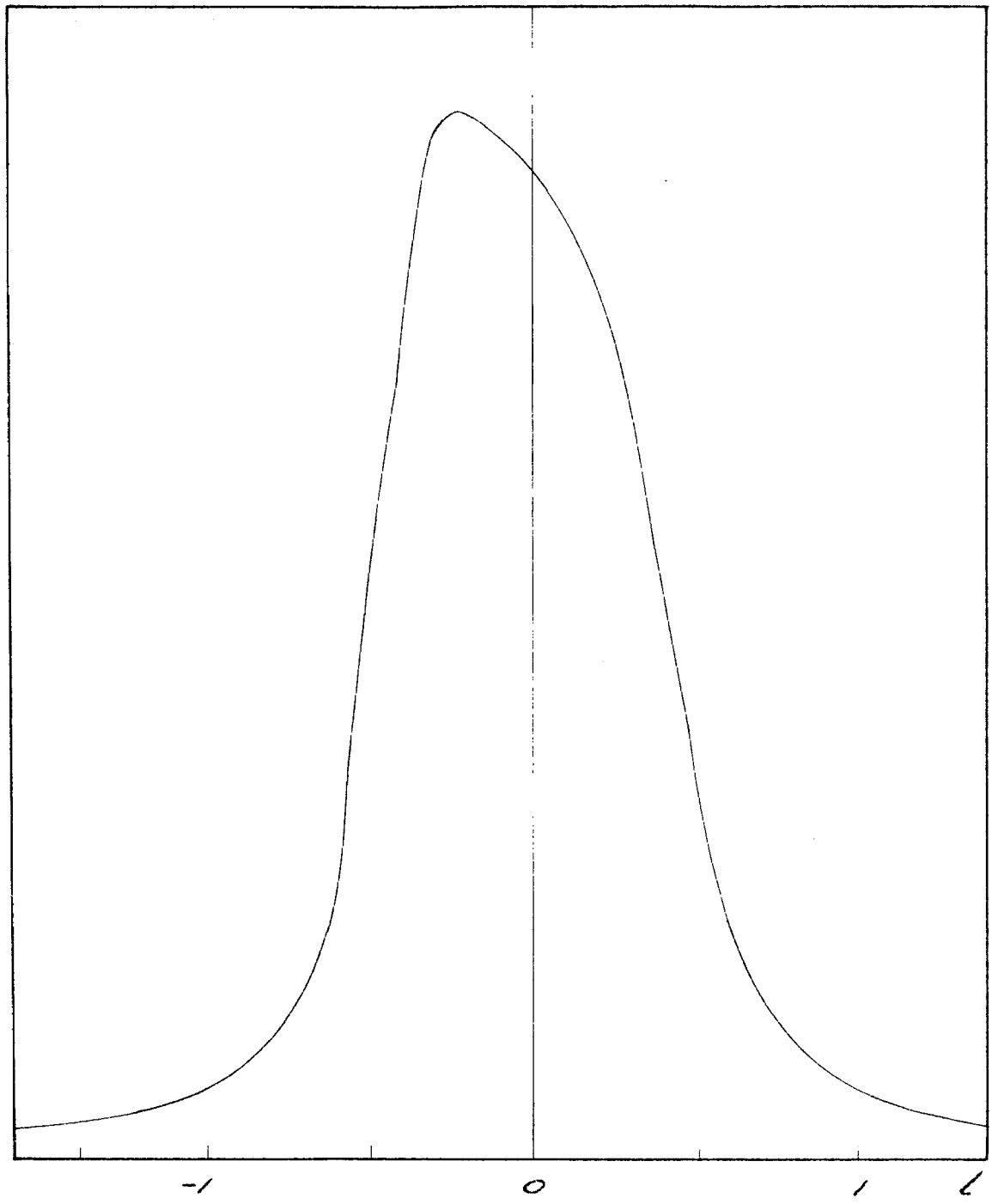

Figure 4. Diffraction pattern for calcite at a wavelength of 2.299 Å showing the effect of absorption.

polarization already mentioned (electric vector parallel to surface and perpendicular to plane of incidence) is referred to as σ-polarization. That type which has the electric vector lying in the plane of incidence is referred to as π-polarization. Completely unpolarized radiation can be resolved into these two components, each having an intensity equal to one half the total intensity of the unpolarized beam.

In the case of π-polarization it is evident that only the component of the incident electric vector which is perpendicular to the reflected ray will be effective in producing radiation in that direction. Therefore in the Darwin formula, F/Z must be replaced by (F/Z) cos 2 θ_0; in the Prins formula (D+iB)F/Z must be replaced by (D+iB)(F/Z) cos $2\theta_0$. The introduction of the cosine factor into the formulae causes a change in the height and width of the diffraction patterns; the π-curves are shorter and narrower than the corresponding σ-curves. The diffraction pattern for unpolarized radiation would be given by

$$I(\ell) = \tfrac{1}{2} I_{\sigma}(\ell) + \tfrac{1}{2} I_{\pi}(\ell) .$$

Parratt's work (17) includes calculations for both $I_{\sigma}(\ell)$ and $I_{\pi}(\ell)$ for longer wavelengths, while Allison (16) lists only $I_{\sigma}(\ell)$ values for the shorter wavelengths. Inasmuch as we are interested primarily in determining a correction for the asymmetry effect as a function of wavelength, the lack of published values of $I_{\pi}(\ell)$ for the shorter wavelengths requires us to base the corrections on $I_{\sigma}(\ell)$ alone.

B. The Two-Crystal Spectrometer

When a divergent X-ray beam which is also heterogeneous in wavelength is incident upon the surface of a crystal, the action of the crystal is similar in result (though for a different reason) to that of a prism placed in a beam of white light. The various wavelength components of the original X-ray beam, upon reflection from the crystal, are separated into bundles of nearly parallel rays, each bundle having a different direction but obeying the Bragg law $\lambda = 2d \sin \theta$.* Let the crystal be mounted on a pivot so that it can be rotated about an axis lying in its reflecting surface and normal to the plane of incidence of the X-rays. A second identical crystal may now be placed in the reflected beam with its axis of rotation lying in its surface and parallel to the axis of rotation of the first crystal. If the radiation of wavelength λ makes an angle θ with the reflecting planes of this second crystal such as to satisfy the Bragg law, $\lambda = 2d \sin \theta$, the beam will undergo a second reflection. Referring to the first crystal as crystal A and the second as crystal B, it is evident that B can have two positions with respect to A and still satisfy the conditions for reflection of radiation. Figure 5 shows the basic arrangement of the two-crystal spectrometer as well as the two possible positions of crystal B. The position in which the planes of crystal B are parallel to those of crystal A (or very nearly so) is called the parallel position; the other position, in which the planes of B still make the angle θ with the rays from A but with B turned through an angle of $(180+2\theta)$ degrees from the

---

* We shall consider only first order reflection, $n = 1$.

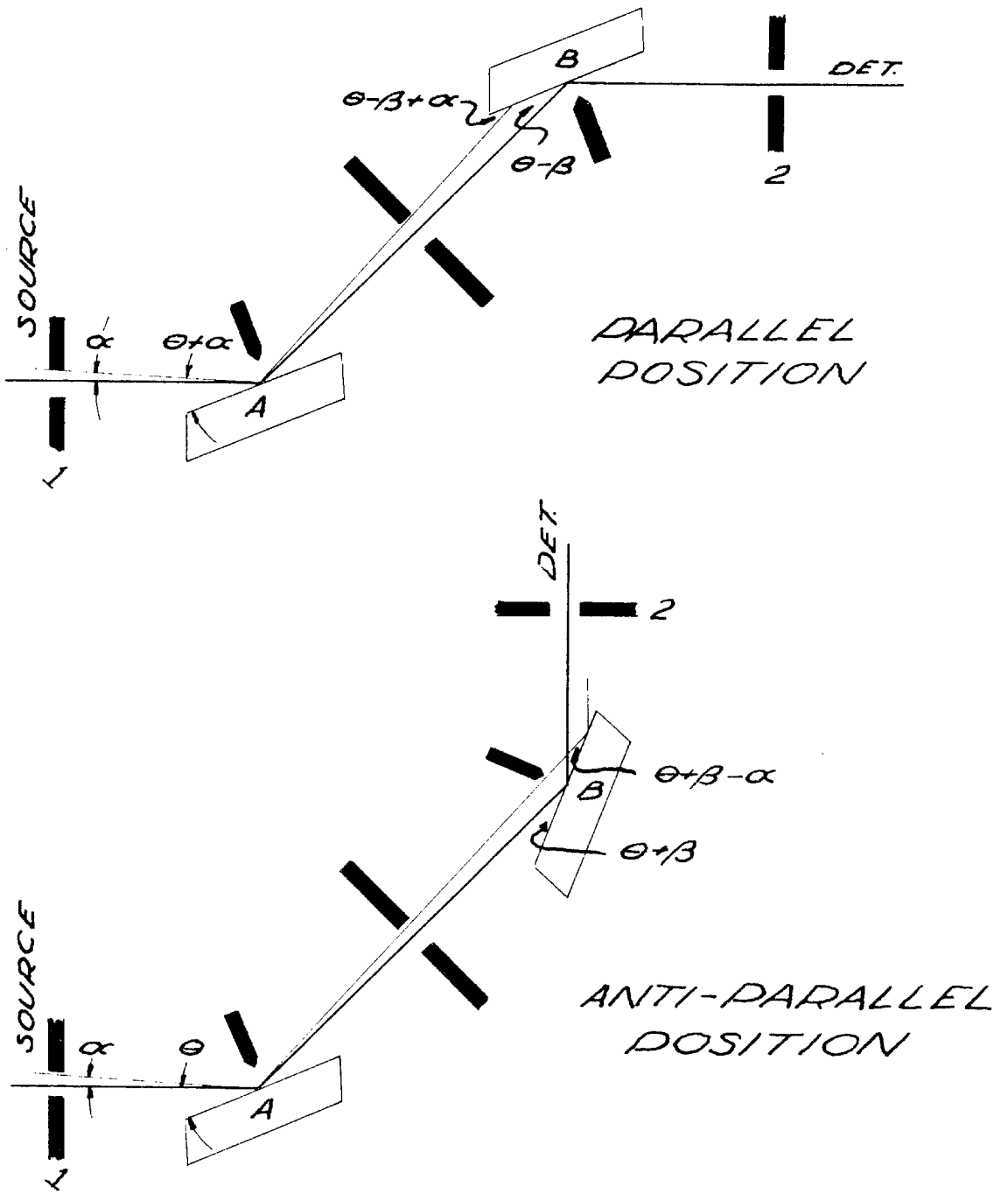

Figure 5. Basic arrangement of the two-crystal spectrometer showing crystal B in parallel and in anti-parallel positions. The angle α is the horizontal divergence. The central ray through the system makes an angle θ with crystal A.

parallel position, is called the anti-parallel position. It is evident that when the crystals are in this position, the Bragg law requires a ray to make the same angle (to a good approximation) with both crystal surfaces in order that it may undergo a double reflection. The various slit systems shown in Figure 5 serve only as rough stops and shields and do not affect the precision of the angle measurements.

As a preliminary to the theoretical discussion, a brief description of the experimental arrangements and mode of operation is not out of place. The crystals themselves are mounted in holders which can be rotated about a vertical axis. We will assume that the crystal A axis and the crystal B axis are parallel and that the crystal holders have been adjusted so that the reflecting planes are parallel to the axis of rotation. We will also assume that the source and detector are maintained at their proper orientation by a suitable mechanical system. In the application of the instrument to the precision measurement of Bragg angles, crystal A is adjusted so that the desired radiation is reflected approximately over the axis of crystal B; crystal B is then rotated to the parallel position, the condition of exact parallelism indicated by a maximum of intensity reaching the detector. Without changing the position of crystal A, crystal B and the detector are rotated around to the anti-parallel position and a survey made of the variation of intensity with rotation of crystal B about the spectral region of interest. It is clear that when the crystals are exactly parallel the Bragg law can be satisfied for a relatively large range of angles (determined by the rough slits used) and hence a wide band of wavelengths. The parallel position is there-

fore used as a reference point from which to measure angles and is of no value in itself for the determination of wavelengths.

The theory of the instrument is conveniently separated into two parts dealing individually with the parallel and anti-parallel positions. The general problem is the following: knowing the theoretical single crystal diffraction pattern and making certain assumptions about the spectral distribution of the source radiation, to account for the intensity curves which are observed experimentally. Certain additional information about the limitations in angular spread of the X-ray beam in the horizontal and vertical directions is also needed in order to account for small asymmetries in the anti-parallel curve.

To make the problem a bit more graphic, typical parallel and anti-parallel curves are shown in Figure 6. These curves are approximately those actually observed near a wavelength of 1 Angstrom, the anti-parallel curve being the profile of a typical L_{β_1} X-ray line. It can be pointed out again that the angular width of the parallel rocking curve is a function only of the angular width of the crystal diffraction patterns and does not depend upon the spectral distribution of the radiation coming from the source. The shape of the anti-parallel curve, however, is almost entirely a function of the manner in which the intensity of the source varies with wavelength, that is, the spectral distribution or line profile.

Compton and Allison* have presented the general theory of the instrument as it pertains to the two positions under discussion in sufficient detail so that this present treatment need be only an

---

* Op. cit., pp. 709-740.

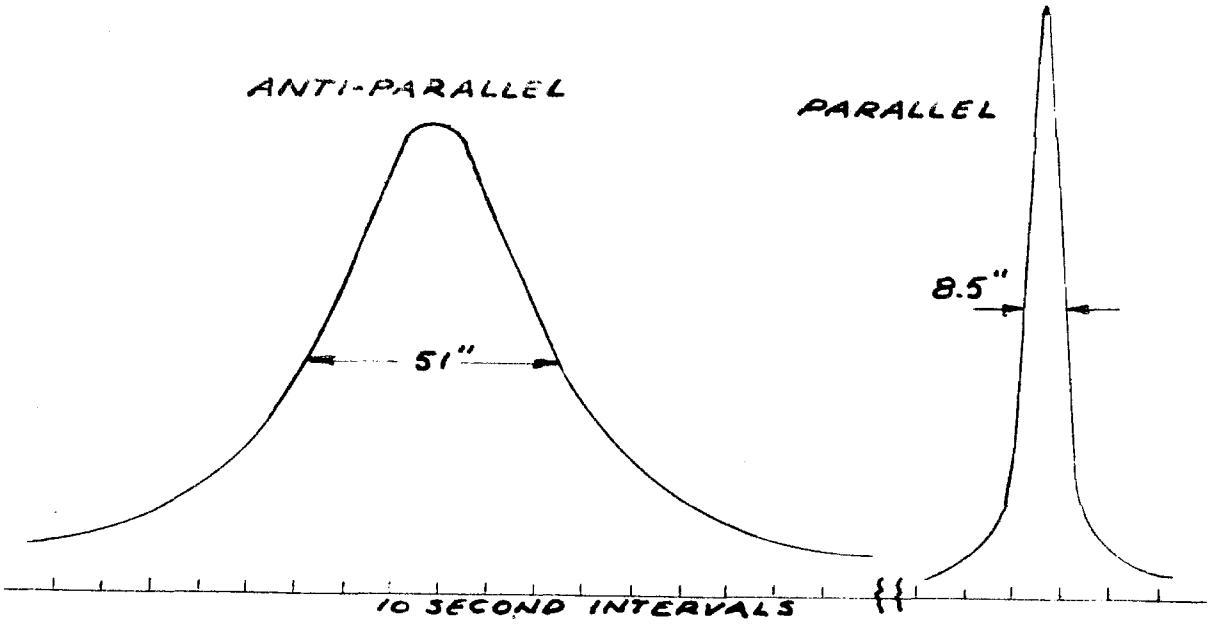

Figure 6. Typical parallel and anti-parallel curves (Bi $L\beta_1$) showing the relative widths.

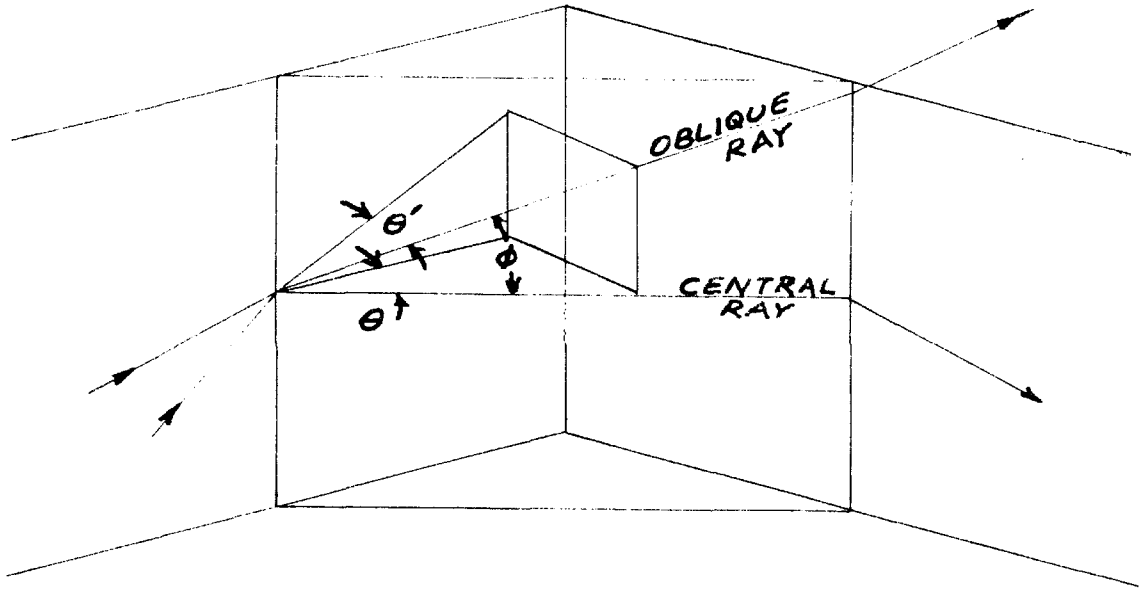

Figure 7. Diagram showing the dependence of the glancing angle on the vertical divergence.

application and/or extension of their theory. In accordance with their terminology and notation we make the following definitions:

Central Ray - The central ray is that ray which passes through the geometrical center of the horizontal and vertical slit systems,* intersecting the axes of rotation of both crystals.

Horizontal Divergence - The horizontal divergence of a ray is the angle α between that ray and its projection on a vertical plane containing the central ray. A positive value of α means that the ray makes a glancing angle with the surface of crystal A which is larger than that made by the central ray.

Vertical Divergence - The vertical divergence of a ray, measured by the angle ϕ, is the angle made by the ray with its projection on a horizontal plane (Figure 7) that is to say a plane perpendicular to the reflecting faces of both crystals. The angle of maximum vertical divergence is given by $\phi_m = (h_1+h_2)/2L$ where h_1 and h_2 are the heights of the vertical slits at the source and detector respectively and L is the distance between them.

Angular Positions of Crystal B - The rotation of crystal B is measured by the angle β relative to a reference position. The reference position for parallel operation is that position in which the surface of B is exactly parallel to that of A, the central ray thus making an angle θ with the surface of B. The reference position

---

* The horizontal slits are formed by pieces of lead with straight vertical edges which limit the angular spread of the beam in the horizontal plane. The vertical slits are formed by pieces of lead with their edges horizontal limiting the vertical spread of the beam. Taken together the system of slits forms two rectangular apertures, one at the source and one at the detector.

for anti-parallel operation is that position in which the central ray also makes an angle θ with the surface of B (Figure 5).

At this point it is necessary to calculate the small change in glancing angle, θ', of an oblique ray from that of the central ray. A typical ray with vertical divergence ϕ is shown in Figure 7 as it is reflected from one crystal to the other in the anti-parallel position. From the triangles shown it is evident that

$$\sin \theta' = \sin \theta \cos \phi \tag{3.5}$$

from which

$$\theta' \cong \theta - \frac{\phi^2}{2} \tan \theta$$

since ϕ is ordinarily a very small angle (of the order of 10^{-2} radians).

An arbitrary ray passing through the system may be characterized by the quantities (λ, α, ϕ), and the intensity reflected from crystal B for a given value of β for values of these quantities in the ranges $(\lambda, \lambda+d\lambda)$, $(\alpha, \alpha+d\alpha)$, $(\phi, \phi+d\phi)$ is shown by Compton and Allison to be given by

$$dP(\beta) = G(\alpha, \phi)\, J(\lambda-\lambda_0)\, I\left[\alpha - \tfrac{1}{2}\phi^2 \tan\theta - (\lambda-\lambda_0)(\partial\theta/\partial\lambda_0)\right]$$

$$I\left[\pm\alpha \mp \beta - \tfrac{1}{2}\phi^2 \tan\theta - (\lambda-\lambda_0)(\partial\theta/\partial\lambda_0)\right] d\alpha\, d\lambda\, d\phi\,. \tag{3.6}$$

In this expression $G(\alpha, \phi)$ is the functional dependence of the beam intensity on geometrical factors such as the slit openings and the distribution of intensity over the source. The function $J(\lambda - \lambda_0)$ gives the spectral distribution of intensity as emitted by the source with λ_0 being some reference wavelength such as the center of a

spectral line. The I functions are the theoretical single crystal diffraction patterns whose arguments are proportional to the variable ℓ defined in (3.2). The upper signs in the argument of the second I function refer to the parallel position, while the lower signs refer to the anti-parallel position. Crystal A is assumed to be set so that the central ray makes the glancing angle $\theta(\lambda_o)$, in which case the term $(\lambda - \lambda_o)\partial\theta/\partial\lambda$ appearing in (3.6) is merely the difference between $\theta(\lambda)$ and $\theta(\lambda_o)$.

DuMond (18) has invented a method of graphical analysis of the operation of the two-crystal spectrometer which may be used here to facilitate the interpretation of (3.6). The X-ray intensity reflected from the surface of a single crystal is regarded as a function of the independent variables λ and θ and can thus be represented as a surface above the λ, θ plane. To avoid three dimensional drawings, the height of the surface is to be thought of as represented by the transparency of the diagram; the regions where little or no intensity is reflected are regarded as opaque, and the regions of maximum intensity, as completely transparent. The transparent region is immediately adjacent to the locus on the diagram, $\lambda = 2d \sin\theta$, and the decrease in transparency on either side of this line is represented by the Prins single crystal diffraction pattern. The extension to one more crystal reflection is accomplished by superimposing another appropriate diagram for crystal B on top of the diagram for crystal A. In the case of the parallel position the crystal B diagram has its θ axis in the same direction as that for crystal A since an increase in θ_A produces a corresponding increase in θ_B (see Fig. 5). In the case of the anti-parallel position the crystal B diagram has its θ axis in the opposite direction to that for crystal A since an increase in θ_A produces a corresponding decrease in θ_B.

Figure 8 is an attempt to apply the graphical technique to (3.6)

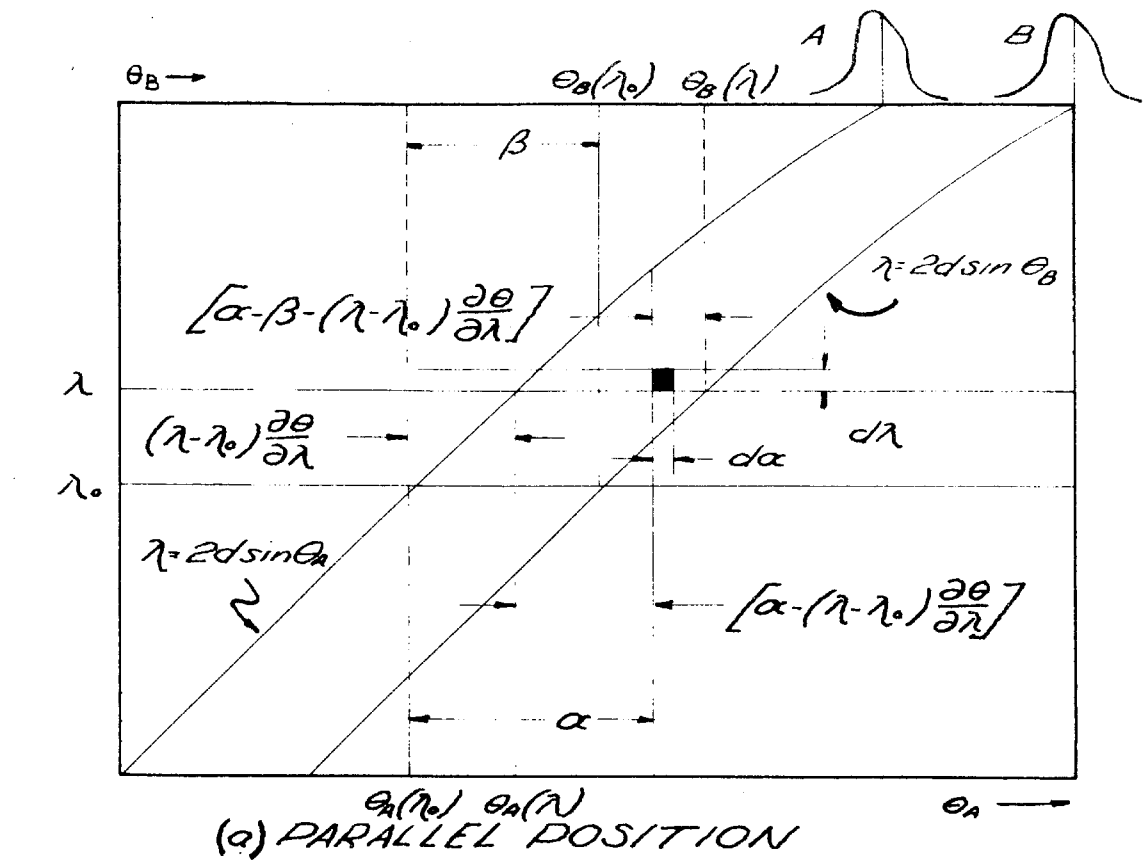

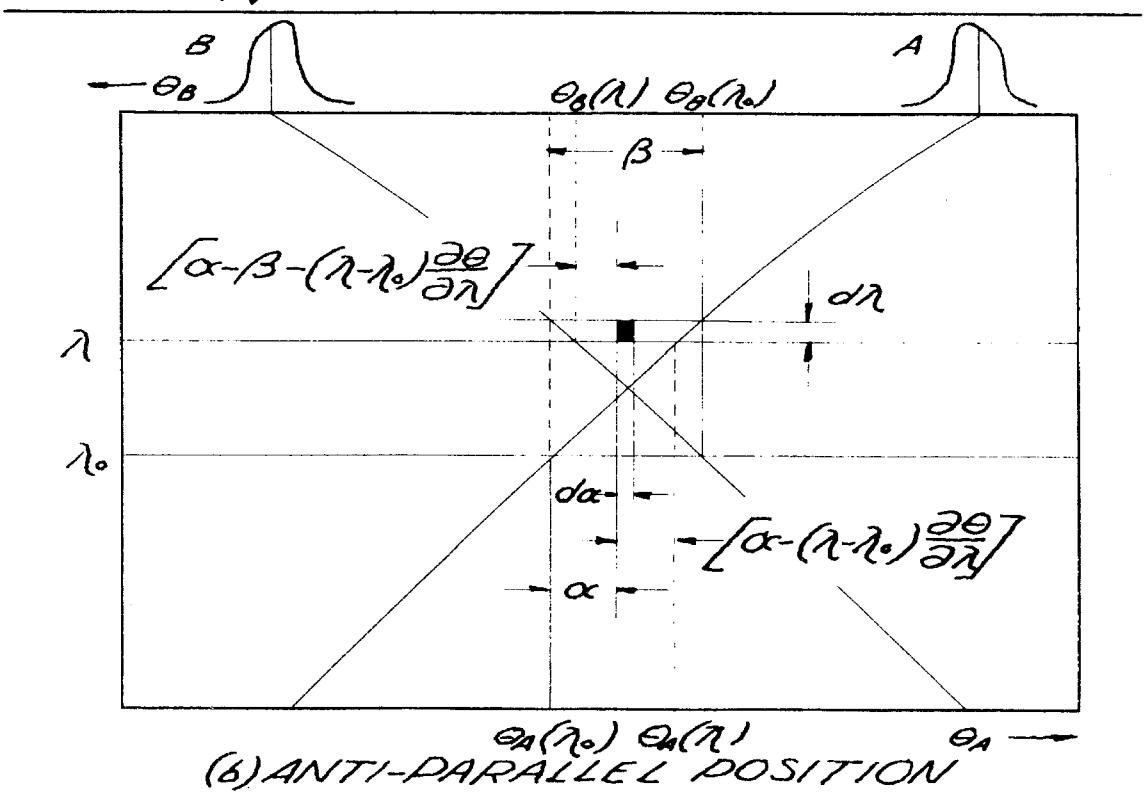

Figure 8. Transparency diagrams of the parallel and anti-parallel positions. The amount of transparency is represented by the curves at the top of each figure.

in order to show the relationships of the arguments of the I functions to each other. Unfortunately, the vertical divergence angle, ϕ, cannot be easily shown on this two dimensional representation; we will therefore assume that the diagrams represent the conditions as they exist in the horizontal plane only. Excluding the effect of the G and J functions, the effective transparency of the double crystal diagrams becomes

$$I\left[\alpha - (\lambda - \lambda_0)\frac{\partial\theta}{\partial\lambda}\right] I\left[\alpha - \beta - (\lambda - \lambda_0)\frac{\partial\theta}{\partial\lambda}\right] \qquad (3.7)$$

for the parallel position and

$$I\left[\alpha - (\lambda - \lambda_0)\frac{\partial\theta}{\partial\lambda}\right] I\left[-\alpha + \beta - (\lambda - \lambda_0)\frac{\partial\theta}{\partial\lambda}\right] \qquad (3.8)$$

for the anti-parallel position. The argument of I_B for the anti-parallel case must be the negative of that shown on the diagram because the abscissa of its diffraction pattern has been reversed in direction.

By means of several qualitative considerations based mainly on the fact that the arguments of the I functions must be close to zero in order to obtain appreciable intensity reflected from crystal B, Compton and Allison show that the expression in (3.6) may be simplified in the case of the parallel position to

$$P(\beta) = \int_{-\phi_m}^{\phi_m} \int_{\lambda_{min}}^{\lambda_{max}} \int_{-\alpha_m}^{+\alpha_m} dP(\beta) = K \int_{-\infty}^{\infty} I(\ell)\, I(\ell - \beta)\, d\ell \,. \qquad (3.9)$$

The constant K is proportional to the intensity of the incident beam and results from the integration of the functions G and J over ϕ and λ. The extension of the integration over α to infinite limits is permissible because the actual range of α is orders of magnitude

larger than the effective "width" of the I functions. The change of variable from α to ℓ results in a convenient scale change for computational purposes. The important conclusions based on (3.9) are that the shape of the parallel curve is independent of the slit openings and of the spectral distribution of intensity of the source. It is also clear that as long as the I function of crystal A is identical to that of crystal B the function $P(\beta)$ will have an axis of symmetry even though the I functions themselves are asymmetrical.

Allison (16) and Parratt (17) have evaluated the above integral for calcite over a wide range of wavelengths assuming the Prins diffraction pattern. The agreement between the theoretical curves and those obtained by experiment was very good indicating that the Prins formula is probably valid for predicting crystal properties. A point of comparison other than the general agreement of the shapes of the theoretical and experimental curves is the width of the curves at the half-maximum value. This quantity is obtained very easily experimentally; the values measured in the present work are shown in Figure 9 plotted against wavelength along with the curve predicted by the theory (obtained from Allison's paper). The disagreement suggests that the crystals used in this work differ slightly from perfect crystals, but the difference is small enough so that the theory may still be used to obtain semiquantitative predictions about the performance of the spectrometer.

Turning now to the problem of the anti-parallel position, we again use (3.6) with the lower signs. As is shown in Compton and Allison, the terms involving λ and ϕ appearing in the arguments of the I functions cannot be integrated out as in the case of the

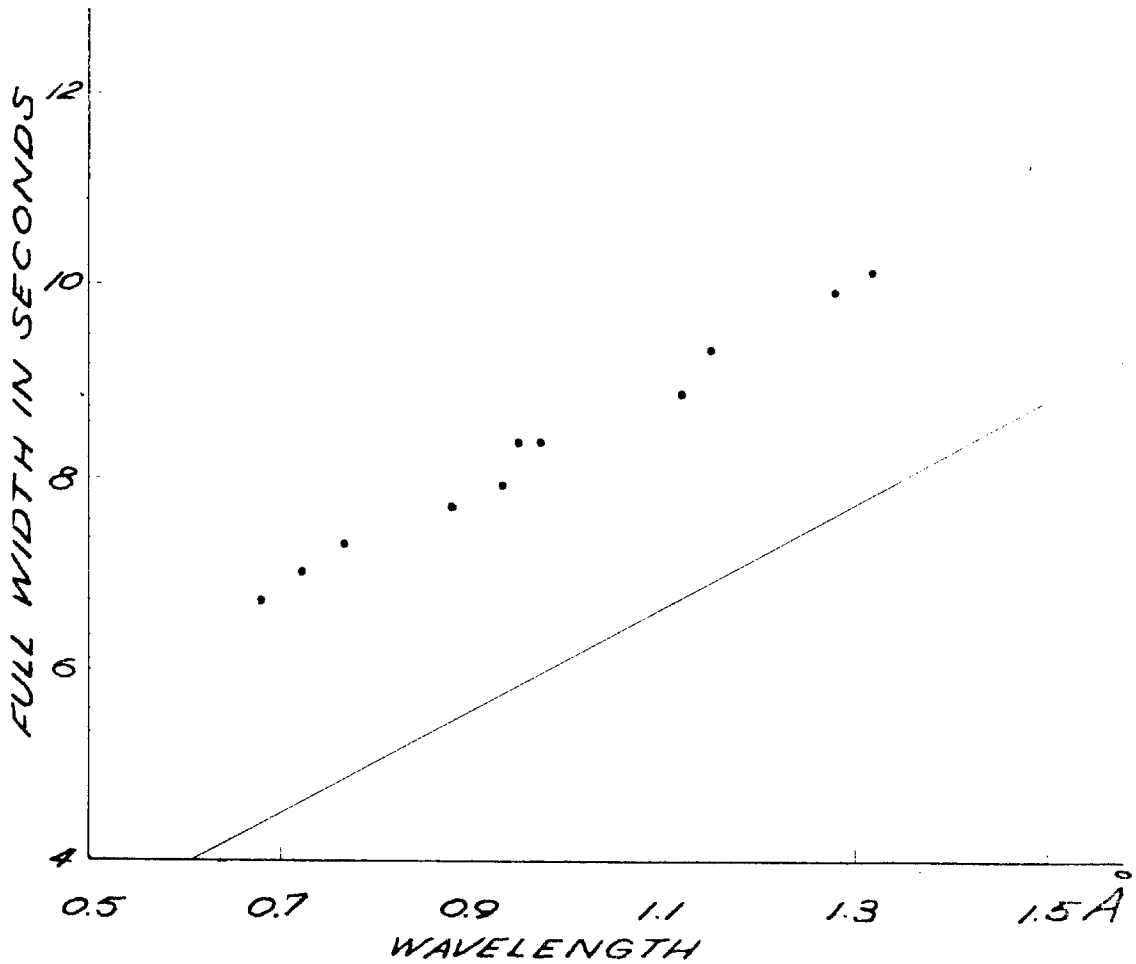

Figure 9. Measured widths of parallel rocking curves plotted against wavelength. The straight line is the theoretical width obtained from the Prins diffraction pattern formula.

parallel position. For this reason it becomes exceedingly difficult to perform computations with the expression as it stands because of the complicated nature of the I functions. By making certain approximations and assumptions, however, the complexity of the expression may be reduced to a point where it will be possible to obtain usable results in the form of curves representing the function $P(\beta)$.

Let us first assume that the incident radiation is completely monochromatic with $\lambda = \lambda_o$ and that the vertical slits are made narrow enough so that $(\frac{1}{2})\phi_m^2 \tan\theta$ is negligibly small. The expression for $P(\beta)$ becomes

$$P_1(\beta) = K_1 \int_{-\infty}^{\infty} I(\ell)\, I(\beta - \ell)\, d\ell \qquad (3.10)$$

where again the integration over α has been extended to infinite limits and the scale has been changed by employing ℓ as the variable; K_1 is merely a constant of proportionality, and the subscript on the P serves to distinguish this monochromatic case from the more general one. Comparing this expression to (3.9) it is evident that if the I functions are symmetrical about $\ell = 0$, that is, $I(\ell) = I(-\ell)$, then (3.9) and (3.10) yield identical curves (except possibly for amplitude). However since the theoretical diffraction patterns do not have an axis of symmetry for the case of non-negligible crystal absorption it will be necessary to investigate the effect of this asymmetry on the shape of the curve representing $P_1(\beta)$ as given by (3.10). Allison (16) has evaluated $P_1(\beta)$ by numerical integration using only the σ-polarization component of the I function for a wavelength of 1.537 Å. His results show that the main effect of the asymmetry is to shift the center of

gravity of the resultant curve toward negative values of β (smaller Bragg angle). This means that if the spectrometer could be used to explore such a monochromatic spectral line the curve of intensity vs. crystal B setting (angle β) would have the shape of $P_1(\beta)$ and would be displaced toward smaller Bragg angles. The effect may be seen qualitatively by noting that the top portion of the quasi-quadrilateral region of intersection of the two curves of Figure 8b is more transparent than the bottom. Allison's results also show that the asymmetry of $P_1(\beta)$ at this wavelength is not pronounced; Figure 10 shows a graph of $P_1(\beta)$ along with a plot of a witch* having the same half-width. Although it is clear that the witch is a poor approximation to the curve for values of β larger than the half-width, the approximate symmetry of $P_1(\beta)$ may be seen by comparison to the witch.

On the basis of the foregoing facts we will make the following simplifying assumption: In the limiting case of zero vertical divergence we will assume that the function $P_1(\beta)$ may be approximated with adequate precision by a witch whose axis of symmetry is at slightly negative values of β. The main justification for such an assumption is that it greatly reduces the complexity of the further analysis of the anti-parallel curves and the corrections which must be applied to them. We may represent the curve, therefore, by the following formula:

$$P_1(\beta) = \frac{A}{1 + \left(\frac{\beta + \epsilon}{b}\right)^2} = \int_{-\infty}^{\infty} P_1(\beta - x)\, \delta(x)\, dx \quad (3.11)$$

---

* The witch (sometimes known as the Cauchy distribution) has the formula $y = (1 + x^2/a^2)^{-1}$ with a being the half-width at half maximum.

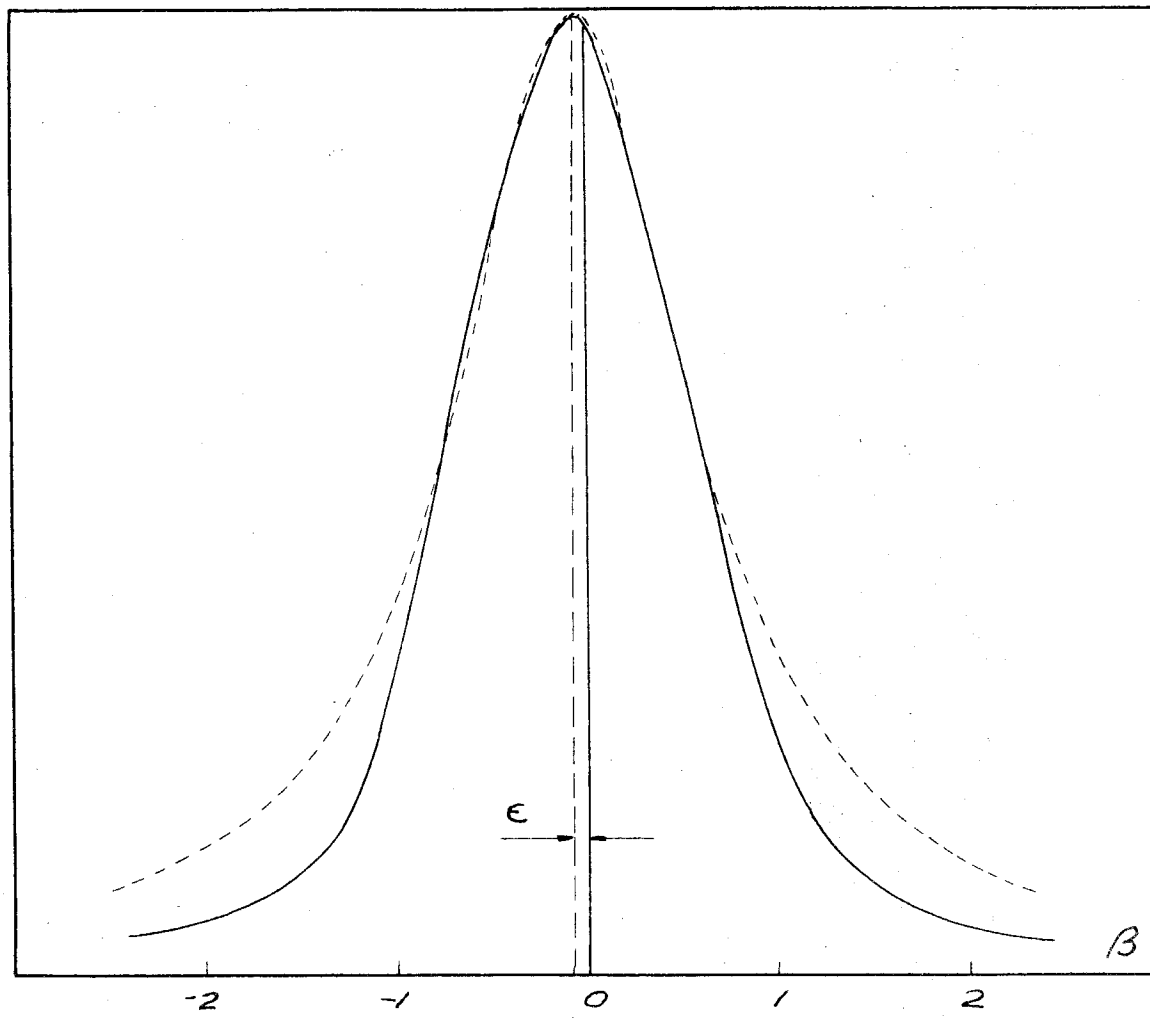

Figure 10. Anti-parallel "monochromatic" curve as obtained by Allison for 1.537 Å. The dashed curve is a witch having the same half-width. The axis of symmetry of the witch is shown at $\beta = -\epsilon$.

where A is the amplitude of the curve, b is the half-width at half maximum, and $\beta = -\epsilon$ is the axis of symmetry. The integral is included to show that $P_1(\beta)$ may be regarded as the fold of itself into a Dirac delta-function (which represents the monochromatic line); $P_1(\beta-x)$ is the window curve of the spectrometer and corresponds to the transparency of the crossover region in Figure 8b with the variable of integration x being measured along the λ axis.

In order properly to extend the method of the fold integral to a spectral distribution $J(\lambda - \lambda_0)$ we must know the relationship of β and λ so that a transformation to a common variable may be made. The required relation is shown by Compton and Allison to be given by the equation

$$\beta = \tfrac{1}{2} D \lambda_0 \phi^2 + D(\lambda - \lambda_0) \qquad (3.12)$$

where $D = 2\,\partial\theta(\lambda_0)/\partial\lambda_0$ for the anti-parallel position and $D = 0$ for the parallel position. The dispersion of the instrument in the anti-parallel position when crystal B alone is rotated is therefore

$$\frac{d\beta}{d\lambda} = D = \frac{1}{d\,\cos\,\theta(\lambda_0)} \qquad (3.13)$$

where we have evaluated $\partial\theta(\lambda_0)/\partial\lambda_0$ from the Bragg law. The quantity D may be regarded as a constant over rather wide ranges of θ; for example, at a Bragg angle of 15°, D = 70.5 sec/XU while $dD/d\theta = 0.006$ sec/XU/min. Under the assumption of zero vertical divergence it is evident that there exists a simple proportionality between β and $\lambda - \lambda_0$ and changes from one variable to the other involve only the scale factor D.

In terms of wavelength (3.11) is therefore written

$$P_1(\lambda - \lambda_0) = \frac{A}{1 + \left(\frac{\lambda - \lambda_0 + \epsilon/D}{b/D}\right)^2} = \int_{-\infty}^{\infty} P_1(\lambda - \lambda')\,\delta(\lambda' - \lambda_0)\,d\lambda', \tag{3.14}$$

and the extension to a distribution of wavelengths simply involves replacing the delta-function with the distribution function $J(\lambda' - \lambda_0)$. Now since we are primarily interested in X-ray spectral lines which several investigators (19) have shown to have the shape of a witch, we may conclude immediately that the output curve of the spectrometer is also a witch having a width equal to the sum of the widths of the two original witches.* The axis of symmetry of the resultant witch is, however, no longer at $\lambda = \lambda_0$, but is displaced toward shorter wavelengths by the amount ϵ/D. The equation representing the spectrometer output is therefore

$$J'(\lambda - \lambda_0) = \frac{C}{1 + \left(\frac{\lambda - \lambda_0 + \epsilon/D}{a}\right)^2} = \int_{-\infty}^{\infty} \frac{A}{1+\left(\frac{\lambda - \lambda_0 + \epsilon/D}{b/D}\right)^2} \frac{B}{1+\left(\frac{\lambda' - \lambda_0}{w}\right)^2}\, d\lambda' \tag{3.15}$$

where $a = b/D + w$, with w being the half-width of the original X-ray line.

We have reached the important conclusion that under the assumptions of zero vertical divergence and a symmetrical window curve, the observed spectral line has a slightly greater width and a slightly lower wavelength at its axis of symmetry than the original spectral line. Corrections for these aberrations are straightforward provided ϵ and b are known. In making the correction for the position

---

* We have used here the result of a well-known theorem on the fold of two witches. For a proof of the theorem see, for example, W. J. West, Thesis, California Institute of Technology, 1948.

of the center of the original line, one may either add the quantity $\epsilon/2$ to the observed Bragg angle or add ϵ/D to the wavelength calculated from this angle. It is more convenient, however, to obtain the magnitude of ϵ in terms of angular measure in which case the correction of the Bragg angle rather than the wavelength is easier. In Part IV a method of obtaining approximate values of ϵ will be given along with an extensive analysis of the effect of vertical divergence.

PART IV

ANALYSIS OF THE EFFECT OF VERTICAL DIVERGENCE AND OTHER CORRECTIONS

The experimental approach to the problem of precision X-ray spectroscopy involves making a wise choice of each of the three major pieces of equipment that enter into the experiment. These items are the source, the spectrometer, and the detecting system. Some of the factors that must be considered are (a) the source's intensity, stability, and versatility; (b) the spectrometer's resolution and luminosity; (c) the detector's sensitivity and spectral response characteristics. There is usually no problem associated with the choice of a spectrometer; one uses the best available which in the present work was a two-crystal spectrometer. With source and detector, however, a certain latitude of choice exists; and since the characteristics of each have a definite relationship to the calculations of this Part we shall digress briefly to discuss the advantages and disadvantages of various types.

As far as a source is concerned, one could use a conventional X-ray tube whose target is the element in question, or a demountable tube with interchangeable targets, or a fluorescent source irradiated with X-rays from a conventional tube. For intensity and stability, the commercial sealed-off tube is the logical choice, but the number of usable target elements in the high atomic number range is quite limited. The range of target elements can be extended somewhat by using a continuously pumped, demountable target tube, but its use introduces the further complications of a vacuum system and instability of operation. A compromise between stability and wide range of target

materials lies in the fluorescent source, but the intensity of this type of source is orders of magnitude lower than that obtained from an X-ray tube. Because of the success of Rogosa and Schwartz (20) who used fluorescent radiation in an experiment similar in many respects to the present one, it was decided to use this type of source and to compensate partly for the lower intensity by using as broad a source as possible.

The choice of detector is not necessarily contingent upon the selection of the source; but in the case of a broad source it is necessary to have a detector which has rather uniform response over sufficient lateral extent so that full advantage is taken of the width of the source. Ordinary end-window Geiger counters are usually satisfactory for this purpose providing the area of the window accomodates the entire X-ray beam. However, the sensitivity of the counter is not uniform over the area presented to the beam mainly because of the necessity of having an insulating bead over the end of the central electrode. For the purposes of calculation it is very desirable to have the characteristic of uniform lateral sensitivity in the detector; hence the Geiger counter was ruled out, and a thin flat NaI crystal was used instead. A more detailed description of both source and detector will be given later, but for the purposes of this discussion it is necessary to point out that the extended source which is necessary for sufficient intensity introduces the complication of large vertical divergence. In order to calculate the effect of this divergence on the observed position and shape of an X-ray line a knowledge of the intensity distribution over the source and the response characteristics of the detector is required.

A. The Geometrical Window Profile of the Spectrometer

In this discussion we shall assume that since vertical divergence is known to produce only a small effect, it may be considered to give rise to a geometrical window for the spectrometer which introduces small aberrations into the spectrometer output. We shall assume further that the magnitude of these aberrations can be obtained by evaluating the product integral of the geometrical window curve and the spectrometer output curve for zero divergence.

We shall begin, therefore, by developing a suitable expression for the function $G(\alpha, \phi)$ defined on page 34. We note at the outset that the extent of horizontal divergence (represented by the angle α_m) has a negligible effect on the output curve of the spectrometer. Allison (16) has shown this to be true in the case of a uniformly intense source, so to avoid unnecessary complications we shall assume that the source used in this experiment has a uniform intensity distribution in the horizontal direction. (Actual pinhole photographs of the source justify this assumption but indicate a slight variation of intensity in the vertical direction.) We may therefore omit the angle α from the argument of G and confine our attention entirely to the behavior of $G(\phi)$ in the vertical plane.

We shall assume that the source, as seen by the spectrometer, may be represented by a vertical plane perpendicular to the central ray, each point of which emits radiation isotropically with an intensity $I(z)$ where z is measured in the vertical direction from some horizontal reference line in the plane. For convenience we shall choose this reference line to pass through the intersection of the central ray and the source plane. Figure 11 shows a schematic

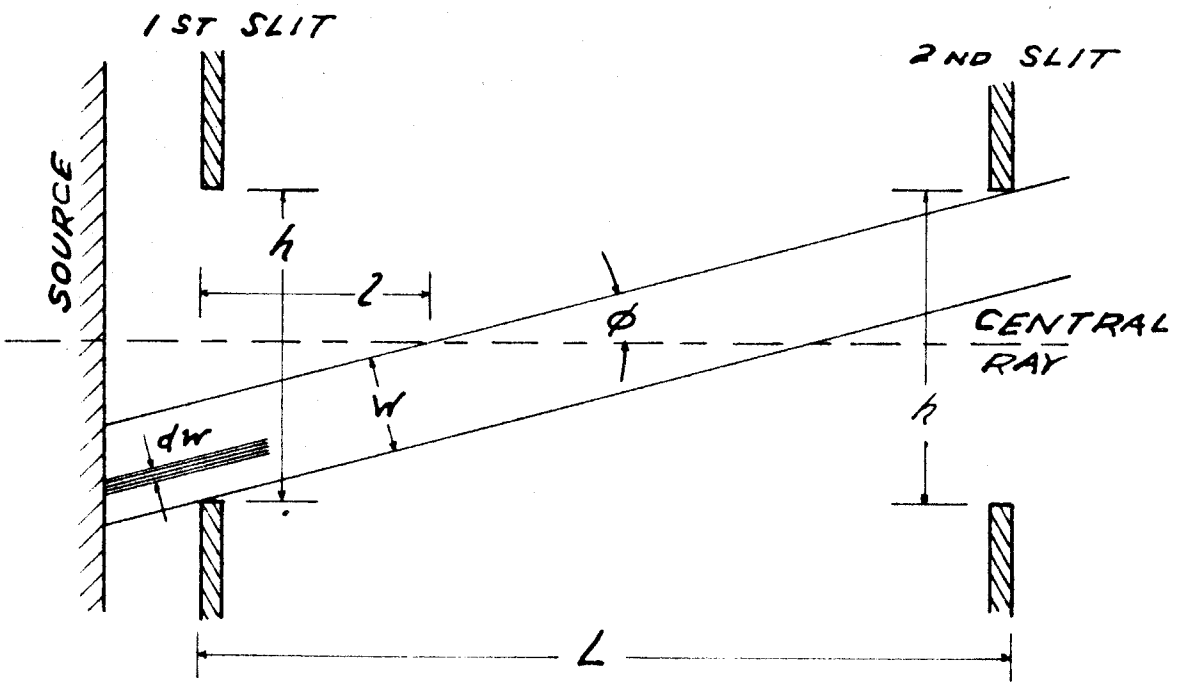

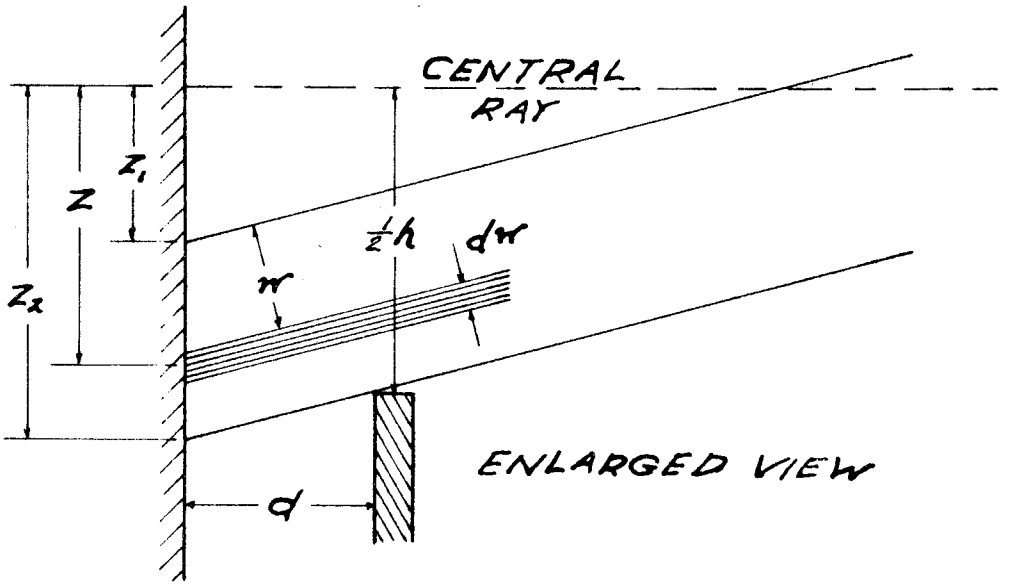

Figure 11. Schematic diagram of source and vertical slit system.

diagram of the source and vertical slit system for the specific case of equal source and detector slits and also serves to define certain quantities which are used in the calculations.

If we let $P(\phi)$ represent the power in the beam of width W which passes through both slits in the direction ϕ and interpret $G(\phi)$ as the ratio of $P(\phi)$ to the maximum power that can get through, we may then write

$$P(\phi) = G(\phi)P_{max} = \int_{w=0}^{w=W} I(z)dw \cong \int_{z_1}^{z_2} I(z)dz \qquad (4.1)$$

where the approximation is valid because of the smallness of ϕ. We must now express the limits of the integral in terms of ϕ, and from the diagram it follows that

$$z_1 = (\ell + d)\phi, \quad z_2 = \frac{h}{2} + \phi d, \quad \frac{h}{2} = (L - \ell)\phi ,$$

and therefore

$$z_2 - z_1 = L(\frac{h}{L} - \phi) = L(\phi_m - \phi) . \qquad (4.2)$$

For a point source at $z = 0$, $I(z) = P_{max}\delta(z)$ and therefore $G(\phi) = 1$. The angular extent of $G(\phi)$ for this simple case cannot be ascertained from (4.1) but is clearly limited by the angle which the second slit subtends at the source. For the more interesting case of a uniform source where $I(z)$ is a constant, (4.1) and (4.2) yield

$$G(\phi) = (1 - \left|\frac{\phi}{\phi_m}\right|) \qquad (4.3)$$

where the absolute value signs are put in to include both plus and minus values of ϕ. Actual measurements indicated that the source used in this experiment was not uniform but decreased slightly in intensity

for both plus and minus values of z. The data suggested a parabolic function for I(z) symmetrical about z = 0; the G function was calculated for such a distribution, but it turned out to deviate from $G(\phi)$ for a uniform source by such a small amount that the extra labor involved in further analysis did not seem worthwhile. We will therefore let (4.3) represent the spectrometer window due to slit and uniform source geometry. It is obvious that the assumption of a uniformly sensitive detector greatly simplifies matters; a non-uniform detector sensitivity could be included, of course, by multiplying the appropriate response function into the integrand of (4.1).

We now wish to express the function $G(\phi)$ in terms of λ since we eventually must multiply it into the spectrometer output curve which is expressed as a function of λ. The required relationship between ϕ and λ follows from writing the Bragg law for an oblique ray with vertical divergence angle ϕ, namely,

$$\lambda' = 2\, d \sin\theta'$$

where the relation between ϕ and θ' is given by (3.5) which is repeated here for convenience:

$$\sin\theta' = \sin\theta \cos\phi \quad . \tag{3.5}$$

From the above two equations and the Bragg law for the central ray we obtain

$$\frac{\lambda - \lambda'}{\lambda} = \frac{\sin\theta - \sin\theta'}{\sin\theta} = 1 - \cos\phi \cong \frac{\phi^2}{2} \tag{4.4}$$

from which we may write

$$\lambda' = \lambda\left(1 - \frac{\phi^2}{2}\right) \tag{4.5}$$

$$\phi = \sqrt{\frac{2(\lambda - \lambda')}{\lambda}} \tag{4.6}$$

$$d\lambda' = -\sqrt{2\lambda(\lambda - \lambda')}\; d\phi \quad . \tag{4.7}$$

The physical interpretation of (4.4) is that for a given setting of crystal B, a ray which passes through the system with vertical divergence ϕ must have a slightly smaller wavelength than that of the central ray. Thus the spectrometer has in addition to its wavelength response curve in the horizontal plane, a wavelength response curve in the vertical plane which cuts off at a maximum wavelength of λ. The shape of this curve is given by $G(\lambda')$, and from conservation considerations we may write

$$G(\lambda')d\lambda' = -G(\phi)d\phi \tag{4.8}$$

or, from (4.7),

$$G(\lambda') = G(\phi)\left[2\lambda(\lambda - \lambda')\right]^{-\frac{1}{2}} \quad . \tag{4.9}$$

For a point source (4.9) becomes

$$\begin{aligned} G(\lambda') &= \left[2\lambda(\lambda - \lambda')\right]^{-\frac{1}{2}}, \quad \lambda_m \leq \lambda' \leq \lambda \\ G(\lambda') &= 0 \;, \qquad \lambda' < \lambda_m \;; \quad \lambda' > \lambda \end{aligned} \tag{4.10}$$

where

$$\lambda_m = \lambda\left(\frac{1 - \phi_m^2}{2}\right) .^{*} \tag{4.11}$$

For a uniform source, combining (4.3), (4.6) and (4.9), we obtain

$$\begin{aligned} G(\lambda') &= \frac{1}{\sqrt{2\lambda(\lambda - \lambda')}} - \frac{1}{\lambda\phi_m} \\ G(\lambda') &= 0, \quad \lambda' < \lambda_m; \quad \lambda' > \lambda \;. \end{aligned} \tag{4.12}$$

---

* To avoid using another subscript we have used the letter m in two senses thus maintaining the association between the maximum vertical divergence angle ϕ_m and the corresponding minimum wavelength λ_m.

We have not expressed ϕ_m in terms of λ_m since ϕ_m is already a constant. Curves showing $G(\phi)$ and $G(\lambda')$ for both point and uniform sources are presented in Figure 12. It will be noted that $G(\lambda')$ has an infinite ordinate at $\lambda' = \lambda$; the area under the curve is, however, finite.

B. The Effect of the Geometrical Window on a Spectral Line

We have seen that under the assumption of zero vertical divergence the intensity output of the spectrometer as a function of wavelength for an X-ray spectral line input is

$$J'(\lambda - \lambda_o) = \frac{C}{1 + \left(\frac{\lambda - \lambda_o + \epsilon/D}{a}\right)^2} \quad . \tag{3.15}$$

Instead of using λ_o as a reference wavelength, we shall find it convenient to use the wavelength of the axis of symmetry of the observed line (with zero divergence). The center of this observed line, which will henceforth be referred to as the unmodified line, is at the wavelength

$$\lambda_c = \lambda_o - \epsilon/D \tag{4.13}$$

In accordance with our initial assumption that the spectrometer output in general is the product integral of the geometrical window profile and the profile of the unmodified line we may write

$$F(\lambda, \lambda_m) = \int_{\lambda_m}^{\lambda} G(\lambda')J'(\lambda' - \lambda_c)d\lambda' \quad . \tag{4.14}$$

We have evaluated $G(\lambda')$ for both a point source and a uniform source, but since the latter is more interesting we shall proceed no further with the point source problem except to mention that it can be solved

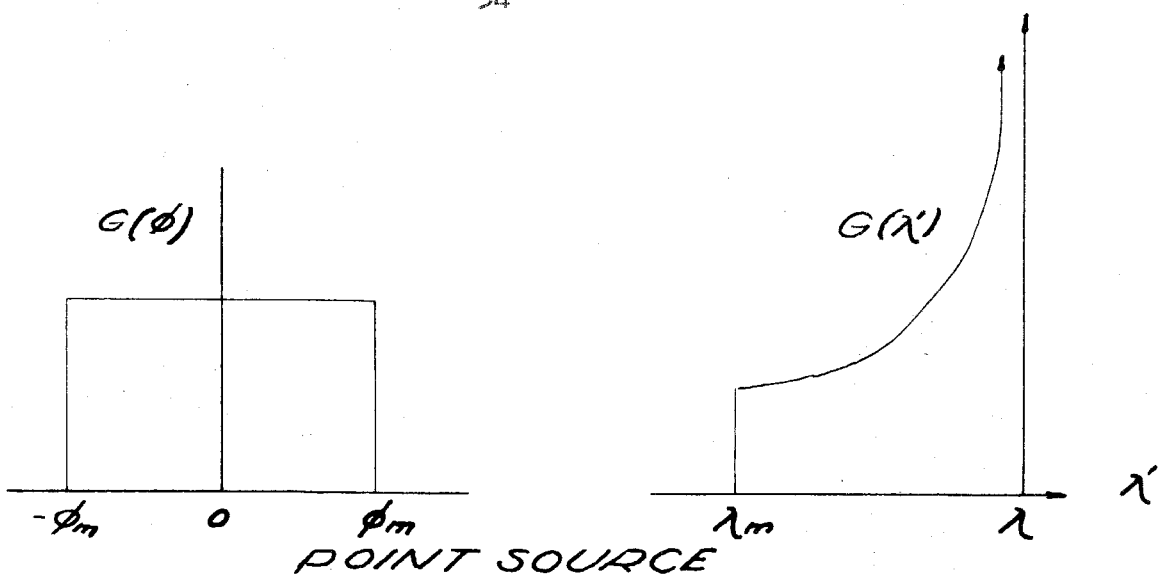

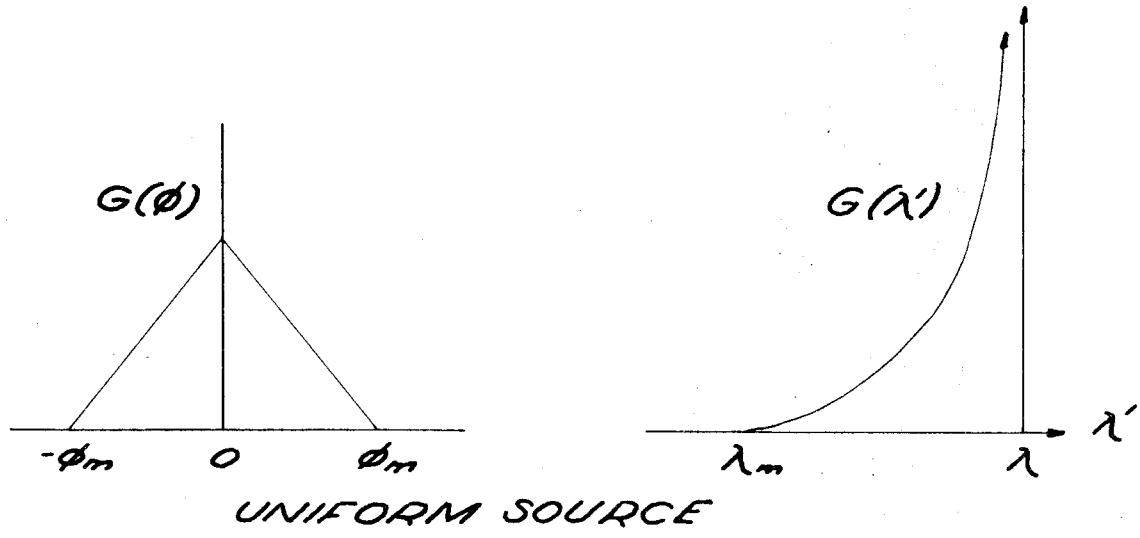

Figure 12. Geometrical spectrometer window curves for point and uniform sources.

as a special case of the uniform source problem.

Substituting from (4.12) and (3.15) into (4.14) we obtain

$$F(\lambda,\lambda_m) = \int_{\lambda_m}^{\lambda} \frac{Cd\,\lambda'}{\sqrt{2\lambda(\lambda-\lambda')}\left[1+\left(\frac{\lambda'-\lambda_c}{a}\right)^2\right]} - \frac{1}{\lambda\phi_m}\int_{\lambda_m}^{\lambda} \frac{Cd\,\lambda'}{1+\left(\frac{\lambda'-\lambda_c}{a}\right)^2}, \quad (4.15)$$

and if we make the substitutions

$$x = \frac{\lambda'-\lambda_c}{a}, \quad t = \frac{\lambda-\lambda_c}{a}, \quad k = \frac{\lambda-\lambda_m}{a} = \frac{\lambda\phi_m^2}{2a} \quad (4.16)$$

the expression for $F(\lambda, \lambda_m)$ simplifies to

$$F(t,k) = \frac{C\phi_m}{2\sqrt{k}} \int_{t-k}^{t} \frac{dx}{\sqrt{t-x}\ (1+x^2)} - \frac{C\phi_m}{2k}\int_{t-k}^{t} \frac{dx}{1+x^2} \quad (4.17)$$

The physical interpretation of the quantities x, t, k follows easily from (4.16). The half-width a of the unmodified line is chosen as a unit of wavelength, and deviations from the wavelength of the center of the unmodified line are measured in terms of a. The variable t is the difference expressed in units of a between the spectrometer setting λ and the reference wavelength λ_c. The parameter k is the ratio of the wavelength width of the geometrical window to the half-width of the unmodified line. The elimination of the common factor $C\phi_m/2$ from (4.17) affects only the amplitude of F(t,k) and does not change its general appearance. In the subsequent treatment we shall assume that this factor is dropped.

The second integral in (4.17) is elementary, but the first one is not usually encountered in the tables and could be done by partial fractions. Fortunately, however, the extensive tables of Gröbner and Hofreiter (21) list an integral (231-23a) which is similar in form,

so we may consider the integration in (4.17) as accomplished. The algebraic details giving rise to the solution as well as the expression for F(t,k) itself are complex enough to be uninteresting and have been relegated to Appendix A.

Actual calculation of a curve of F(t,k) involves knowing the appropriate value of k which is really not a constant since it depends on λ, the spectrometer setting, which changes as a spectral line is explored. However, we make very little error (less than $\frac{1}{2}\%$) by assigning to k its average value, namely,

$$k = \frac{\lambda_c \phi_m^2}{2a} \tag{4.18}$$

We still are unable to evaluate k with any degree of precision because the value of a, the half-width of the unmodified line, is unknown and cannot be measured directly. It would be possible to calculate a if b, the crystal window width, and w, the original spectral line width were known. Even if w were known accurately (rather improbable) the value of b for a given spectrometer is largely a matter of speculation. It is theoretically possible to solve for the values of t at the half maximum points of F(t,k) thus obtaining the ratio of the modified width to the unmodified width, but since F(t,k) contains t in the arguments of several transcendental functions, this method is a practical impossibility.

Instead of evaluating F(t,k) for a particular spectral line, we may estimate the range of k likely to be covered in the experiment and then plot curves of F(t,k) for a number of different values of k. By this graphical technique it is possible to obtain a fairly complete knowledge of the effect of vertical divergence.

Because of the complexity of the expression for F(t,k), ordinary hand computation of just a few points on one curve involves many hours of desk calculator work. It therefore was decided to have this series of calculations done by the electronic digital computer method. Eleven different curves were computed for values of k ranging from 0.1 to 1.5, each curve consisting of 65 points in the range $-5 \leq t \leq 5$. It is of some interest to note that these 715 separate calculations, which took about one hour of machine time, would require an estimated three and one-half months using a desk calculator.

The eleven graphs of F(t,k) were plotted and the following measurements taken off the graphs: (1) the maximum and half maximum values; (2) the values of t corresponding to the half maximum value (t_1, a negative number and t_2, a positive number). From the two values of t obtained above we can compute two more quantities of interest:

$$\delta = \frac{t_1+t_2}{2}$$
$$\tau = \frac{t_2-t_1}{2} \qquad (4.19)$$

where δ represents the deviation of the midpoint of the line joining the half maximum values of the curve from the line t = 0 and hence is a measure of the shift in wavelength of the observed spectral line, while τ is the half-width at half maximum of the curve F(t,k). The quantities τ and δ are shown on Figure 13 which is a graph of F(t,k) for k = 1; shown also is the original witch so that the effect of vertical divergence on the width and position of the unmodified line can be easily seen. The quantity τ-1 is the relative increase in half-width since the half-width of the original line is 1. Graphs of δ and $100(\tau-1)$ are shown in Figure 14 as functions of the

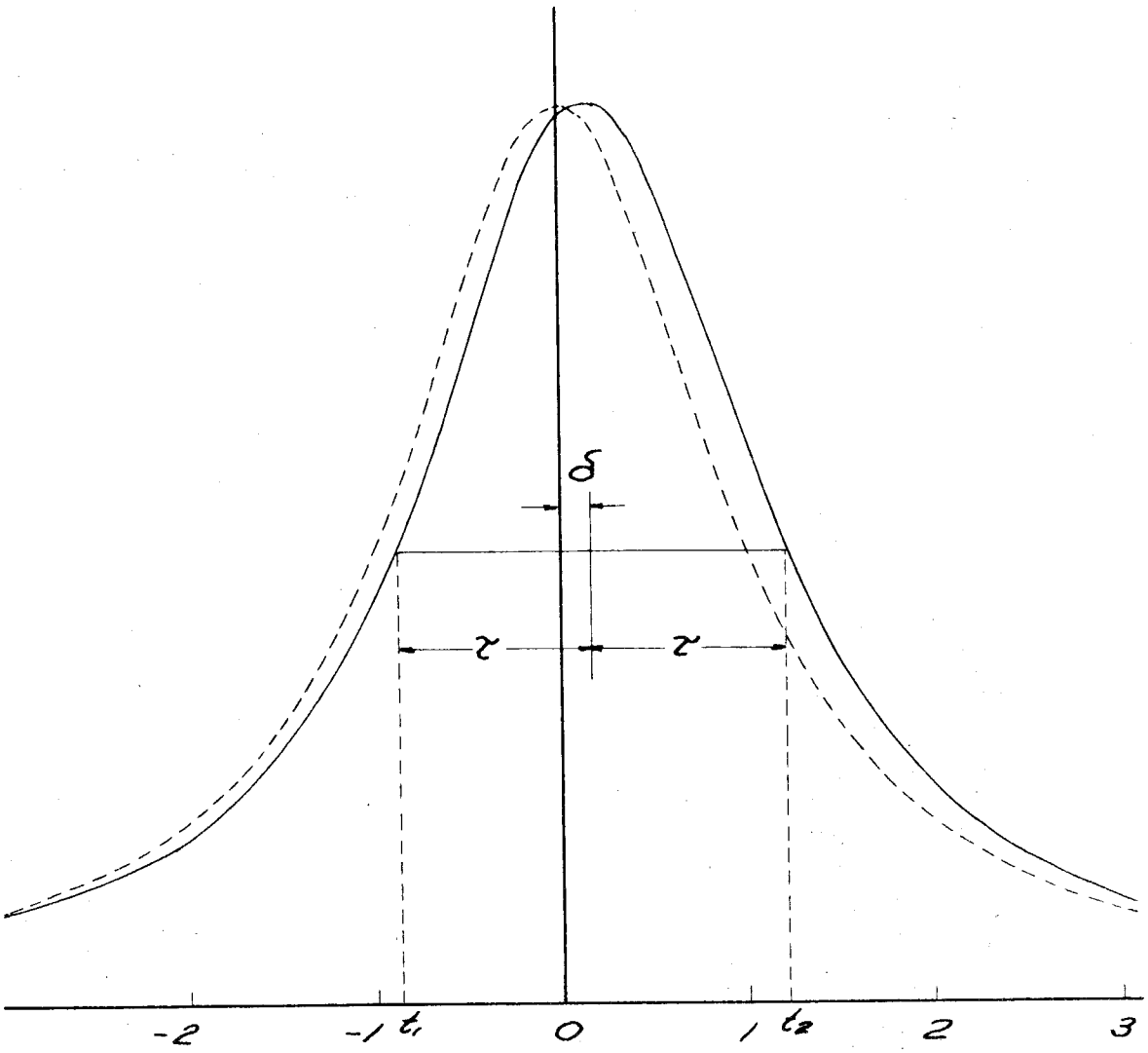

Figure 13. Plot of F(t,k) for k = 1.0 showing the significance of δ and τ. The unmodified witch is shown by the dashed curve.

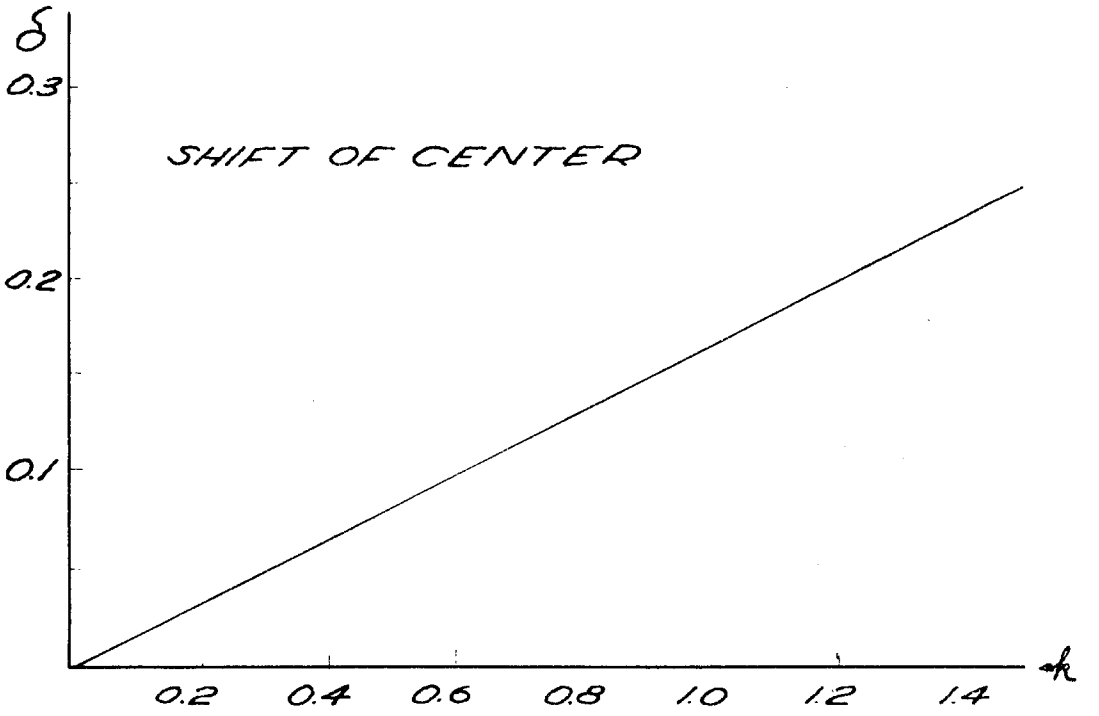

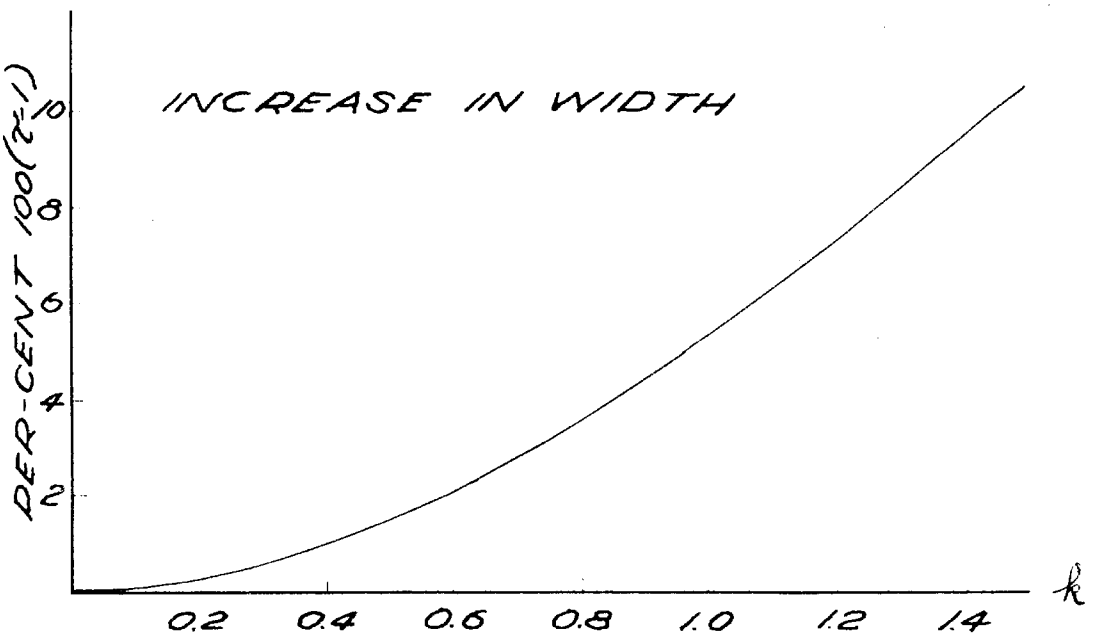

Figure 14. Curves showing the quantities δ and $100(\tau - 1)$ as functions of k.

parameter k. It is interesting to note that δ is directly proportional to k while τ is a function of some higher power of k. An attempt was made to find a simple analytic expression which would fit the τ graph, but it was without success. The δ graph, however, can be expressed quite accurately by the equation

$$\delta = k/6 \tag{4.20}$$

From the above relation it is possible to derive a simple formula which gives the angle to be subtracted from the observed Bragg angle when the latter is determined from the center of the observed spectral line. The shift in wavelength is found by multiplying δ by a, the half-width of the unmodified line; from the differential of the Bragg equation we obtain

$$\Delta\theta_v = \frac{a\,\delta\,\tan\theta}{\lambda_c}$$

where $\Delta\theta_v$ is the <u>increase</u> in observed angle because of vertical divergence and therefore must be <u>subtracted</u> from the observed Bragg angle. Combining the above expression with (4.18) and (4.20) we obtain

$$\Delta\theta_v = \frac{\phi_m^2}{12}\tan\theta \tag{4.21}$$

which gives us the desired correction in terms of the maximum vertical divergence angle.

Other investigators have derived similar expressions; Spencer (22) obtained 1/6 as the coefficient in (4.21) rather than 1/12, while Williams (23) gives as a correction formula

$$\Delta\theta_v = \frac{h_1^2 + h_2^2}{24L^2}\tan\theta$$

which reduces to (4.21) if $h_1 = h_2$. The solution of the problem of the

effect of vertical divergence for unequal slit heights by the method of this Part is straightforward but is made much more complicated by the additional parameter required. In practice the slit heights were made unequal in order to realize a greater intensity; the difference in θ_v as given by the above two formulae is negligible.

The determination of a, the half-width of the unmodified line, can be obtained from a', the half-width of the modified line, by using the curve in Figure 14b. The correct value of k to use in reading the curve is obtained from (4.18) which, unfortunately, contains a, the quantity sought. A good approximation to k may be found, however, by noting that k', calculated using a', is smaller than k by the same factor that a' is larger than a. This approximation to the true value of k is therefore

$$k = k' \tau \ . \qquad (4.22)$$

One further point which is of interest is the overall distortion of the unmodified line by the geometrical window of the spectrometer. To show this we have drawn the theoretical profile F(t,k) for the extreme case of k = 1.5 and have fitted a witch with the same width and height to this curve, matching the two at the half maximum values. These curves are shown in Figure 15 along with a witch representing the unmodified line for comparison. This value of k is over twice as large as the highest value encountered in the present experiment, so as far as L X-ray lines are concerned, a witch is probably an excellent approximation to the modified line. For measurements on the K lines of some of the lighter elements which have larger values of $\lambda/2a$, the parameter k could conceivably have a value of 1 or larger depending on the amount of vertical divergence.

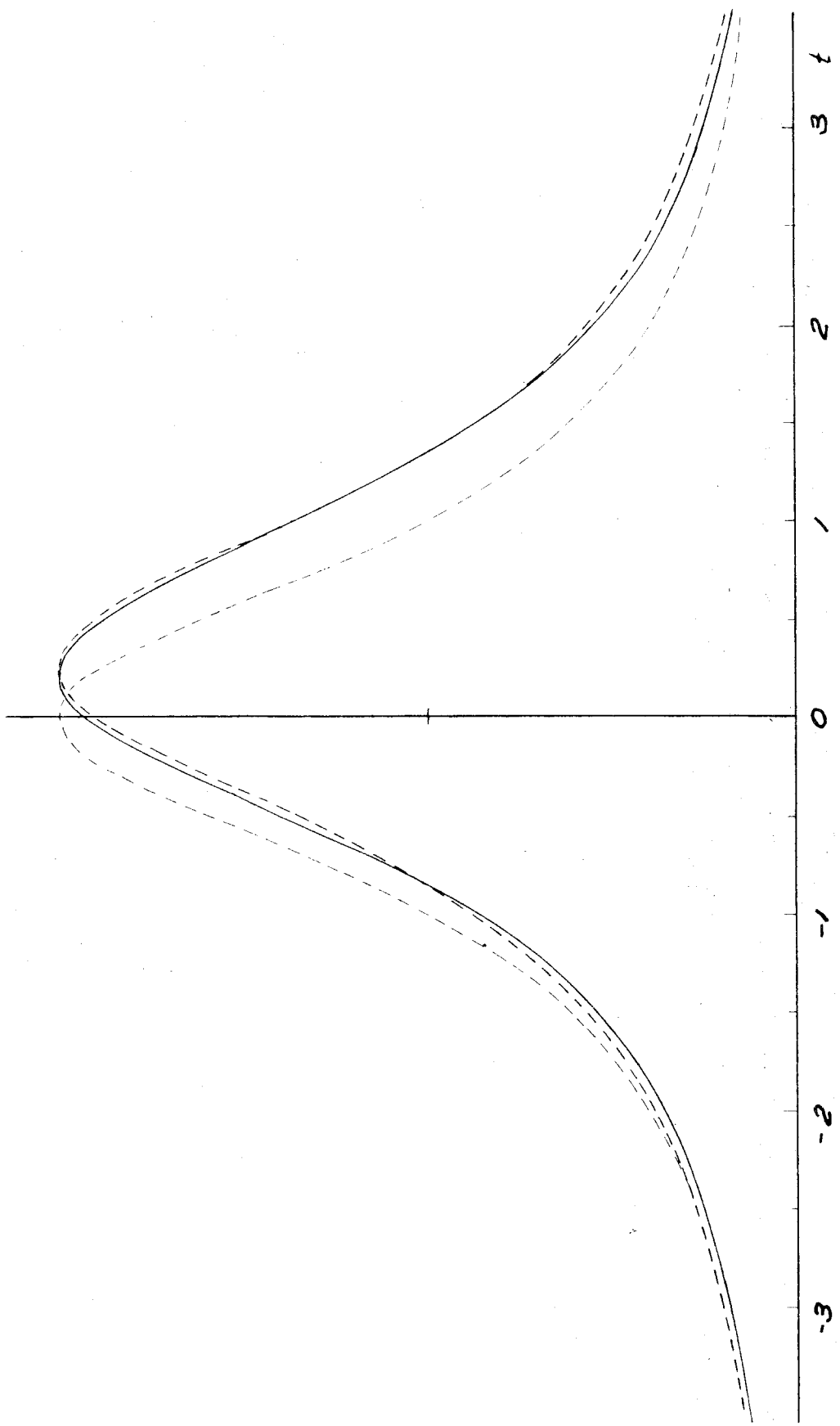

Figure 15. Comparison of the curve F(t, 1.5) (solid) to a witch (dashed) normalized to the same height and width. The curve symmetrical about t = 0 is the unmodified line.

C. The Effect of Differential Absorption of a Spectral Line

When an X-ray spectral line of full width 2a and wavelength λ_0 passes through an absorber, the longer wavelength portions of the line are absorbed more than the shorter wavelength portions because of the cubic dependence of the absorption coefficient upon wavelength. We wish to find the shift in the center of the line due to this non-symmetric absorption.

Assume that the profile of the line before absorption is given by $y = A\left[1 + (\lambda - \lambda_0)^2/a^2\right]^{-1}$ and that after absorption it is given by

$$y = \frac{A}{1 + (\frac{\lambda-\lambda_0}{a})^2} \; e^{-\mu(\lambda)x} \tag{4.23}$$

where x is the thickness of the absorber and $\mu(\lambda)$ is its linear absorption coefficient. We shall assume that λ is far enough from any absorption discontinuities of the absorber so that the approximate cubic dependence of $\mu(\lambda)$ upon λ may be assumed. We may then set

$$\mu(\lambda) = \mu_0 + (\lambda - \lambda_0)\frac{3\mu_0}{\lambda_0} + \ldots$$

by a Taylor expansion about the point λ_0. The amplitude of the line after absorption may be found to sufficient accuracy by setting $\lambda = \lambda_0$ in (4.23); the shift in wavelength of the center may be found by solving for the values of λ corresponding to one-half this peak value of y. We obtain therefore

$$\tfrac{1}{2} = \frac{e^{-(\lambda-\lambda_0)3\mu_0 x/\lambda_0}}{1 + (\frac{\lambda-\lambda_0}{a})^2}$$

which can be simplified by replacing the exponential by its expansion:

$$\frac{1}{2} \cong \frac{1 - 3\,\mu_o\, x(\lambda - \lambda_o)/\lambda_o}{1 + (\lambda - \lambda_o)^2/a^2} \qquad (4.24)$$

The expression (4.24) can be reduced to a quadratic in $(\lambda - \lambda_o)/a$ which has the solution

$$\frac{\lambda-\lambda_o}{a} = -\frac{3\,\mu_o x a}{\lambda_o} \pm \sqrt{\left(\frac{3\,\mu_o x a}{\lambda_o}\right)^2 + 1} \quad .$$

If the second order term in the radical is neglected, the two values of λ corresponding to the half maximum points on the line are given by

$$\lambda = \lambda_o \pm a - \frac{3\,\mu_o x a^2}{\lambda_o}$$

from which we obtain for the relative shift in wavelength of the absorbed line:

$$\frac{\Delta\lambda}{\lambda_o} = -3\,\mu x\left(\frac{a}{\lambda_o}\right)^2 . \qquad (4.25)$$

The correction to be applied to the observed Bragg angle is therefore

$$\Delta\theta = +3\,\mu x\left(\frac{a}{\lambda_o}\right)^2 \tan\theta$$

which should also be expressed in seconds in order to compare it to the required precision of measurement. If a is expressed in milli-angstroms and λ is expressed in angstroms, the correction angle is

$$\Delta\theta \cong 0.6\,\mu x\left(\frac{a}{\lambda}\right)^2 \tan\theta \text{ seconds.} \qquad (4.26)$$

The quantity μ changes with wavelength more rapidly than any other quantity in (4.26), so the evaluation of $\Delta\theta$ at the longest wavelength would give its highest value. Since $(a/\lambda)^2$ is approximately a constant equal to 0.2 for most L lines and tan θ at the longest

wavelength of 1.5 Å is approximately 0.25, (4.26) reduces to

$$\Delta\theta = 0.03 \ \mu x \ \text{seconds} . \qquad (4.27)$$

The correction would have to be 0.1 sec or greater to be considered non-negligible, in which case the μx values for the various absorbers in the path of the beam should add up to about 3.3 or more. The absorbers which contribute significantly to $\Sigma \mu x$ are

air path $\mu x = 0.8$

various windows* $\mu x = 0.6$,

and these evidently give rise to a negligible correction.

We have not yet considered the effect of the absorption of the X-rays in the source itself. Because of the difficult nature of this problem we can only hope to obtain an order of magnitude for the correction for this effect. While a more detailed description will be given later, for the purposes of this discussion the source may be considered to be a flat strip of metal inclined at 30° to the horizontal. The exciting radiation is provided by an X-ray tube placed immediately above the source, and the fluorescent radiation as seen by the spectrometer emerges in a horizontal direction. We shall make the following simplifying assumptions:

(a) parallel incident radiation

(b) semi-infinite source with surface perpendicular to incident rays

(c) parallel radiation only accepted by spectrometer.

---

* The windows referred to here are the various absorbers through which the beam must pass before it enters the NaI crystal detector such as the beryllium cover for the crystal and the black paper light shield over the opening in the detector housing.

Figure 16 shows the geometrical configuration of the source and the incident and fluorescent beams. The quantities used in the subsequent treatment are defined in this figure.

Per unit width of the source, the power arriving at the volume element dV for a wavelength λ_1 is

$$dP = I_o e^{-\mu_1 r} dt$$

where I_o is the intensity in the incident beam. Since

$$r \sin(\phi - \alpha) = s \sin \alpha$$

with

$$dr \sin \phi = dy, \quad ds \sin \phi = dt,$$

we may write

$$dP = I_o e^{-\mu_1 r} \sin \phi \, ds .$$

Now the fluorescent X-rays from dV in the horizontal direction have a power proportional to the amount of absorption in the path dr:

$$\begin{aligned} dP_f &= cI_o e^{-\mu_1 r} \mu_1 dr \sin \phi \, ds \\ &= cI_o e^{-\mu_1 sb} \mu_1 dy ds \end{aligned} \tag{4.28}$$

where c is a constant of proportionality and

$$b = \frac{\sin \alpha}{\sin(\phi - \alpha)} . \tag{4.29}$$

The intensity of the fluorescent X-rays at the surface is obtained by integrating (4.28) from s = 0 to s = ∞ and dividing by dy:

$$I_f = cI_o \mu_1 \int_0^\infty e^{-s(\mu_1 b + \mu_o)} ds = \frac{cI_o \mu_1}{\mu_1 b + \mu_o} \tag{4.30}$$

where μ_o is the linear absorption coefficient of the source for the

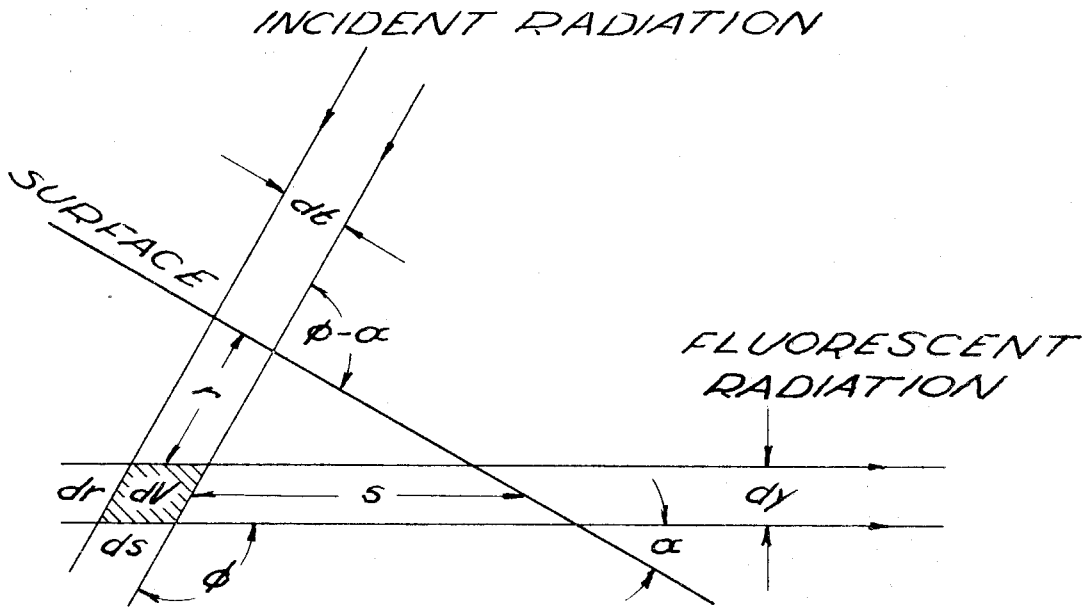

Figure 16. Schematic diagram showing relationship of incident and fluorescent beams of radiation.

fluorescent radiation. If $\mu_o = 0$ the fluorescent intensity would be

$$I_f' = \frac{cI_o}{b} ,$$

and the ratio of I_f/I_f' is therefore a measure of the effective absorption of the source material. We may define an effective depth of emergence, $\bar{x}$, by the equation

$$e^{-\mu_o \bar{x}} = \frac{I_f}{I_f'} = \frac{\mu_1 b}{\mu_1 b + \mu_o} = \frac{1}{1 + \mu_o / \mu_1 b} \qquad (4.31)$$

so that

$$\begin{aligned} \mu_o \bar{x} &= \ln(1 + \mu_o / \mu_1 b) \\ &= \ln(1 + 2\,\mu_o / \mu_1) \end{aligned} \qquad (4.32)$$

where we have substituted the angles $\alpha = 30^\circ$ and $\phi - \alpha = 90^\circ$ in (4.29) to evaluate b.

Even though (4.32) is valid for only one value of wavelength of the incident radiation, it may be used to obtain an estimate for $\mu_o \bar{x}$ providing a judicious choice can be made for λ_1 and hence μ_1. The range of λ_1 effective in producing fluorescent radiation is from the critical absorption wavelength of the source to the short wavelength limit of the continuous spectrum of the exciting radiation, while μ_1 varies roughly from a maximum to a minimum in this range of wavelength. We shall obtain the largest value of $\mu_o \bar{x}$ by choosing the smallest value of μ_1 and the largest value of μ_o; experimentally this corresponds to measurements on W which has a mass absorption coefficient of 159 at the L_{α_2} wavelength and 6.9 at the short wavelength limit of the continuous spectrum of the incident radiation. For this case $\mu_o \bar{x} \cong 3.8$, and when this value is combined with the $\Sigma \mu x$ value for

the other absorbers (which totals 1.4 for this same wavelength) the Bragg angle correction as given by (4.27) amounts to about 0.15 seconds which is on the borderline of being significant.

It is believed that the above estimate of $\mu_o \bar{x}$ is pessimistic enough so that the correction due to differential absorption of spectral lines may be neglected for wavelengths below 1.5 Å but should be considered if fluorescent measurements above this wavelength were undertaken.

D. Correction for the Effect of Crystal Diffraction Pattern Asymmetry

In Part III we have shown that the asymmetry of the Prins single crystal diffraction pattern introduces a small shift toward smaller Bragg angles of the axis of symmetry of the observed spectral line. The amount of shift was designated by the letter ϵ which is an angle measured in the same units in which the rotation of crystal B is measured. In order to calculate a correction which can be added to the observed Bragg angle the function $P_1(\beta)$, which was defined by (3.10) and which represents the spectrometer output for a monochromatic input, should be graphed for a sufficient number of wavelengths so that the dependence of ϵ on λ could be determined.

The single crystal I functions, from which $P_1(\beta)$ is obtained, are of such complexity, however, that it is not feasible to calculate $P_1(\beta)$ for many wavelengths. We have already mentioned the fact that Allison (16) and Parratt (17) have made several contributions along these lines, Allison having published a curve of $P_1(\beta)$ for λ=1.537Å and Parratt having published a table of values of $I_\sigma(\ell)$ for λ=2.299Å. Since the asymmetry of the diffraction pattern becomes negligible as λ approaches zero, it is evident that $\epsilon(\lambda)$ is zero at $\lambda = 0$;

we will attempt to estimate its functional behavior for $\lambda > 0$ by evaluating it at $\lambda = 1.537\text{Å}$ and $\lambda = 2.299\text{Å}$.

Careful measurements made on Allison's curve (see Figure 10) indicate that ϵ has a value of about 0.5 sec at $\lambda = 1.537\text{Å}$. In order to obtain ϵ at the longer wavelength it was necessary to perform the integration indicated in (3.10) by numerical methods. Measurements off the resulting curve of $P_1(\beta)$ yield a value of $\epsilon = 1.1$ sec at $\lambda = 2.299\text{Å}$. If we assume a power law dependence of ϵ on λ, the above two values of ϵ may be used to evaluate the constants in the equation $\epsilon = A\lambda^n$. The approximate result is

$$\epsilon = 0.2\lambda^2 \text{ seconds} . \qquad (4.33)$$

The size of this correction varies from about 0.5 sec for WL_{α_2} to about 0.1 sec for PuL_{β_1}. For the purposes of the present work it is more important to know accurately the differences between the various corrections applied to the L_{α_2} and L_{β_1} angle measurements rather than to know the absolute value of a given correction with high accuracy.

PART V

DESCRIPTION OF EXPERIMENTAL APPARATUS

Several references have been made already to the three major components of the experimental apparatus, namely, the X-ray source, the spectrometer, and the detector. In this Part a more detailed description will be given, with emphasis on those features which are considered unique or which tend to aid in the obtaining of maximum precision.

A. The X-ray Source

We have limited the term source to mean the piece of metal which gives rise to fluorescent radiation when irradiated with X-rays of sufficient quantum energy. We shall include in this discussion, however, the X-ray tube which provides the exciting radiation as well as the high voltage power supply.

The six elements studied in this work, namely, W, Pt, Bi, Th, U, and Pu, are all available in metallic form and hence are quite easy to mount on a source holder of almost any design. The design chosen was quite similar to that used by Rogosa and Schwartz (20) which held the plane of the source material at an angle of 30° with the horizontal. In order to facilitate the monitoring of the intensity of the source, the mounting plane of the source holder was tilted so that the surface of the fluorescent material could be seen both by the spectrometer and by a monitoring Geiger counter placed on the horizontal line passing through the source approximately at right angles to the central ray.

The source holder was machined from a rectangular aluminum bar and mounted on a steel plate which could be moved parallel to the central ray and fastened securely in any position. Aluminum was selected rather than some heavier metal because its own fluorescent radiation is so soft that most of it is absorbed by the air. Aluminum clamps are provided on the mounting surface to hold the various fluorescent materials in place. A perspective view of the source holder is shown in Figure 17.

The exciting radiation was obtained from a Machlett type OEG-50T high intensity X-ray tube. This tube has a single beryllium window and a tungsten target, is provided with water cooling, and is capable of running continuously at 50KV, 50ma input. The tube was positioned over the source so that the normal through the center of its window was normal to the plane of the source and intersected this plane at the same point as did the central ray. The surface of each source, regardless of the thickness, could be brought into the proper position with respect to the X-ray tube and the central ray by merely sliding the source holder backward or forward as indicated in the figure.

The source, X-ray tube, and monitor with its shielding were mounted on a thick steel base plate and enclosed in a lead-lined box. The box was provided with adjustable vertical and horizontal slits immediately in front of the source holder. The base plate itself was fastened to a steel frame with adjustable screws for leveling purposes, and the whole assembly was rigidly fastened to a concrete bench.

The X-ray tube was powered by a Phillips water cooled diffraction unit which could provide a full-wave rectified output, variable from 0 to 60KV peak. The voltage regulation of this unit is quite good,

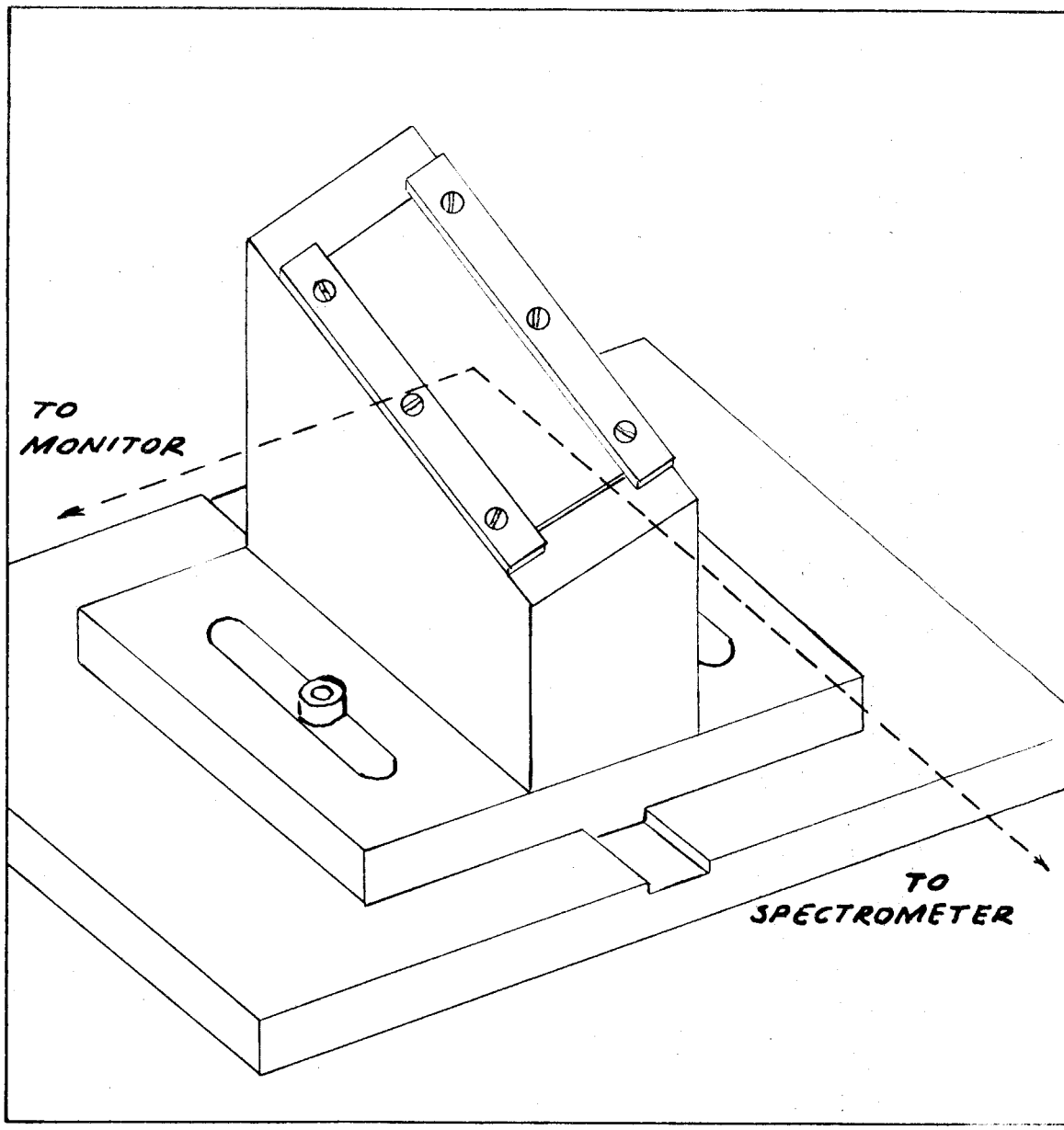

Figure 17. The fluorescent source holder.

but to insure greater stability of operation of the tube, the primary voltage was regulated with a Sorensen 2.5KVA regulator.

As an additional check on the stability of source intensity during measurements on a spectral line, the total number of counts recorded by the monitoring Geiger counter could be watched for significant variations. The radiation input to the counter was adjusted by a series of apertures to a high enough value so that the relative statistical fluctuations in the counting rate were small. The input to the monitor was also filtered by means of a critical absorber whose K absorption edge was slightly on the short wavelength side of the L line undergoing measurement. In this way the monitor was more sensitive to changes in intensity of the fluorescent line than it would have been without the filter, since much of the continuous radiation from the tube is scattered by the source material and could be picked up by the monitor.

An electronic system was developed which allowed the integrated monitor output to control the length of time that counts from the X-ray detector would be recorded. Counts from the monitor were scaled down and stored in an electro-mechanical register which automatically turned off both monitor and detector scalers when a predetermined number of counts was reached. Thus if the source intensity dropped slightly during measurements at a particular spectrometer setting, the detector scaler would remain on for enough additional time to compensate for the decreased intensity.

B. The Two-Crystal Spectrometer

The spectrometer used in this work was designed and built by DuMond and Marlow (24) and is distinctive because of its versatility

and high precision. The instrument is provided with four independent motions of rotation actuated by worm wheel drives which permit (a and b) precision settings of the two crystal tables to a few tenths of a second of arc, (c) angular setting of the instrument as a whole about an axis coincident with that of crystal A relative to the primary X-ray beam, and (d) angular setting of the arm supporting the X-ray detector about an axis coincident with that of crystal B. The worm gears on which the crystal tables are mounted have been specially lapped and optically calibrated; the error curve is shown in Figure 18.

Figure 19 is a perspective view of the instrument showing the crystal holders, the control wheels which turn the worm gears, and the supporting arm for the detector. The crystal holders shown provide means for adjusting the angle of tilt of the crystals so that the reflecting planes may be made parallel with the axis of rotation; there is also a translational adjustment so that the crystal surface may be brought into coincidence with the axis of rotation. The spectrometer is equipped with several additional adjustments so that the top surface may be made level and set to the desired height above the floor. Without altering either of these adjustments, the main body of the instrument may be moved in a horizontal direction perpendicular to the X-ray beam so that the axis of rotation of crystal A may be made to intersect the central part of the X-ray beam.

The calcite crystals used in this work are rather large, being about 2 3/4 inches on a side and about 1 inch thick. They are of uncertain origin but probably were split from a single piece as indicated by the similarity of the cleavage steps on their surfaces.

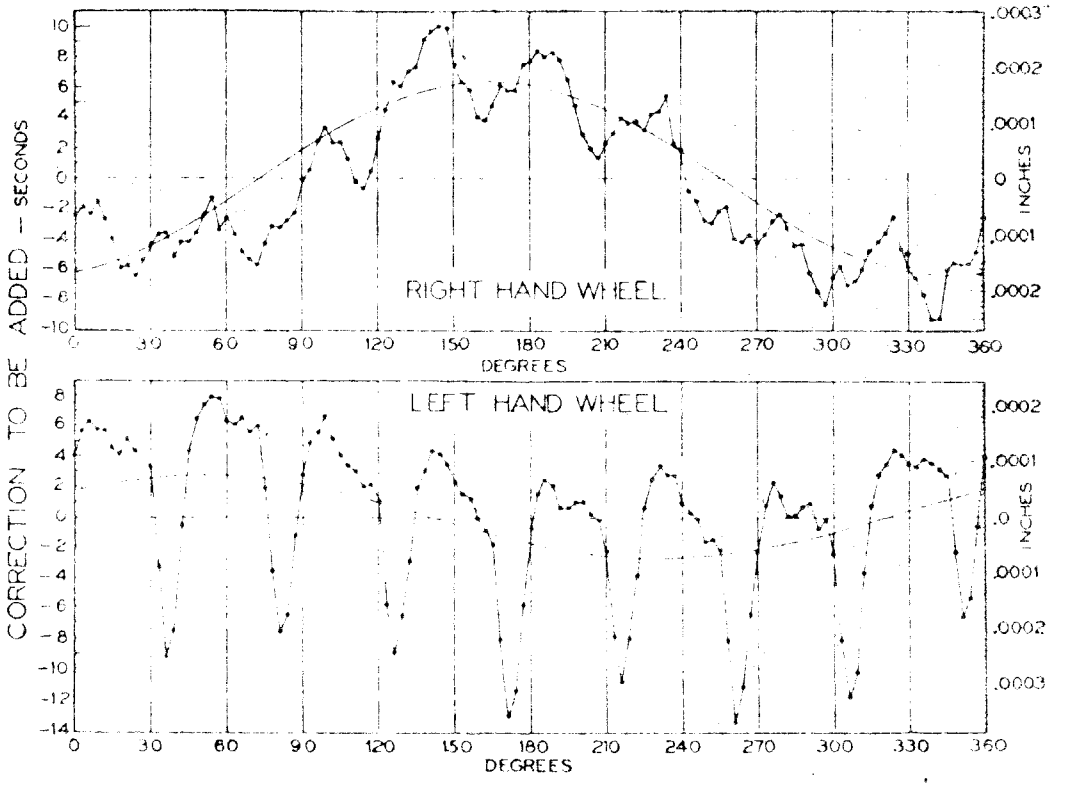

Figure 18. Error graphs obtained by optical calibration of the two worm wheels in the two-crystal X-ray spectrometer. (Copied from reference 24.)

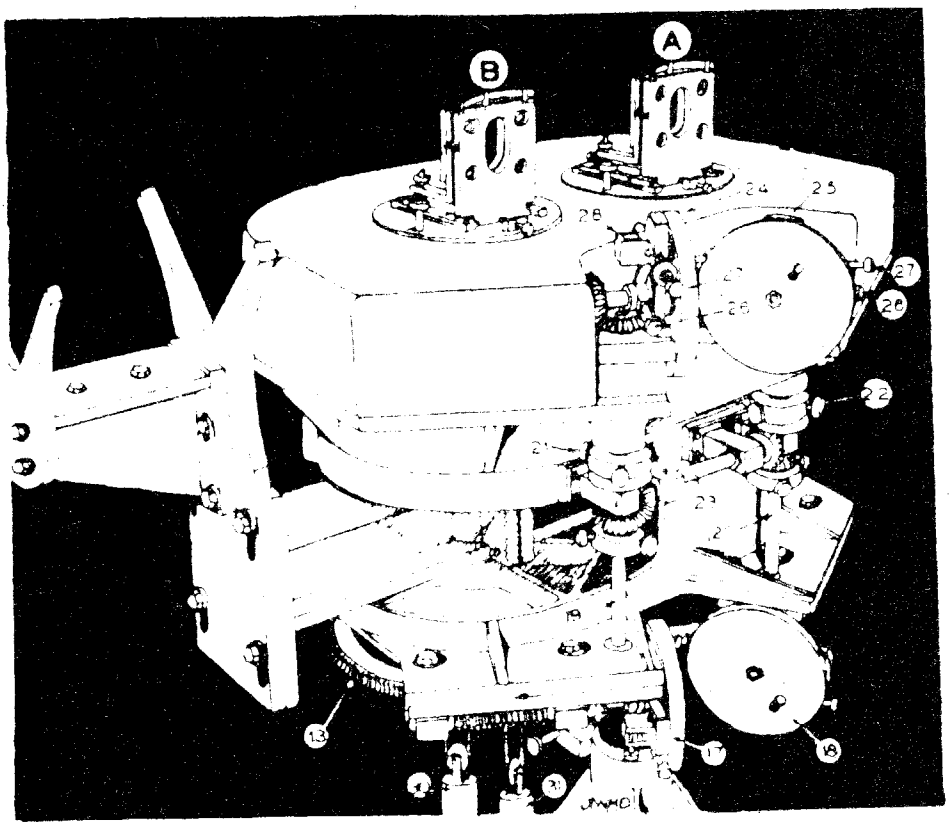

Figure 19. Two-crystal X-ray spectrometer showing crystal holders A and B, gear drives, clutches coupling the upper and lower worm wheel drives, and detector support arm. (Copied from reference 24.)

Since the cleavage steps cast shadows in the reflected beam which cause its intensity to vary sporadically as the crystal is rotated, it was thought best to grind out these steps and make the crystal surface as flat as possible. During the grinding process, precautions were taken to insure that the ground surface would be as parallel as possible to the reflecting planes. After grinding and polishing, the crystal surfaces were etched lightly with dilute HCl as suggested by Manning (25) in order to dissolve out any debris which might cause widening of the crystal diffraction pattern. Several measurements of the parallel rocking curve width were made during this process as a check on the effectiveness of the polishing and etching. The process was discontinued as soon as widths were obtained which were comparable to those obtained by other investigators.

The tilt adjustment of a crystal (making its reflecting planes parallel to the axis of rotation) is relatively easy providing the crystal surface is parallel to the planes and is a good optical reflector. A telescope with a Gauss eyepiece is adjusted so that it is perpendicular to the axis of rotation; the crystal is then mounted in its holder and the angle of tilt adjusted so that the telescope cross-hairs are reflected back on themselves. The grinding process, however, not only destroys the optical reflecting properties of the surface but also introduces an uncertainty into the angle between the surface and the reflecting planes. This difficulty was alleviated in the present work by utilizing the back cleavage surfaces of the crystals which were still fair optical reflectors. The crystal mounts as well as the adjustable holders shown in Figure 19 have large holes in them so that such optical tests may be easily made. The only

assumption necessary in using the rear planes of a crystal to adjust the front planes is, of course, that there is no flaw in the crystal which might cause the planes near the two surfaces to be non-parallel. No such flaw was evident in these crystals.

In a theoretical analysis of the action of the two-crystal spectrometer, Schwartzchild (26) has shown that the parallel rocking curves have an increased width if the crystal reflecting planes are not parallel to the axis of rotation. Therefore, by making a series of parallel position runs, each with a different tilt adjustment for one of the crystals, a curve of width vs. tilt angle may be obtained, the minimum of which indicates the correct tilt adjustment. Compton (27) has used such a technique, and his procedure was followed in the present work in order to check the accuracy of the optical adjustments. The conclusion reached was that the correct tilt adjustment obtained optically also yielded the narrowest rocking curves. Therefore the optical method, being so much quicker and easier, is to be preferred.

The angular setting of either of the two crystals is made by turning the appropriate upper control wheel shown in Figure 19. One revolution of the control wheel results in one degree rotation of the crystal. The rim of the wheel is divided into minute and ten-second intervals, and a vernier allows settings to be made directly to one second of arc. The accuracy of angle setting of crystal B using the vernier is, however, not sufficient for the purposes of this experiment. Reproducibility and accuracy were improved considerably by viewing the graduations on the control wheel through a low power microscope which was mounted on the spectrometer. The microscope eyepiece contains a reticule having 20 major divisions,

and the magnification of the microscope was adjusted, using an additional lens, so that these 20 divisions correspond to two ten-second intervals on the rim of the control wheel. The accuracy of setting of the crystal B control wheel is now limited only by the size of the random errors in the positions of the graduations which is approximately 0.1 second.

C. The X-ray Detector

In Part IV it was shown that the feature of having uniform response over the sensitive area of the detector was highly desirable. This reason, in addition to others, led to the choice of a NaI crystal detector over a conventional end-window Geiger counter. Some of the other advantages are: (1) the smaller volume reduces the background counting rate; (2) the cosmic ray counts may be eliminated by a discriminator thus reducing the necessity for lead shielding; (3) the efficiency of the crystal detector is higher for the shorter wavelength X-rays than the Geiger counter.

The NaI detector used in this work was designed and built by Mr. Robert Swank of the Argonne National Laboratories. The crystal itself is a round, thin wafer of NaI which is mounted in a holder having a beryllium window for the X-rays and a glass window for the light output. The detector is designed to be fastened directly to the face of a photomultiplier tube with some kind of clear grease or plastic compound. A diagram of the construction of the detector and a drawing of the complete detector assembly with its shielding are shown in Figure 20.

The output of the DuMont 6292 photomultiplier tube is fed into a pre-amplifier mounted on the detector support arm, and the pulses

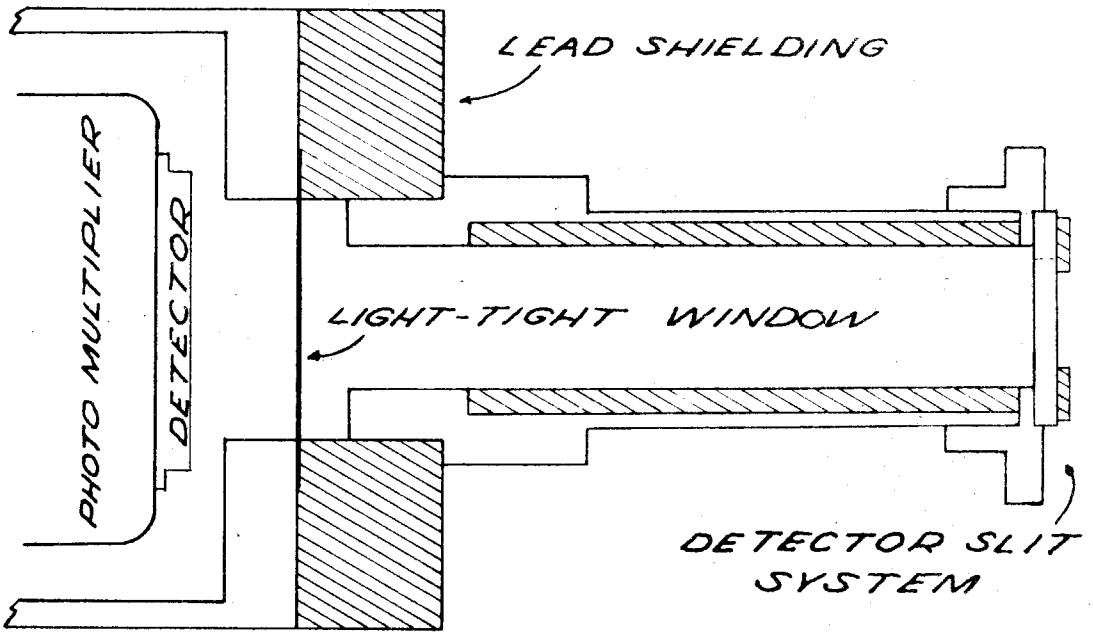

DETECTOR HOUSING AND SHIELDING

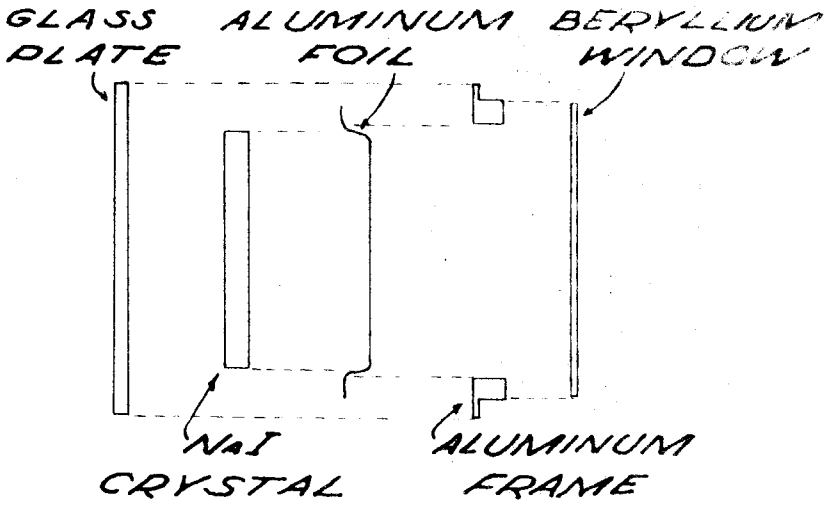

CRYSTAL DETECTOR ASSEMBLY

Figure 20. The scintillation crystal detector and its housing.

are then sent to a linear amplifier before being discriminated. The discriminator, while not an essential component of the detecting system, serves to eliminate two sources of background, namely, the photomultiplier tube noise and the cosmic ray pulses. The discriminator output is fed into a binary scaler and recorded on a mechanical register.

In order to insure that the shape and position of the observed X-ray line is determined by the spectrometer alone and is not influenced by the spectral response curve of the detecting system, an attempt must be made to obtain uniform response characteristics over a relatively wide spectral region in the vicinity of each of the lines measured. The spectral response curve may be investigated experimentally by setting the spectrometer at the peak of an X-ray line and noting the change in detector output as the base line* setting of the discriminator is varied. If the base line is then set to the value corresponding to the peak of this curve, the danger of having the shape of the observed line modified by the detector response is minimized. The discriminator channel width is, of course, set to the maximum value, since the discriminator itself is not being used as a spectrometer.

The detector slit system (both horizontal and vertical slits) is mounted on the end of the extended shielding tube shown in Figure 20. The horizontal slit opening serves to define the width of the X-ray beam that passes through the system, since the radiation that is reflected from crystal B is essentially parallel. As crystal B and

---

* The base line setting refers to the adjustment which determines the minimum pulse height in volts which will trigger the discriminator.

the detector arm are rotated during the measurement of a spectral line the X-ray beam defined by the detector slit migrates across the surface of crystal A and also across the source. It is important, therefore, that the source as well as the various slits and stops in the path of the beam be wide enough so that as the beam moves through its maximum lateral extent it maintains the same width as defined by the detector slit. For the widest X-ray line encountered the maximum rotation of crystal B was approximately 3 minutes of arc or about 10^{-3} radian. The distance from the axis of rotation of crystal B to the source slit is about 20 inches. Therefore, the maximum excursion of the beam at the source end is about 1/2 mm; such a small increase in the effective width of the beam can easily be allowed for in the adjustment of the slits and stops prior to a measurement.

D. The Temperature Control Equipment

The effective grating space of calcite for first order reflection is*

$$d_1 = 3029.04 \text{ XU at } 18^\circ\text{C} \quad , \tag{5.1}$$

and since the coefficient of thermal expansion is known it is possible to correct d_1 to any other temperature. The correction to be added to the observed Bragg angle is calculated from the coefficient of thermal expansion and the Bragg law:*

$$\Delta\theta_t = 2.10(t-18^\circ) \tan\theta \text{ seconds} \quad . \tag{5.2}$$

From this equation we may obtain the necessary precision in the temperature measurement and control in order to make the uncertainty in the temperature correction negligible. If an error of 0.1 sec or

---

* Compton and Allison, op. cit., p. 682.

less is used as a measure of the precision required in the measurement of the Bragg angle, it follows that the temperature should be maintained at a constant value over the time required for a run to better than 0.5° C.

In order to control the temperature of the room in which the spectrometer was located, it was necessary to heat the room electrically to several degrees above normal and maintain the temperature with some kind of thermostat. A Fenwal Thermoswitch was positioned near the top of the spectrometer and through a series of relays was made to control two electric heaters. One of the heaters with a 2KW rating was installed over the fresh air inlet to the room with a continuously operating fan behind it; the other heater rated at 1.6KW was suspended near the spectrometer (hence, near the Thermoswitch) and served to shorten the time of the control cycle with a consequent reduction in the temperature variation.

Inasmuch as the depth of penetration of the X-rays into the surfaces of the crystals is quite small (of the order of magnitude of a few thousand atomic planes), and since the crystal surfaces are rather sensitive to rapid changes in temperature, it is quite possible that the variations in the quantity $\Delta\theta_t$ might well exceed 0.1 sec for short periods of time. It is therefore necessary to keep air currents in the room, which are subject to relatively wide variations in temperature, from striking the crystal surfaces. An aluminum cover for the top of the spectrometer was constructed having entrance and exit windows for the X-ray beam made of 0.00025 inch Mylar film having a negligible μx value even at long wavelengths. The temperature

of the cover was measured with a mercury thermometer having 0.1° C graduations which was suspended in an oil cup fastened to the top of the cover. After the electrical equipment and room lights had been operating for an hour or so, the temperature of the crystal cover and hence the crystals themselves did not vary more than one or two tenths of a degree.

PART VI

EXPERIMENTAL RESULTS AND COMPARISON WITH THE THEORY

A. Preliminary Measurements on the $M_0K_{\alpha_1}$ Bragg Angle

Before beginning the measurements on the L lines of the heavy elements chosen for this investigation a series of measurements of the Bragg angle of the K_{α_1} line of M_0 was undertaken. This particular X-ray line has been measured by many investigators, and its Bragg angle for calcite is very accurately known. The measurements of Compton (27) on this angle using two-crystal spectrometer techniques, when corrected for vertical divergence using Williams' formula (p. 60), yield a value of

$$\theta = 6^\circ\ 42'\ 35.9_5''\ . \qquad (6.1)$$

It was believed that the results of the preliminary measurements on $M_0K_{\alpha_1}$ would shed light on the following factors which affect the precision of subsequent measurements:

(1) the reliability of the worm wheel calibration curve,

(2) the assumption that the grating space of the calcite crystals is the same as the commonly accepted value,

(3) the assumption that the calcite crystals are approximately "perfect,"

(4) the effectiveness of the measurement techniques in obtaining maximum precision.

Factor (1) was checked by making measurements in three different portions of the crystal B worm wheel; the error correction curve shown in Figure 18 was thus verified in three distinct regions. Factor (2) could be checked by comparing the mean of several

determinations of θ to the value given in (6.1). Factor (3) is rather difficult to investigate thoroughly, but by comparing the widths of the parallel rocking curves and the observed lines to those obtained by others whose crystals were not in doubt, a rough measure of the perfection of the crystals may be obtained. Factor (4) may be evaluated by noting the spread of the results of the several measurements.

Using a fluorescent M_o *source, five independent sets of measurements* of the Bragg angle were made, each measurement consisting in the complete delineation of a parallel and anti-parallel curve. The angular displacement between the centers of the two curves is equal to $180^\circ + 2\theta$ where θ is the Bragg angle uncorrected for worm wheel errors, vertical divergence and temperature. In some of the measurements the beam was deviated to the left by crystal A, and in others to the right. We shall denote runs of the former type by the letter L and runs of the latter type by the letter R. Subscripts will be appended to these letters to distinguish the various positions of the worm wheel that were used.

The results of the preliminary measurements on $M_oK_{\alpha_1}$ are shown in Table III. The worm wheel correction $\Delta\theta_w$ is equal to the difference between the parallel position correction and the anti-parallel position correction; the sign is determined by whether the anti-parallel angle is subtracted from the parallel angle to determine $180^\circ + 2\theta$ or vice versa. The correction $\Delta\theta_w$ is added to $180^\circ + 2\theta$ while $\Delta\theta_t$ is added to θ. When the values of θ listed in Table III are corrected for vertical divergence using Williams' formula (p. 60), which gives $\Delta\theta_v = 1.4''$, the mean of the five values

with its standard deviation is

$$\theta = 6^\circ\ 42'\ 35.9 \pm 0.2'' \ . \qquad (6.2)$$

The remarkable agreement between this value and that given in (6.1) may be somewhat fortuitous, but it indicates that factors (1), (2), and (4) mentioned above are not tending to produce significant errors.

Table III

Results of $M_oK_{\alpha_1}$ Bragg angle measurement, uncorrected for vertical divergence

Run No.	$180^\circ+2\theta$	Worm Wheel $\Delta\theta_w$	Temperature $\Delta\theta_t$	Bragg angle θ
L_1	$193^\circ\ 25'\ 14.9''$	$-4.3''$	$1.6''$	$6^\circ\ 42'\ 36.9''$
R_1	$193^\circ\ 25'\ 14.5''$	$-4.3''$	$1.7''$	$6^\circ\ 42'\ 36.8''$
R_2	$193^\circ\ 25'\ 17.1''$	$-5.0''$	$1.6''$	$6^\circ\ 42'\ 37.7''$
L_2	$193^\circ\ 25'\ 17.0''$	$-5.0''$	$1.7''$	$6^\circ\ 42'\ 37.7''$
L_3	$193^\circ\ 25'\ 19.1''$	$-8.0''$	$1.7''$	$6^\circ\ 42'\ 37.3''$

The average values for the full widths of the parallel and anti-parallel curves were:

parallel 7 seconds

anti-parallel 25 seconds.

The large value of vertical divergence used in this series of runs resulted in a k value of nearly 1.5. Referring to Figure 14 it is seen that this value of k causes an approximate increase in line width of 10 per cent. The unmodified line width is therefore about 22.7" which compares favorably with 21", the lowest value reported. (20) Manning (25) obtained 7.0" as the full width of the parallel

rocking curve while Brogan (28) reports a value of 5.2", the smallest published value found; the theoretical minimum is about 4.6". We may thus conclude that while the crystals probably are not "perfect", the amount of imperfection is not sufficient to impair their usefulness in precision wavelength measurements.

B. Experimental Procedure in the L Line Measurements

Four independent measurements of the Bragg angle of both the L_{α_2} and L_{β_1} lines of each of the six selected elements were planned using two different portions of the crystal B worm wheel. A left and right deviation run would be completed for each element before the crystal was rotated with respect to the worm wheel; the entire series of measurements would then be repeated. As previously stated each line measurement includes a parallel and an anti-parallel run which must be made in sequence, the position of crystal A remaining unchanged.

In order to facilitate the setting of the four control wheels of the spectrometer and to aid in the location of the various lines, the Bragg angles of each of the twelve lines were calculated using the tabulated wavelengths of Cauchois (12). In the case of Pu, where no published data were found, a Moseley extrapolation was used with good results. As soon as the Bragg angles were available it was possible to calculate the crystal width projected on a plane perpendicular to the X-ray beam. This projected width determined the maximum horizontal width of the detector slit which, when combined with the length of the strip of metal used for the source, determined the heights of the vertical slits at both the source and detector. The relation between the slit and source sizes is based on a

geometrical formula developed for the purpose of obtaining maximum intensity consistent with the fact that the extended shielding tube on the detector housing has a circular aperture of 3/4 inch diameter. A complete set of interchangeable, non-adjustable slits for the detector slit holder was constructed along with a set of spacer blocks for the adjustable vertical slit at the source. The slit sizes were known to a few thousandths of an inch and could be set up for a given X-ray line measurement quickly and accurately.

Before an actual line run could be started, several preliminary details had to be taken care of. The source, appropriate slits, and monitor filter had to be installed and adjusted. A precursory run was then made over the region of the line to determine its peak intensity and approximate position; with this information the length of time that should be spent at each point in order to accumulate approximately 8000 counts at the peak of the line (giving about one per cent statistics) could be estimated, and a point by point program of spectrometer settings could be planned in advance so that the time might be used most efficiently. With the spectrometer set on the peak of the line a discriminator run was made to determine the best position of the base line setting. This latter run did not have to be made before each measurement, of course, nor for each line, since a linear relationship exists between the quantum energy of the radiation and the output pulse height of the photomultiplier.

The line run itself consisted in making the spectrometer settings according to the pre-arranged program and recording the number of counts accumulated at each point. The monitor controlled the length of the counting interval which was automatically timed by an electric

clock which turned on and off with the scalers. This time was also recorded so that any significant changes in X-ray power could be quickly detected and so that all intensity measurements could be normalized to counts per unit time. The crystal temperature was recorded every few points.

For all L_{α_2} lines and for the Pu L_{β_1} line the intensity was so low that two and sometimes three separate runs over the line profile were necessary to accumulate the required number of counts. This procedure was used rather than making a single run with more time per point because of the excessive amount of total time involved. For example, twelve hours were required for three runs over the Pu L_{α_2} line. Special attention was given to the problem of holding the temperature of the crystals to the same value for each of the runs.

Additional data taken during the line measurements included a background count made with a piece of lead in the path of the X-ray beam and measurements on the peak intensity and position of other lines in the immediate vicinity of the line in question. This latter was done so that the background contributed by the extraneous lines could be properly subtracted off. The cases in which other lines were close enough to the desired line so that a correction had to be made were (a) all the α_2 lines since the α_1 line is only 10 XU away, (b) the Bi L_{β_1} line where the L_{β_2} line is 3 XU away, (c) the Th L_{β_1} line where the L_{β_5} line is at essentially the same wavelength.

The parallel position run associated with a particular line measurement was made either before or after the line run but always with the same setting for crystal A and under the same temperature conditions. The techniques employed in making the parallel run were slightly different than those for the anti-parallel run because of

the different characteristics of the two curves. The intensity available in the parallel position was usually sufficient so that the X-ray tube could be run at a much lower power input. Under these conditions the stability of X-ray intensity was good enough so that the monitor control of the length of the counting interval could be discontinued in favor of ordinary timing devices. Because of the narrowness of the parallel curves a preliminary run was unnecessary, the spectrometer being advanced a second of arc at a time over the steep portions of the curves. The parallel rocking curve runs were always repeated at least two times to get a more accurate value for this reference angle.

C. Calculation of Experimental Results

For a required precision of about one second of arc in the determination of the Bragg angle, one could simply plot the raw data for both parallel and anti-parallel curves, find their midpoints, evaluate $180^{\circ} + 2\theta$, and apply the various corrections to the resultant value of θ. The one step in this method which is most likely to give rise to errors is the one involving the determination of the midpoint of the anti-parallel curve. The method usually used is to draw a smooth curve through the plotted points using a french curve and then to determine the midpoint of the line joining the half maximum values of the curve. When sufficient intensity is available and many points can be taken with good statistics, this method is capable of giving good results. When a limited number of points are available, as in the present work, the "correct" curve to draw through the points is largely a matter of personal judgment

and hence is subject to some variation.

The high precision required in this investigation was considered to be sufficient justification for a more involved but less subjective method of arriving at the correct value of the anti-parallel position angle. The theoretical line profiles F(t,k) discussed in Part IV were taken as the idealized line shape and the observed data fitted analytically to these curves. In so doing the effect of vertical divergence was automatically taken care of, since the center of the unmodified line corresponds to t = 0 on the theoretical curve; hence no further correction for vertical divergence was required. It should be pointed out that while the curve F(t,k) was evaluated using a wavelength scale for the abscissa it is equally valid if an angular scale is used, since the only change is the scale factor D (the dispersion) which we have shown to be essentially a constant. The variable t may be interpreted, therefore, as the angular deviation (measured in half-widths of the unmodified line) of the spectrometer setting from the center of the unmodified line.

The procedure used in fitting the observed data to the theoretical line profile is rather complicated and can probably be set forth in a more succinct way by simply outlining the various steps followed. Certain preliminary corrections to the raw data were necessary, however; the background count was subtracted from each of the intensity readings, and the background due to extraneous lines was subtracted assuming a witch profile for the unwanted lines. The corrected data were then plotted on graph paper and the following steps taken:

(1) The amplitude and half-width of the curves were estimated as accurately as possible.

(2) Using (4.18) and the dispersion D, a value of k was calculated which was corrected by the method described on page 61. With the corrected k the half-width of the unmodified line was determined from the graph in Figure 14b.

(3) From the eleven original curves of F(t,k) which were calculated by machine, a k value was selected which was nearest to the one found in (2) above. By a method described in Appendix B the theoretical curve was adjusted to correspond to the correct k value and was then plotted on a large scale.

(4) Using a convenient spectrometer setting near the center of the observed curve as an origin, the t'-values of each of the other spectrometer settings were determined using the angular half-width of the unmodified line as determined in (2). The prime is used to distinguish between this value of t measured from an arbitrary origin and the t measured from the center of the unmodified line.

(5) The intensity values of the observed points were multiplied by a normalizing constant so that the amplitudes as well as the widths of both the observed and theoretical curves were equal within the accuracy obtainable in (1). Under these conditions the normalized data and the theoretical line profile could be plotted on separate pieces of translucent graph paper; one graph could then be placed over the other and adjusted so that the points fell on the theoretical curve. An indication of the goodness of fit as well as the value of t' corresponding to t = 0 could thus be obtained. This graphical technique was used only to check the normalization and to indicate those few points which were so far from the curve that they should be rejected. A typical graph for Bi $L\beta_1$, R_1 run, is shown

in Figure 21.

(6) The intensity of each point, designated as a y value, was used to locate a corresponding t value on the large scale plot of F(t,k) mentioned in (3). Ordinarily a difference would exist between this value of t and the value of t' for the observed point. The size of the difference was a measure of how far the arbitrary origin selected in (4) was from the true origin, t = 0. Now if each of the observed points fitted the theoretical curve exactly, the difference, t' - t, would have the same value for each point. However, statistical fluctuations and errors in spectrometer setting cause a variation of the t' - t values from one point to the next. If the variations are random, the weighted average of all the t' - t values for each of the observed points would indicate the correct value of spectrometer setting corresponding to the center of the unmodified spectral line.

(7) It is clear that some of the points on the spectral line are more important in determining its position than others. When the position is determined by the y values of the observed data the points that lie far out on the curve and near the peak are less reliable for positioning the line than those points on the steeper portions of the curve. A weight function was derived for the t'-t values on the basis of this reasoning. The derivation is presented in Appendix C.

(8) The angle corresponding to the center of the unmodified line is found by multiplying the weighted average of the t' - t values by the half-width determined in (2) and adding the result to the spectrometer setting corresponding to the arbitrary origin of (4).

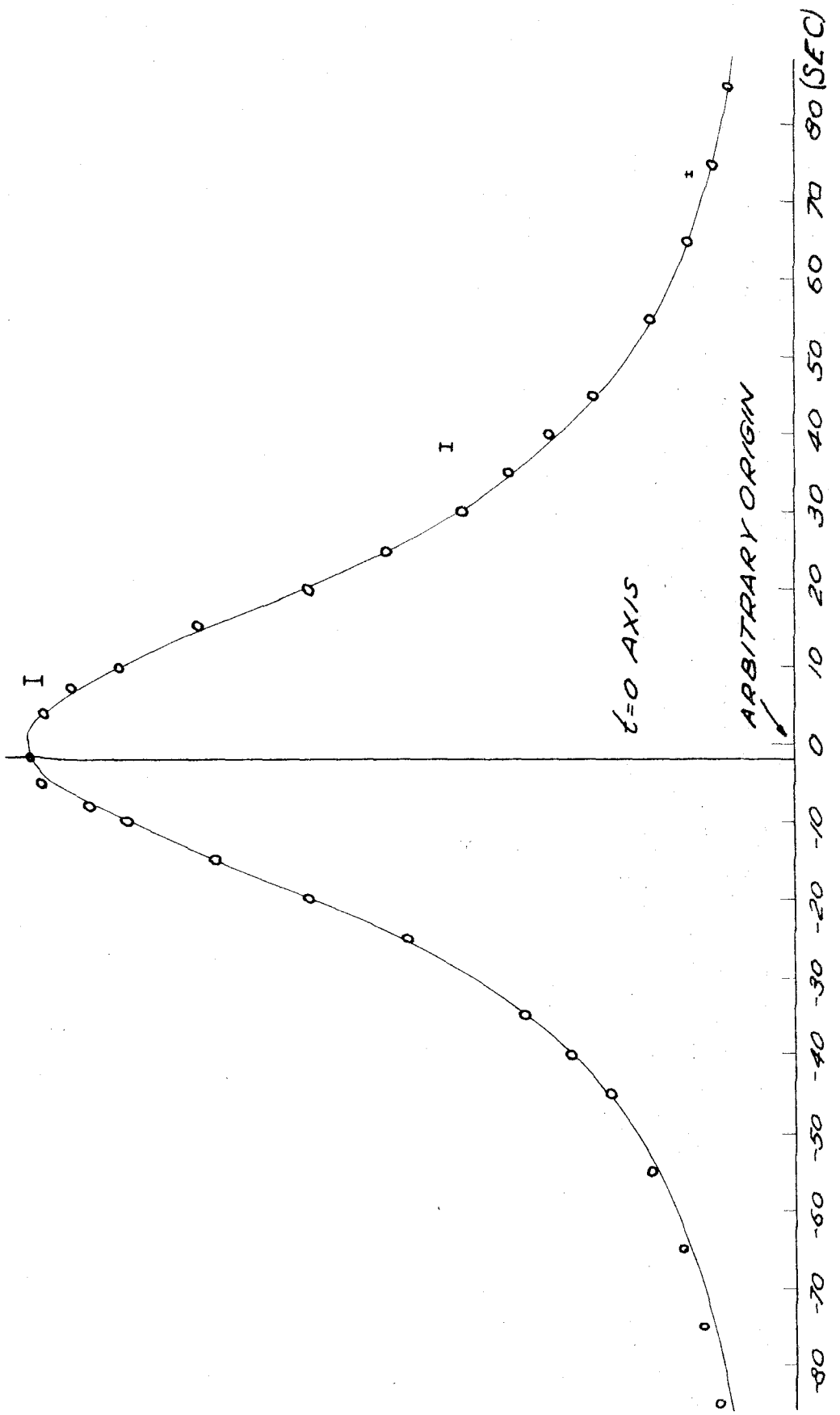

Figure 21. Typical anti-parallel curve (Bi $I_{B_1} - R_1$) showing the fit of the observed data to the theoretical line profile F(t,k).

These eight steps represent a considerable amount of numerical work; for the 48 anti-parallel runs made, more than 10,000 separate steps or calculations had to be performed. The one rewarding feature of the method is that it gives the center of the line to better than 1/200 of the half-width. For lines having k values less than about 0.7, the witch is an excellent approximation to the modified line shape, so considerably less work with the same order of precision would result from fitting the data to a witch and making the necessary vertical divergence correction as a separate step. Unfortunately this method did not suggest itself until after the more laborious procedure was completed.

The centers of the parallel curves were much easier to locate because of their narrowness. Instead of drawing a smooth curve through the observed points which were plotted on a large scale, the points were connected by straight line segments. The midpoints of several horizontal lines at different heights drawn from one side of the curve to the other were averaged to give the angle of the parallel position.

Once the anti-parallel and parallel position angles have been determined, the Bragg angle calculations follow in the same manner as outlined in Section A for $M_0K_{\alpha_1}$ except for the vertical divergence correction. Typical angle calculations are shown in Table IV for the Bi L_{α_2} and L_{β_1} lines. Included in these calculations is the small correction for crystal diffraction pattern asymmetry given by (4.33).

The Bragg angles for each of the measured lines are given in Table V with their standard deviations. The wavelengths were calculated

TABLE IV

TYPICAL BRAGG ANGLE CALCULATIONS FOR Bi L_{α_2} and L_{β_1} LINES

(a) Bi L_{α_2} runs

Run No.	Parallel Position	Anti-Parallel Position	Worm Wheel Correction	2θ (uncorrected)	$\Delta\theta_t + \epsilon/2$	θ (corrected Bragg angle)
L_1	250° 41' 9.2"	48° 44' 32.6"	-8.1"	21° 56' 28.5"	3.5 + 0.1"	10° 58' 17.9"
R_1	48° 44' 16.3"	250° 40' 53.8"	-8.1"	21° 56' 29.4"	3.6 + 0.1"	10° 58' 18.4"
L_2	296° 37' 42.5"	94° 41' 8.2"	-5.4"	21° 56' 28.9"	4.0 + 0.1"	10° 58' 18.5"
R_2	94° 40' 43.5"	296° 37' 16.4"	-5.4"	21° 56' 27.5"	4.1 + 0.1"	10° 58' 18.0"

Mean value of Bragg angle for Bi L_{α_2}: $\theta = 10° 58' 18.2 \pm 0.2"$

(b) Bi L_{β_1} runs

Run No.	Parallel Position	Anti-Parallel Position	Worm Wheel Correction	2θ (uncorrected)	$\Delta\theta_t + \epsilon/2$	θ (corrected Bragg angle)
L_1	248° 44' 11.3"	50° 41' 28.4"	-8.6"	18° 2' 34.3"	2.9 + 0.1"	9° 1' 20.2"
R_1	50° 41' 9.2"	248° 43' 53.0"	-8.6"	18° 2' 35.2"	2.9 + 0.1"	9° 1' 20.6"
L_2	294° 40' 47.2"	96° 38' 6.6"	-6.3"	18° 2' 34.3"	3.2 + 0.1"	9° 1' 20.5"
R_2	96° 37' 39.9"	294° 40' 21.7"	-6.3"	18° 2' 35.5"	3.2 + 0.1"	9° 1' 21.0"

Mean value of Bragg angle for Bi L_{β_1}: $\theta = 9° 1' 20.6 \pm 0.2"$

TABLE V

EXPERIMENTAL RESULTS

X-ray Line	Bragg Angle	λ_s (X-units)	ν/R
W L_{α_2}	14° 10' 59.8 ± 0.3"	1484.378 ± 0.008	612.656 ± 0.003
W L_{β_1}	12° 11' 23.9 ± 0.1"	1279.186 ± 0.003	710.931 ± 0.001
Pt L_{α_2}	12° 36' 2.6 ± 0.2"	1321.604 ± 0.005	688.113 ± 0.003
Pt L_{β_1}	10° 37' 51.5 ± 0.4"	1117.611 ± 0.010	813.712 ± 0.008
Bi L_{α_2}	10° 58' 18.2 ± 0.2"	1153.001 ± 0.005	788.735 ± 0.003
Bi L_{β_1}	9° 1' 20.6 ± 0.2"	950.031 ± 0.006	957.246 ± 0.006
Th L_{α_2}	9° 10' 28.3 ± 0.1"	965.914 ± 0.004	941.505 ± 0.004
Th L_{β_1}	7° 14' 30.2 ± 0.2"	763.655 ± 0.005	1190.868 ± 0.007
U L_{α_2}	8° 44' 29.0 ± 0.2"	920.676 ± 0.006	987.767 ± 0.006
U L_{β_1}	6° 48' 41.3 ± 0.1"	718.505 ± 0.004	1265.701 ± 0.007
Pu L_{α_2}	8° 20' 16.2 ± 0.1"	878.480 ± 0.002	1035.212 ± 0.002
Pu L_{β_1}	6° 24' 35.4 ± 0.2"	676.321 ± 0.006	1344.647 ± 0.011

from the Bragg law using the effective first order grating space, d_1, given in (5.1) and values of sin θ which were computed to 8 decimal places using four terms of the power series. The transition energies are given in units of the Rydberg with the necessary conversion from X-units to milliangstroms made using λ_g/λ_s=1.002039 and with R = 109737.309 cm^{-1}. (16)

On the basis of the general agreement of the results of the four independent determinations of θ for each line and the results of the measurements on $M_oK_{\alpha_1}$ it is believed that the standard deviations shown in Table V are a fair representation of the accuracy of the experimental results.

D. Comparison With the Schawlow-Townes Theory

Another indication of the overall precision of the measurements may be obtained from a plot similar to the one in Figure 1. If the results are as reliable as is claimed then the six points at Z = 74, 78, 83, 90, 92, 94 obtained by comparing experiment to theory should lie on some relatively smooth curve (assuming, of course, that the scatter of the points in Figure 1 can be attributed to experimental errors). In order to make the comparison, the experimental values of the fine structure splitting, $L_{II} - L_{III}$, are needed. These values are obtained from Table IV by subtracting the ν/R value of the L_{α_2} line from that for the L_{β_1} line and are shown in Table VI with their relative errors expressed in parts per million.

Table VI

Experimental values of the fine structure splitting

Element	$\Delta\nu/R$	Relative Error ppm
$_{74}W$	98.275 ± 0.004	37
$_{78}Pt$	125.599 ± 0.008	64
$_{83}Bi$	168.511 ± 0.007	42
$_{90}Th$	249.364 ± 0.009	34
$_{92}U$	277.935 ± 0.009	33
$_{94}Pu$	309.435 ± 0.011	36

The theoretical expression for the $L_{II}L_{III}$ energy level splitting including the Schawlow-Townes correction for the nuclear size effect is given by (2.26). We shall write it in the following form to simplify the calculations:

$$\left(\frac{\Delta\nu}{R}\right)_{Th} = \phi(\alpha Z) + BZ^2 - \left(\frac{\Delta\nu}{R}\right)_{Exp} De^{b(Z-60)} \qquad (6.3)$$

where

$$\phi(\alpha Z) = \frac{2}{\alpha^2} S(\alpha Z) - 2\alpha^2 Z^3 f(\alpha Z) - 2(0.0178)\alpha^4 Z^5 . \qquad (6.4)$$

The significant difference between (6.3) and (2.26) comes from using the experimental value of $\Delta\nu/R$ to calculate the theoretical decrease in fine structure splitting due to nuclear size rather than the value of $\Delta\nu/R$ given by the point nucleus expression. We have also made explicit the fact that nuclear size causes a <u>decrease</u> in splitting by writing the correction term as a negative quantity which requires D to be a positive number. In (6.4) we have included the small correction term which Christy and Keller have estimated to make up for the omission of higher order terms in the interaction Hamiltonian used to calculate $f(\alpha Z)$.

The first step in the calculations is the evaluation of the quantity $\phi(\alpha Z)$ in which the slowly varying function $f(\alpha Z)$ must be interpolated or extrapolated from the values listed in Table II. It was mentioned previously (page 15) that Lagrange interpolation of log $f(\alpha Z)$ expressed as a function of $1 - \sqrt{1-\alpha^2 Z^2}$ should be more reliable than interpolation using $f(\alpha Z)$ itself. The interpolation formula expressed as a power series is

$$\log \left[10\, f(\alpha Z)\right] = C_0 + C_1 x + C_2 x^2 - C_3 x^3 + C_4 x^4 \qquad (6.5)$$

with

$$C_0 = 6.794690 \times 10^{-1}$$
$$C_1 = 6.83439 \times 10^{-3}$$
$$C_2 = 2.648 \times 10^{-5}$$
$$C_3 = 5.26 \times 10^{-7}$$
$$C_4 = 1.09 \times 10^{-8}$$

and with

$$x = 100 \left[1 - \sqrt{1 - \alpha^2 Z^2}\right] .$$

The results of the calculation of the quantities making up the function $\phi(\alpha Z)$ are shown in Table VII.

Table VII

Evaluation of point nucleus expression (6.4)

Z	$\frac{2}{\alpha^2} S(\alpha Z)$	$2\alpha^2 Z^3\, f(\alpha Z)$	$0.0356\, \alpha^4 Z^5$	$\phi(\alpha Z)$
74	122.4447	26.7910	0.2240	95.4297
78	155.1396	32.4429	0.2915	122.4052
83	206.1783	40.9392	0.3976	164.8415
90	301.8214	56.2056	0.5961	245.0197
92	335.5598	61.4630	0.6653	273.4315
94	372.6790	67.1968	0.7409	304.7413

Before proceeding with the calculations it is necessary to discuss briefly a significant correction factor. Although it is not too clear from their paper (7), Schawlow and Townes made a correction for the effect of the anomalous electron moment which increases the fine structure by the factor $1 + \alpha/\pi$ to first order.* Therefore to compare the experimental measurements of $\Delta\nu/R$ to the theory which does not include the effect of the anomalous moment we may simply reduce the experimental values by the factor $(1 + \alpha/\pi)^{-1}$.

Continuing with the comparison with the theory, we shall first assume that D = 0 (no nuclear size effect) and evaluate the constant B in (6.3) by a least squares fit of the theoretical to the experimental values of $\Delta\nu/R$ which have been modified by the factor $(1+\alpha/\pi)^{-1}$. The value of B thus determined is used in (6.3) to calculate the relative deviation between theory and experiment as follows:

$$\frac{(\Delta\nu)_{Th} - (\Delta\nu)_{Exp}}{(\Delta\nu)_{Exp}} = B\,\frac{Z^2}{\Delta\nu/R} - \left[1 - \frac{\phi}{\Delta\nu/R}\right]. \qquad (6.6)$$

Equal weighting is used in the least squares analysis because the relative errors in the experimental measurements are all about the same (see Table VI). The results of this first comparison are shown in Figure 22 with the deviations expressed in parts per million. The statistical error for the various points is the relative experimental error obtained from Table VI. It is clear that the improved precision of the X-ray measurements has made the systematic deviation between theory and experiment at large Z even more evident than appears in Figure 1a.

---

* Professor Townes has clarified this point in a private communication.

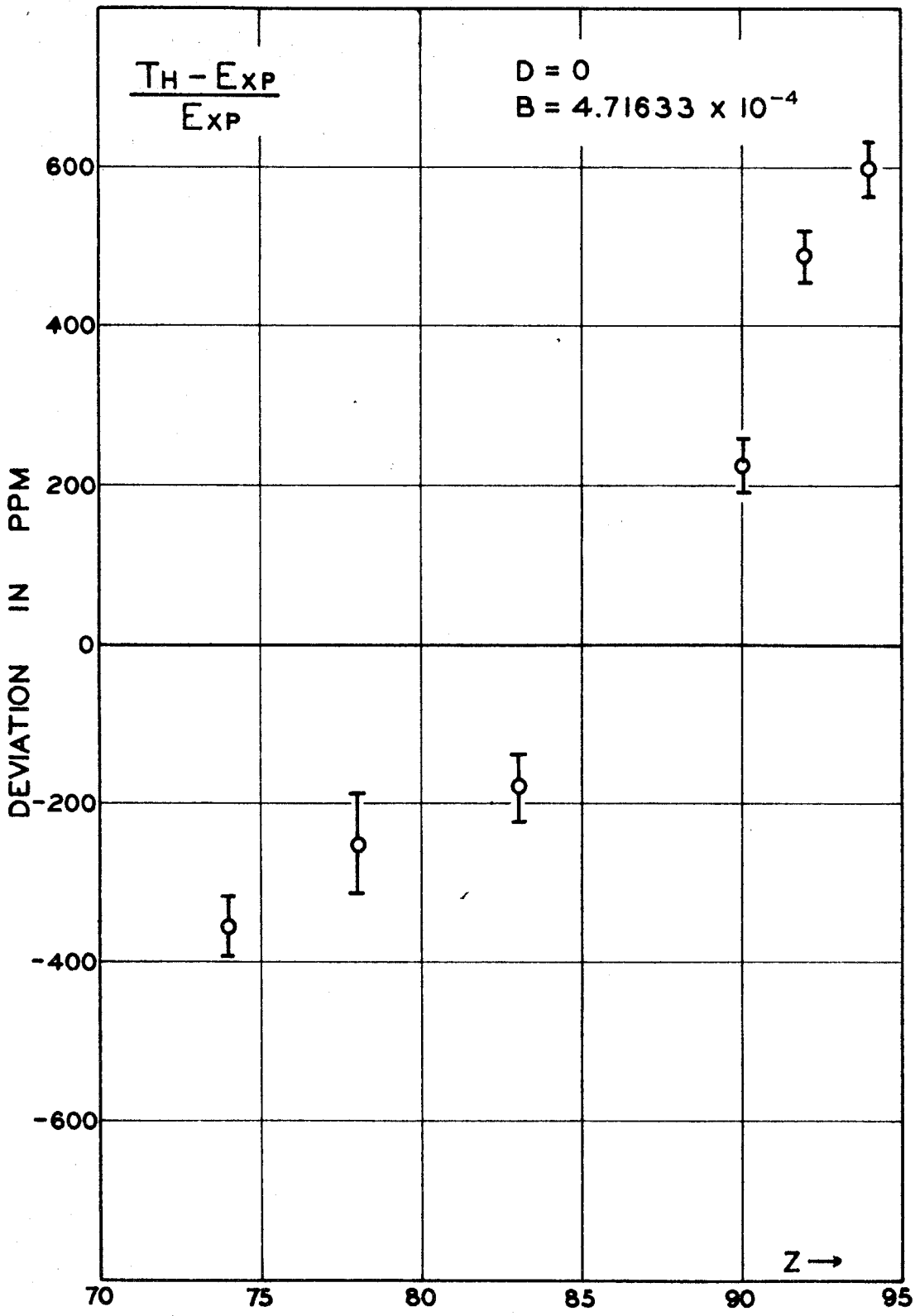

Figure 2. Relative deviation of theory and experiment without the nuclear size correction.

When the nuclear size effect is included, two approaches may be followed. We may assume that the deviation between the point nucleus values of $\Delta\nu$ and the experimental values is due entirely to a uniformly charged spherical nucleus of unknown radius. The values of D and B in (6.3) may then be adjusted to give a best fit to experiment; the value of D obtained in this way is then a measure of the size of this fictitious nucleus. On the other hand, we may accept the results of other measurements on nuclear size and charge distribution and compute the value of D corresponding to this more realistic nucleus. The resulting plot of (Th - Exp)/Exp* is then an indication of the magnitude of further corrections which must be applied to the theory. In either case the values of $\Delta E/h\Delta\nu$ computed by Schawlow and Townes and listed in Table I should be corrected for normalization and for a nucleus which is not sharply bounded having an rms radius constant, $r_o = 1.2 \times 10^{-13}$ cm.

We shall take as a correction factor for normalization to be applied to each of the values in Table I, the value 0.75. (7) Ford and Hill (6) show that the difference in ΔE caused by a uniformly charged nucleus and one which has an extended tail is small enough so that a uniformly charged nucleus may be assumed. The correction of $\Delta E/h\Delta\nu$ to correspond to $r_o = 1.2 \times 10^{-13}$ cm rather than 1.5×10^{-13} cm is accomplished merely by multiplying each of the values in the second column of Table I by $(1.2/1.5)^{2\sigma}$ in accordance with the equation preceding (2.13), since $\langle r^{2\sigma} \rangle_{Av} = r^{2\sigma}$ in the case of a uniformly charged nucleus. The corrected values of $\Delta E/h\Delta\nu$ may be expressed quite accurately by the formula

---

* The abbreviation "Th" means $(\Delta\nu/R)_{Th}$ with a similar meaning for "Exp".

$$\frac{\Delta E}{h\Delta\nu} = De^{b(Z-60)} = 0.54 \times 10^{-4}\, e^{0.0878p} \qquad (6.7)$$

where $p = Z - 60$.

The relative deviation of theory and experiment when only the effect of an unknown nuclear size is included may be written as

$$\frac{\text{Th-Exp}}{\text{Exp}} = B\frac{Z^2}{\Delta\nu/R} - \left[1 - \frac{\phi}{\Delta\nu/R}\right] - De^{bp} \qquad (6.8)$$

where D and B are evaluated by least squares yielding $B = 4.81722 \times 10^{-4}$ and $D = 0.44 \times 10^{-4}$ with the root mean square deviation being 60 parts per million. This value of D corresponds to a nuclear radius with $r_o = 1.07 \times 10^{-13}$ cm. A comparison of this value of r_o with the value $r_o = 2.1 \times 10^{-13}$ cm obtained by Schawlow and Townes suggests that small errors in the already existing X-ray data might account for the anomalously large nuclear radius deduced by them. It was found that most of the difficulty could be traced to errors in the measurements of the wavelengths of the L_{α_2} lines of several of the heavy elements. Since this line is quite weak and only about 10 XU removed from the strong L_{α_1} line, special precautions are necessary in order to get high precision in wavelength measurements. A comparison of the ν/R values listed in Table V (excepting plutonium) to those calculated from reference 12 sheds a fair amount of light on the problem. The root mean square deviation between the present and older values of ν/R for the L_{β_1} line is 28 parts per million while for the L_{α_2} line it is 87 parts per million. The signs of the deviations are also significant; the ν/R values for the L_{α_2} line for $Z = 83$ and above are all <u>larger</u> than the present values and thus give too <u>small</u> a value for $\Delta\nu/R$ for these heavier elements by several hundred parts per million.

The value of nuclear radius deduced above, namely $r_o = 1.07 \times 10^{-13}$ cm, suggests that when the theory is corrected for a nuclear radius with $r_o = 1.2 \times 10^{-13}$ cm additional correction terms will be needed in order to maintain agreement between theory and experiment. One such correction is due to the effect of vacuum polarization. Wichmann and Kroll (29) have made an accurate determination of the contribution of vacuum polarization to the L_{II}-L_{III} splitting. They have calculated the contribution in Rydbergs for various values of Z and present the results as $\delta_p^{(1)}$ in Table I of their paper. It was found that the fraction $\delta_p^{(1)}/(\Delta\nu/R)$ could be represented accurately by the formula

$$\frac{\delta_p^{(1)}}{\Delta\nu/R} = Ve^{cp} \qquad (6.9)$$

with $V = 1.73 \times 10^{-4}$, $c = 0.0462$, and $p = Z - 60$. The expression corresponding to (6.8) which includes both nuclear size and vacuum polarization corrections is

$$\frac{\text{Th-Exp}}{\text{Exp}} = B\frac{Z^2}{\Delta\nu/R} - \left[1 - \frac{\phi}{\Delta\nu/R}\right] - De^{bp} + Ve^{cp}. \qquad (6.10)$$

With D fixed at 0.54×10^{-4} ($r_o = 1.2 \times 10^{-13}$ cm) and B adjusted by least squares the resulting relative deviations (shown in Figure 23) indicate that still further corrections are needed in the theory.

It is generally conceded that the quantum electrodynamical effect commonly known as the "Lamb shift" plays an important role in modifying the calculated fine structure splitting. Quantitative evaluation of the correction for large values of Z are very difficult and have not been accomplished as yet; however, E. H. Wichmann, in a private communication, suggests that the correction for the Lamb shift

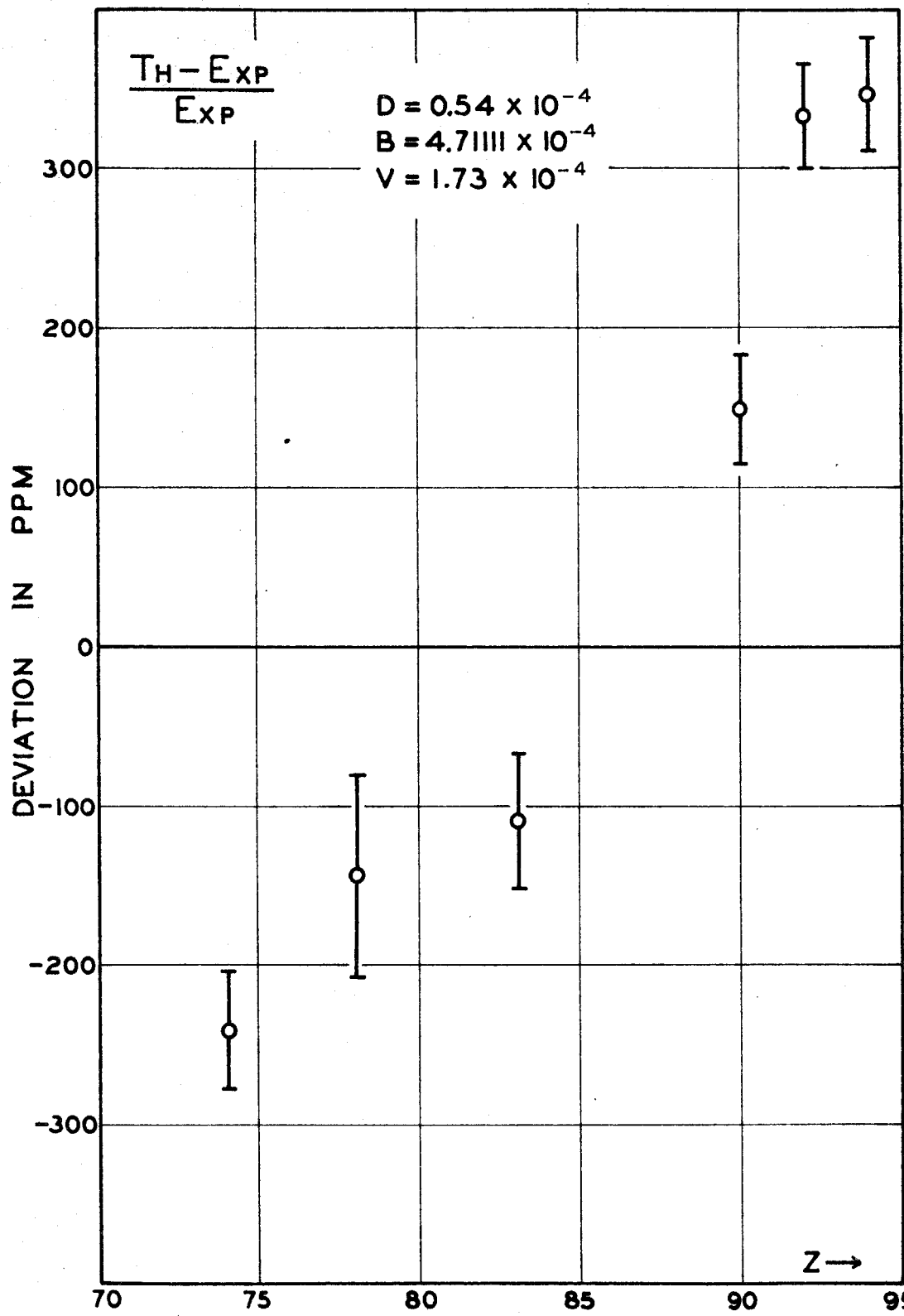

Figure 2°. Deviation of theory and experiment when corrections for vacuum polarization and a nuclear radius of $r_0 = 1.2 \times 10^{-13}$ cm are included.

is of the same order of magnitude as that for vacuum polarization and of opposite sign. It is therefore of some interest to determine from the remaining discrepancy between theory and experiment shown in Figure 23 the magnitude and Z dependence of the correction required to minimize the discrepancy.

We shall assume that the required correction term is exponential in Z having the form Le^{ap} where both L and a are to be determined by least squares. No doubt other functional forms might be used with similar Z dependence, but the one suggested is certainly adequate for the present purpose. The appropriateness of the choice of function can be tested by evaluating the root mean square deviation between theory and experiment and comparing it to the size of the experimental errors.

As before we shall write

$$\frac{\text{Th-Exp}}{\text{Exp}} = B\frac{Z^2}{\Delta\nu/R} - \left[1 - \frac{\phi}{\Delta\nu/R}\right] - De^{bp} + Ve^{cp} - Le^{ap} \qquad (6.11)$$

and adjust B, L, and a by least squares. In practice the exponential term was "linearized" by employing an approximation to a, namely a_o, and setting $e^{ap} \cong e^{a_o p}(1+\alpha p)$ where $a = a_o + \alpha$. The results of the adjustment are $B = 4.76333 \times 10^{-4}$, $L = 10.7 \times 10^{-6}$, $\alpha = -0.005$ with $a_o = 0.12$. When these values are substituted in (6.11) and the rms deviation calculated the result is 39 parts per million which is to be compared to the average experimental error of 41 ppm. It may be concluded, therefore, that the assumption of a single correction term of exponential form is adequate in view of the present experimental accuracy.

It is not suggested that the formula

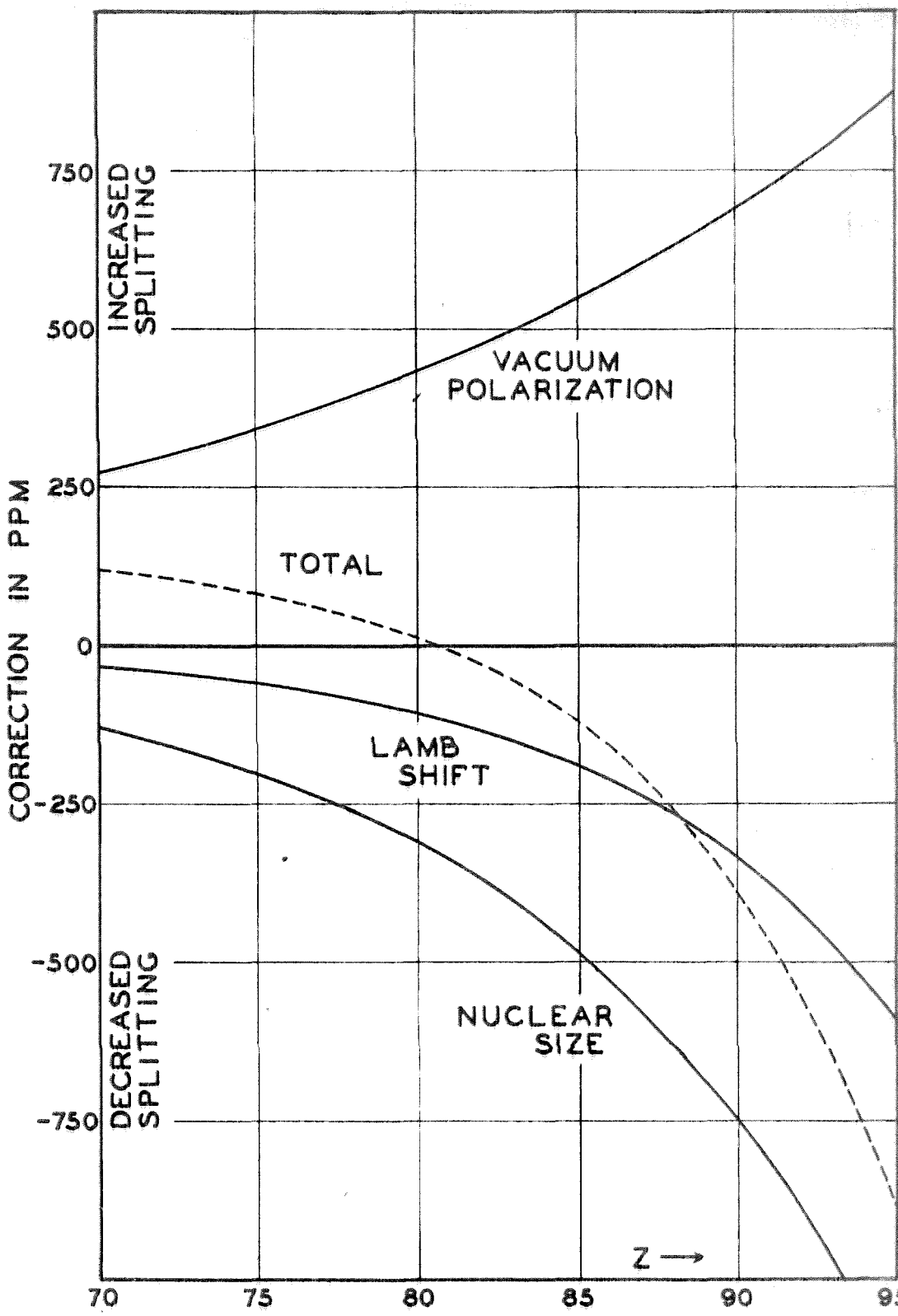

Figure 24. Showing how the various correction terms affect the fine structure splitting as given by the Christy-Keller point nucleus formula.

$$Le^{a(Z-60)} = 10.7 \times 10^{-6}\ e^{0.115(Z-60)} \qquad (6.12)$$

actually represents the fractional correction to the fine structure splitting due to the Lamb shift alone, since very likely there are further corrections necessary in the Christy-Keller point nucleus formula. However, it is clear that (6.12) represents rather accurately the sum of whatever further corrections are needed in the theory, and because of the strong Z dependence it is quite probable that a large part of the correction may, indeed, be attributed to the Lamb shift effect. The three corrections to the fine structure splitting as well as their sum are shown in Figure 24 as functions of Z. If the remaining uncertainties in the theory due to the screening correction and the Lamb shift could be removed or at least reduced, this method might prove to be of some value in obtaining an accurate value for α, the fine structure constant, using the technique of Christy and Keller.

References

1. M. H. Johnson and E. Teller, Phys. Rev. 93, 357 (1954).

2. R. Hofstadter, B. Hahn, A. W. Knudsen, and J. A. McIntyre, Phys. Rev. 95, 512 (1954).

3. D. L. Hill, B. E. Freeman, and K. W. Ford, Phys. Rev. 99, 649 (1955).

4. V. L. Fitch and J. Rainwater, Phys. Rev. 92, 789 (1953).

5. L. N. Cooper and E. M. Henley, Phys. Rev. 92, 801 (1953).

6. K. W. Ford and D. L. Hill, Phys. Rev. 94, 1630 (1954).

7. A. L. Schawlow and C. H. Townes, Phys. Rev. 100, 1273 (1955).

8. J. E. Rosenthal and G. Breit, Phys. Rev. 41, 459 (1932).

9. E. K. Broch, Archiv for Math. og Naturvindenskab 48, 25 (1945).

10. R. F. Christy and J. M. Keller, Phys. Rev. 61, 147 (1942).

11. E. R. Cohen, J. W. M. DuMond, T. W. Layton, and J. S. Rollett, Rev. Mod. Phys. 27, 363 (1955).

12. Y. Cauchois and H. Hulubei, Longueurs d'Onde des Emissions X et des Discontinuities d'Absorption X, Hermann et Cie, Paris (1947).

13. A. H. Compton and S. K. Allison, X-Rays in Theory and Experiment, D. Van Nostrand Co., 1935, pp. 709-740.

14. C. G. Darwin, Phil. Mag. 27, 325; 675 (1914).

15. Prins, Zeits. f. Physik 63, 477 (1930).

16. S. K. Allison, Phys. Rev. 41, 1 (1932); 44, 63 (1933).

17. L. G. Parratt, Phys. Rev. 41, 561 (1932).

18. J. W. M. DuMond, Phys. Rev. 52, 872 (1937).

19. A. Hoyt, Phys. Rev. 40, 477 (1932); J. H. Williams, Phys. Rev. 40, 791 (1932); G. Brogan, Archiv. f. Fysik 8, 391 (1954).

20. G. L. Rogosa and G. Schwarz, Phys. Rev. 92, 1434 (1953).

21. W. Gröbner and N. Hofreiter, Integraltafel, Springer-Verlag, 1949.

22. R. C. Spencer, Phys. Rev. 38, 618 (1931).

23. J. H. Williams, Phys. Rev. 40, 636 (1932).

24. J. W. M. DuMond and D. Marlow, Rev. Sci. Inst. 8, 112 (1937).

25. K. V. Manning, Rev. Sci. Inst. 5, 316 (1934).

26. M. Schwarzschild, Phys. Rev. 32, 162 (1928).

27. A. H. Compton, Rev. Sci. Inst. 2, 365 (1931).

28. G. Brogan, Archiv f. Fysik 6, 479 (1953).

29. E. H. Wichmann and N. M. Kroll, Phys. Rev. 100, 1273 (1955).

APPENDIX A

We wish to evaluate the expression appearing in (4.17):

$$F(t,k) = \frac{1}{\sqrt{k}} \int_{t-k}^{t} \frac{dx}{\sqrt{t-x}\,(1+x^2)} - \frac{1}{k} \int_{t-k}^{t} \frac{dx}{1+x^2} \quad . \qquad (1)$$

The second integral is elementary, having the value

$$\frac{1}{k} \tan^{-1} \frac{k}{t(t-k)+1} \quad . \qquad (2)$$

The first integral was found in a table of integrals (21), and when the limits of integration are substituted into the tabulated solution the result is:

$$F(t,k) = \frac{1}{\sqrt{k}} \left\{ \frac{\beta_2}{2\rho^2} \left[\log \frac{t^2+1}{A^2+B^2} - \log \frac{(t-k)^2+1}{(A-\gamma_1 k-\sqrt{k})^2 + (B-\gamma_2 k)^2} \right] \right.$$

$$\left. + \frac{\beta_1}{\rho^2} \left[-\tan^{-1} \frac{k}{t(t-k)+1} + \tan^{-1} \frac{B}{A} - \tan^{-1} \frac{B-\gamma_2 k}{A-\gamma_1 k-\sqrt{k}} \right] \right\}$$

$$- \frac{1}{k} \tan^{-1} \frac{k}{t(t-k)+1} \quad . \qquad (3)$$

The abbreviations used in the above expression are as follows:

$$\rho^2 = \sqrt{t^2+1} \qquad \beta_1 = -\sqrt{\rho^2/2 + t/2} \qquad \beta_2 = \sqrt{\rho^2/2 - t/2}$$

$$\gamma_1 = -\beta_1/2\rho^2 \qquad \gamma_2 = \beta_2/2\rho^2$$

$$\delta_1 = -\gamma_2 + t\beta_1/\rho^2 \qquad \delta_2 = \gamma_1 - t\beta_2/\rho^2$$

$$A = \gamma_1 t + \delta_1 \qquad B = \gamma_2 t + \delta_2 \quad .$$

APPENDIX B

It is necessary to be able to evaluate F(t,k) for k not equal to one of the eleven values used in the machine computation of the function. We let

$$\Delta F = \frac{\partial F}{\partial k} \Delta k \tag{1}$$

where F = F(t,k) is given in (1), Appendix A.

Now

$$\frac{\partial F(t,k)}{\partial k} = -\frac{1}{\sqrt{k}} \frac{1}{\sqrt{k}\left[1+(t-k)^2\right]} - \frac{1}{2k^{3/2}} \int_{t-k}^{t} \frac{dx}{\sqrt{t-x}\ (1+x^2)}$$

$$+ \frac{1}{k} \frac{1}{1+(t-k)^2} + \frac{1}{k^2} \int_{t-k}^{t} \frac{dx}{1+x^2} \tag{2}$$

$$= -\left\{ \frac{1}{2k} \frac{1}{\sqrt{k}} \int_{t-k}^{t} \frac{dx}{\sqrt{t-x}\ (1+x^2)} - \frac{1}{2k} \frac{1}{k} \int_{t-k}^{t} \frac{dx}{1+x^2} \right.$$

$$\left. - \frac{1}{2k} \frac{1}{k} \int_{t-k}^{t} \frac{dx}{1+x^2} \right\}$$

$$= \frac{1}{2k} \left\{ \frac{1}{k} \int_{t-k}^{t} \frac{dx}{1+x^2} - F(t,k) \right\}. \tag{3}$$

Therefore

$$\Delta F = \left\{ \frac{1}{2k} \tan^{-1} \frac{k}{t(t-k)+1} - \frac{1}{2} F(t,k) \right\} \frac{\Delta k}{k} . \tag{4}$$

Since the first term of this expression is also part of the expression for F(t,k) it was a simple matter to program the evaluation of the quantity in the braces in (4) along with the computation of F(t,k). The computer program was arranged so that this quantity was printed out along with the value of F(t,k) for each value of t. Any one of the eleven computed curves could therefore be adjusted to a different value of k near the original k without doing the calculation by machine.

APPENDIX C

Assuming that the observed spectral line has the shape of a witch, $y = A(1+t^2)^{-1}$, we wish to calculate the uncertainty, dt, in the horizontal position of a point due to an uncertainty, dy, in the value of y. We have

$$t^2 = \frac{A}{y} - 1 \quad \text{and} \quad tdt = -\frac{A}{2y^2}\,dy$$

so that

$$\frac{dt}{t} = \frac{dy}{y}\left(\frac{A/2}{y-A}\right) = -E\,\frac{dy}{y} \tag{1}$$

where

$$E = \frac{1/2}{1 - y/A} \quad . \tag{2}$$

Now when the value of y is determined by the accumulation of a total of c counts, the relative statistical error in y is given by

$$\frac{dy}{y} = \frac{1}{\sqrt{c}} \quad . \tag{3}$$

In the process of fitting the observed points to the theoretical line profile to determine the center of the unmodified line we must find the average value of t'-t which represents the separation of the origins of the two curves. The weight to be attached to an individual value of t'-t should be inversely proportional to the square of the uncertainty in the measurement of t', that is,

$$w = \frac{k}{(dt')^2} = \frac{k}{t'^2\left(\frac{dt'}{t'}\right)^2} = \frac{k}{t'^2\left(\frac{dy}{y}\right)^2 E^2} = \frac{kc}{t'^2E^2} = fkc \tag{4}$$

where w is the weight to be assigned to the value of t'-t corresponding to the observed point at t', k is a constant of proportionality,

and $f = 1/t'^2E^2$. The quantity f may be expressed as a function of t' and a table of values set up for convenient ranges of t'. The appropriate weight w for a value of $t'-t$ is found by multiplying the f value for that particular point by a number proportional to the counts accumulated at that point.